CODEN:LUTEDX/(TEIE-5376)/1-80(2016)

Industrial Electrical Engineering and Automation

Locating Faults on Energized Airfield Lighting Power Cables

Simon Anderjon
Dennis Honkanen

Division of Industrial Electrical Engineering and Automation
Faculty of Engineering, Lund University

Master Thesis

Locating Faults on Energized Airfield Lighting Power Cables

Lunds Tekniska Högskola

Simon Anderjon, Dennis Honkanen

June 14, 2016

Supervisor (LTH): Bengt Simonsson, Senior Instructor at IEA, LTH
Examiner (LTH): Gunnar Lindstedt, Associate Professor at IEA, LTH

Supervisors (ADB-Safegate): Anders Eriksson, Systems Engineer, ADB-Safegate
Eva Ewertz, Project Manager, ADB-Safegate

Abstract

The purpose of this study is to investigate the feasibility of both online and offline fault location and state of health technologies for airport series circuits used to provide power to light fixtures on the runway. In current series circuits, only some ground faults can be detected and no automated fault location or state of health features are available. Fault location is currently performed with an isolation tester and a "divide and conquer"-methodology which is very time consuming and personnel intensive.

The foundation of this work is based on an extensive literature study, where fault location and state of health methods used in the power distribution were identified. The method evaluation of the thesis is based on a concept generation methodology by Karl T. Ulrich and Steven D. Eppinger. Technical evaluations were performed with primarily LTspice as a simulation tool, time domain reflectometry was also tested in the lab and on real series circuits at Arlanda airport.

The results reveal that adopting fault location technologies used in the power distribution industry for series circuit fault location is very difficult, mainly due to the current transformers placed on the series circuit and the high-resistance nature of the majority of ground faults. The transformers pose as impedance discontinuities which contribute with significant high frequency attenuation and dispersion, which obstructs the utilization of any high frequency transients for fault location purposes. Ground faults with high resistances in the $k\Omega$-range does not produce any high frequency transients and does not cause significant steady state-deviations which is problematic for impedance based fault location methods. Current state of health methods proved to be time consuming and personnel intensive, but could potentially be beneficial for Safegate engineers who could benchmark existing cable systems when commissioning new series circuits. Although, large scale tests are recommended in order to validate these results. Further research into utilizing Airfield Smart power and each individual fixture for fault location and state of health is also of interest for future work.

Acknowledgments

The writing of this thesis has been an exciting and instructive journey. During our time at ADB Safegate we have been given a glimpse into an exciting industry with great potential and interesting challenges ahead.

First of all we would like to thank our supervisors at ADB Safegate, Anders Eriksson and Eva Ewerts, for taking care of us at the company, helping us with technical problems and allowing us to visit Arlanda airport where we had interesting experiences learning about airport operations. We would also like to give our warm thanks to Joakim Arnsby, Peter Körner, Andreas Wirandi and Victor Norell at ADB Safegate for your support and help during our master thesis.

We would also like to thank our supervisors, Senior Instructor Simonsson and Assoc. Prof. Lindstedt, from the IEA institution for their constructive criticism and administrative guidance.

Last but not least we would like to thank our friends and families for supporting us throughout this master thesis and for recharging our mental batteries to maintain our focus at it's peak.

Abbreviations and Indices

AC	Alternating Current
AFL	Airfield Lighting
AI	Artifical Intelligence
ANN	Artificial Neural Network
ASP	Airfield Smart Power
CCR	Constant Current Regulator
CT	Current Transformer
DAQ	Data Acquisition
DC	Direct Current
FL	Fault Location
FLog	Fuzzy Logic
HPC	High Power Converter
KCL	Kirchoff's Current Law
KVL	Kirchoff's Voltage Law
LED	Light Emitting Diode
OHL	Overhead Lines
PD	Partial Discharge
PLC	Power Line Communication
PMU	Phasor Measurement Unit
P.U	Per Unit
PVC	Polyvinyl Chloride
SCADA	Supervisory Control and Data Acquisition
SCF	Series Circuit Filter
SCI	Series Circuit Inductance
SCM	Series Circuit Modem
SoH	State of Health
TW	Traveling Wave
TDR	Time Domain Reflectometry
UV	Ultraviolet
VT	Voltage Transformer
WLT	Wavelet Transform
XLPE	Cross-linked Polyethylene

Contents

1 Introduction **1**
- 1.1 Background . . . 1
- 1.2 Problem Statement . . . 1
- 1.3 Goal . . . 1

2 Airfield Lighting System **2**
- 2.1 Constant Current Regulator . . . 2
- 2.2 Primary Series Circuit . . . 2
- 2.3 Isolation Transformers . . . 3
- 2.4 Light Fixtures . . . 3
- 2.5 Airfield Smart Power . . . 4
- 2.6 Series Circuit Filtering . . . 4

3 Theory **5**
- 3.1 Transmission Line Theory . . . 5
  - 3.1.1 Coaxial Cable Structure . . . 5
  - 3.1.2 Fundamental Electrical Parameters . . . 6
  - 3.1.3 Skin Effect . . . 7
  - 3.1.4 Telegrapher´s Equations . . . 7
  - 3.1.5 Characteristic Impedance . . . 8
  - 3.1.6 Wave Propagation . . . 8
  - 3.1.7 Electrical Field of a Coaxial Cable . . . 10
  - 3.1.8 Transmission Line Shielding . . . 10
- 3.2 Current Transformers . . . 11
  - 3.2.1 Equivalent Circuit . . . 12
  - 3.2.2 Frequency Response & Wave Propagation . . . 13
  - 3.2.3 CT Saturation . . . 13
- 3.3 Electrical Faults . . . 14
  - 3.3.1 Ground Faults . . . 15
  - 3.3.2 Series Faults . . . 15
  - 3.3.3 Intermittent Faults . . . 16
  - 3.3.4 Fault Inception Angle . . . 16

4 Method **17**
- 4.1 Project Plan . . . 17
- 4.2 Tools . . . 17
- 4.3 Specification & Evaluation . . . 18
- 4.4 Method Validation . . . 18

5 Fault Location Strategies **19**
- 5.1 Impedance Based Methods . . . 19
- 5.2 Time Domain Reflectometry . . . 22
- 5.3 High Voltage Pulse Surging . . . 23
- 5.4 Traveling Wave Methods . . . 23
- 5.5 Wavelet Transform . . . 25
- 5.6 Artificial Neural Networks & Fuzzy Logic . . . 27

6 State of Health **29**
6.1 Electric Trees . . . 29
6.2 Partial Discharge . . . 31
6.3 Tan δ . . . 32
6.4 SoH Diagnostics . . . 32

7 Simulations **33**
7.1 Transmission Line Model . . . 33
7.2 Current Transformer Model . . . 35
7.3 Series Circuit Models . . . 37

8 Results & Discussion **39**
8.1 Traveling Wave . . . 39
8.1.1 1 & 2 Terminal Measurements . . . 39
8.1.2 Sampling Frequency . . . 40
8.1.3 Algorithm Implementation . . . 41
8.1.4 Effect of Impedance Discontinuities & Attenuation on Traveling waves . . . 42
8.1.5 Fault Conditions . . . 44
8.1.6 Noise and Transient Analysis . . . 47
8.2 Impedance based methods . . . 50
8.2.1 Algorithm Implementation . . . 50
8.2.2 Fault Conditions . . . 51
8.3 Time Domain Reflectometry . . . 54
8.3.1 Transmission line . . . 54
8.3.2 Effect of impedance discontinuities on TDR . . . 56
8.4 Arlanda Customer Case . . . 58
8.4.1 Operative Study . . . 59
8.4.2 TDR Tests . . . 60
8.5 Concept Evaluation & Scoring . . . 61
8.5.1 Concept Scoring for Fault Location Methods . . . 61
8.5.2 Concept Scoring for State of Health Methods . . . 63

9 Conclusions & Future Work **64**

Appendix A LTspice **69**
A.1 LossyTL Constructor . . . 69
A.2 Complete airport circuit Schematic . . . 70

Appendix B Test Data & Calculations **71**
B.1 Inter-turn Capacitance Calculation . . . 71
B.2 Transformer Data . . . 72

Appendix C Simulations Raw Data **73**
C.1 Inception Angle . . . 73
C.2 Fault Resistance . . . 74
C.3 Fault Location . . . 74

1 Introduction

1.1 Background

Since air traffic is expected to double within the coming 15 years [1], safety and efficiency of airports are subjected to new challenges. The airfield lighting system (AFL) consists of LED-lights which are connected in long loops which can be several kilometers long. One of the challenges with maintaining the cable circuits is to detect and locate different intermittent faults. Common causes of faults are water and moisture intrusion due to faulty splices or connectors.

ADB-Safegate is one of the industry leaders in automated airside systems today, and they offer a variety of solutions for airports. Their portfolio includes automated docking systems and smart airfield lighting systems. Safegate has sold equipment to airports worldwide, Arlanda Airport in Sweden, Hobart Airport in Australia and Doha International Airport in Qatar being a few of them. [2]

The amount of thesis work was divided equally between the authors. Although, Dennis focused on online fault location methods while Simon focused on offline fault location methods and state of health.

1.2 Problem Statement

In AFL systems today, the light fixtures are connected in series while being decoupled from the series circuit using isolation transformers. The series circuits are designed to operate for several years and have proven to be very reliable. Although, occasionally the AFL suffers from electrical faults. The constant current regulator (CCR) is able to measure resistance to ground and successfully detect some electrical faults, but lacks the possibility to pinpoint and locate faults. Therefore, the lack of a fault locating system requires that airport traffic is temporarily suspended and that a maintenance team is dispatched out to the runway to pinpoint the fault location. This is done by using offline methods measuring one segment at a time which can be very time consuming when a fault occurs far out on the series circuit. A fault location system would greatly minimize traffic suspension time and thus reduce maintenance costs for electrical faults on the cable system.

1.3 Goal

The purpose of this study is to try and meet the increasing demands on automation and operational safety of the airport. The thesis work involves development and evaluation of methods that can detect and localize electrical faults on the series circuits, and possibly also determine the state of health of the system.

The method should be able to operate on series circuits of all lengths and loads. In order to ensure compatibility with older series circuits it should not require series circuit communication.

The goals of the thesis work is to fulfill the following criteria:

- Perform a feasibility-study of the potential of existing fault location and state of health technologies and identification of factors that influence the possibility for future implementation in an AFL-system.
- Perform a technical evaluation and comparison of existing fault location and state of health methodologies for future implementation in an AFL-system.

2 Airfield Lighting System

The airfield lighting system is used to light up runways and taxiways on airports around the world, it consists of a constant current regulator that provides power to the primary cable. Along the primary cable, isolation transformers are placed in series, where the secondary winding of each transformer is connected to an individual light fixture. [4]

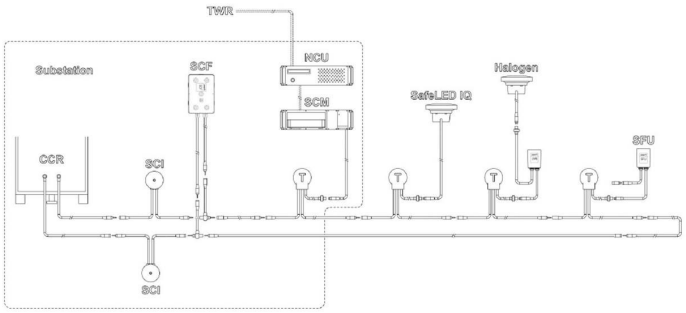

Figure 1: AFL-series circuit setup

2.1 Constant Current Regulator

The constant current regulator (CCR) is an AC-AC converter consisting of a phase controlling thyristor-bridge and a high voltage transformer that can transform the voltage from grid-level up to 5kV (50-60Hz). The CCR keeps a constant output current of 6.6A by regulating the voltage level in order to follow load changes on the series circuit. The CCR is currently able to measure earth-impedance and the minimum limit is $50M\Omega$, but the CCR is not able to locate the fault. These earth-impedance measurements can be routed to a central SCADA system which displays the data to airport personnel. [6]

2.2 Primary Series Circuit

The primary series circuit consists of a single pole coaxial cable. The primary cable can be shielded or unshielded depending on local requirements at each individual airport. The primary series circuit connects the CCR to each individual light fixture by using isolation transformers to decouple the lights from the primary series circuit, this allows other lights in the series circuit to continue operating if one or more light suffers from breakdown.

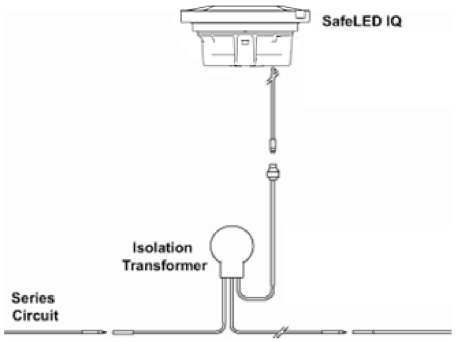

Figure 2: Light/Transformer-connection. [4]

2.3 Isolation Transformers

Current transformers are generally used in metering and over-current relay protection applications. But, in AFL-systems, they are used to overcome the "Christmas tree light"-problem. Since all light fixtures are connected in series, the entire series circuit will break down if 1 fixture fails. Utilizing current transformers to decouple the light fixture from the series circuit maintains a current path on the series circuit that will ensure operation of the remaining light fixtures. When a light fails, the secondary circuit becomes open and the transformer is saturated due to current still running through the primary winding.

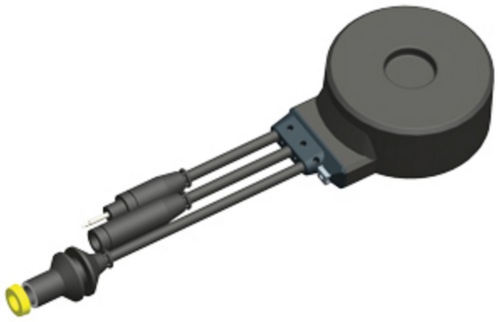

Figure 3: Isolation Transformer from EFLA. [3]

The EFLA transformers recommended by Safegate to their customers are rated at 6.6A rms and from 10W to 500W. Transformers are often "over-sized" in relation to their load in order to lengthen the lifetime of the transformer. [3]

2.4 Light Fixtures

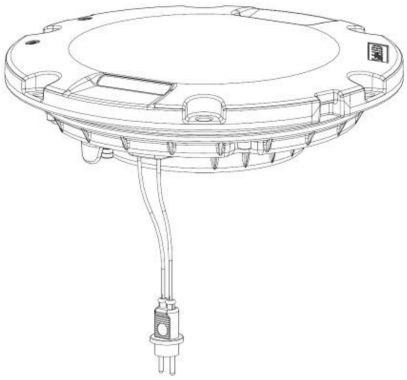

(a) SafeLED, Inset-Light [4]

(b) SafeLED, Elevated Light [5]

Figure 4: Safegate Light Fixtures

There are a number of different light fixtures available from Safegate, which are designed for different applications on the airfield. They can be categorized in 2 different types, elevated light fixtures and inset light fixtures. Inset lights are designed to be implemented into the ground on the runway and to have minimum vertical intrusion up onto the runway, while the elevated lights are usually placed on the edge of the runways and taxiways where vertical intrusion is of less importance.

The fixtures are available with both LED and halogen type lights, halogen lights are significantly less efficient and are continuously being phased out of airports. The power level of the lights depend on light intensity. Although, the maximum power rating for these lights is 58W per light fixture for the LED type. [5]

2.5 Airfield Smart Power

Each light in the AFL-system can be controlled individually by utilizing the Series Circuit Modem (SCM). The SCM is mounted along the series circuit according to Figure 1. The SCM superimposes high frequency communication on to the 50/60 Hz power frequency. By doing so, the number of transmission lines are kept to a minimum. This technique is called power line communication (PLC).

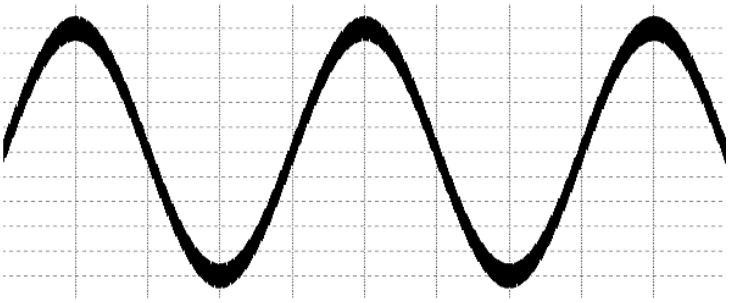

Figure 5: Super-imposed communication on carrier signal.

Since some of series circuits are intelligent and bi-directional communication is possible using the SCM, individual light control and monitoring is possible. The operator can then be notified of individual light faults, location and fault type for fast and easy maintenance. This system is called Airfield Smart Power (ASP). [7]

2.6 Series Circuit Filtering

In order to protect the constant current control loop of the CCR from external and communication noise, filtering is required. Therefore, the series circuit filter (SCF) and series circuit inductance (SCI) are implemented at the terminals of the series circuit.

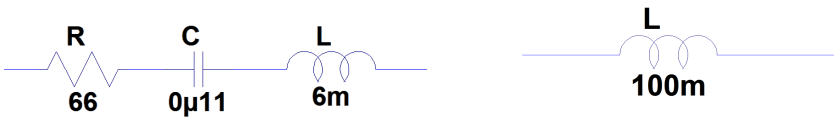

(a) Series Circuit Filter (b) Series Circuit Inductance

Figure 6: Series Circuit Filtering

3 Theory

3.1 Transmission Line Theory

A conductor can be considered a transmission line when a significant fraction of the wavelength of a signal becomes comparable to the length of the conductor. The behaviour of a signal can then be described as a wave-front propagating through a medium. [11]

3.1.1 Coaxial Cable Structure

The underground transmission line that Safegate recommends to customers, is a 5kV shielded underground coaxial cable designed for airport lighting circuits provided by Kabelwerk EUPEN AG. This specific cable is also the one that have been subject to testing in the lab and simulations in LTspice in this master thesis project.

Figure 7: Coaxial Transmission Line from EUPEN. [8]

1. Stranded tinned copper conductor
2. Extruded semi-conducting compound
3. XLPE Insulation
4. Semi-conducting tape, helically applied
5. One lay of brass tape, helically applied, 30% overlapping
6. Separation Tape
7. PE outer sheath - black

As can be seen above, the cable consists of a copper conductor, then followed by a semiconducting layer, XLPE insulation, yet another semiconducting layer and then finally the conductive shield, which is grounded. The outer sheath usually consists of a PVC plastic to provide chemical, UV and weather resistance.

Since the magnitude of the electrical field is equal to the voltage difference between two points, the semi-conductive layers relieve voltage stress along the crossover points between insulation and conductor where the voltage stress is especially high. [9]

Table 1: Physical Parameters, EUPEN Cable. [8]

Cross-Section	**Insulation Thickness**	**Screen Tape**	**Sheath Thickness**	**Overall Diameter**
1x6 mm^2	2.3 mm	0.08x22 mm	1.6 mm	11.5-13.0 mm

3.1.2 Fundamental Electrical Parameters

In a transmission line, electrical parameters are distributed along the length of the line. There are several different ways to represent a transmission line, where the equivalent π-circuit, lumped model and ABCD-model are a few of them. [14]

A coaxial transmission line can be modeled as a series of lumped LC-circuits. The lumped LC-circuits will sufficiently model the characteristics of a short transmission line, where resistive effects are negligible.

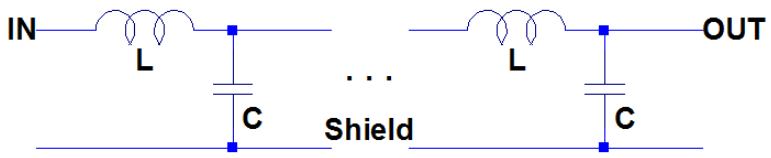

Figure 8: Equivalent circuit of a lossless transmission line.

The distributed inductance per unit length in [H/m] at low frequency for a coaxial cable is:

$$L = L_{int} + L_{ext} = \frac{\mu_c}{2\pi r} + \frac{\mu_{xlpe}}{2\pi} ln\left(\frac{D}{d}\right) \tag{1}$$

Where, μ is the permeability of the materials, copper and XLPE. D is the inner diameter of the shield and d is the exterior diameter of the copper conductor. With higher frequency, the internal inductance will decrease inversely of the square root of frequency at high frequency due to skin effect.

The capacitance per unit length in [F/m] is:

$$C = \frac{2\pi\epsilon}{ln(D/d)} \tag{2}$$

where, ϵ is the dielectric constant of the XLPE insulation. The distributed capacitance is not frequency dependent.

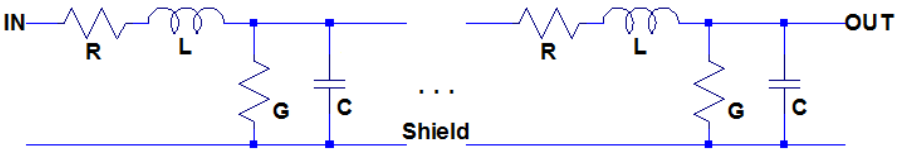

Figure 9: Equivalent circuit of a lossy transmission line.

When transmission lines become long enough, losses can not be neglected. Therefore, distributed resistance R and conductance G are introduced into the model displayed in figure 9, referred to as a lossy transmission line.

The distributed resistance R per unit length $[\Omega/m]$ is:

$$R = \frac{\rho}{A} \tag{3}$$

where ρ is the electrical resistivity of the material per unit length and A is the cross-section of the effective conductance area in m^2 [10]. With low frequency, one can assume a uniform current distribution of the conductor. At higher frequencies, current is concentrated at the surface of the conductor, thus decreasing the effective conductance area. Resistance increases proportionately to the square root of the frequency.

The conductance G per unit length $[S/m]$ is described as:

$$G = \sigma A \tag{4}$$

where σ is the electrical conductivity of the conductor per unit length. Since G is also related to the effective conductance area, G decreases proportionately to the square root of the frequency. [12]

3.1.3 Skin Effect

The skin effect is described as a phenomenon where the current distribution of an AC-signal is not uniform along the radius of the conductor. As frequency increases, current is concentrated along the surface of the conductor. This phenomenon influences resistance, inductance and conductance of a conductor at higher frequencies.

The skin effect originates from the fact that a time-varying magnetic field is accompanied by a time-varying induced electric field, which in turn induces secondary so called eddy currents inside the conductor.

The skin depth of a conductor can be described in [m] with the following equation:

$$\delta = \sqrt{\frac{2}{\omega \mu \rho}} \tag{5}$$

where $\omega = 2\pi f$. For a circular conductor such as a coaxial cable, the effective conductive area can be derived from this. [13]

3.1.4 Telegrapher´s Equations

The telegrapher´s equations, are a set of linear differential equations that can be derived from Maxwells's equations, which describes voltage and current at a given time and distance on a transmission line. The telegrapher´s equations were formulated by Oliver Heaviside in the 1880's when he was working for an American telegraph company. The telegrapher´s equations can be derived for both lossless and lossy transmission lines. [10]

For lossless transmission lines:

$$\begin{cases} \frac{d}{dx}V(x,t) = -L\frac{d}{dt}I(x,t) \\ \frac{d}{dx}I(x,t) = -C\frac{d}{dt}V(x,t) \end{cases} \tag{6}$$

$$\begin{cases} \frac{d^2}{dt^2}V(x,t) = \frac{1}{LC}\frac{d^2}{dx^2}V(x,t) \\ \frac{d^2}{dt^2}I(x,t) = \frac{1}{LC}\frac{d^2}{dx^2}I(x,t) \end{cases} \tag{7}$$

where, t is time, and x represents the distance from the terminal of the transmission line.

For lossy transmission lines:

$$\begin{cases} \frac{d}{dx}V(x,t) = -L\frac{d}{dt}I(x,t) - RI(x,t) \\ \frac{d}{dx}I(x,t) = -C\frac{d}{dt}V(x,t) - GV(x,t) \end{cases} \tag{8}$$

$$\begin{cases} \frac{d^2}{dx^2}V(x,t) = LC\frac{d^2}{dt^2}V(x,t) + (RC+GL)\frac{d}{dt}V(x,t) + GRV(x,t) \\ \frac{d^2}{dx^2}I(x,t) = LC\frac{d^2}{dt^2}I(x,t) + (RC+GL)\frac{d}{dt}I(x,t) + GRI(x,t) \end{cases} \tag{9}$$

3.1.5 Characteristic Impedance

The characteristic impedance (also called surge impedance), is the ratio of current and voltage amplitude of a wave traveling along the transmission line. The characteristic impedance is independent of transmission line length, and is only influenced by the geometry of the transmission line. One can derive the characteristic impedance from the telegrapher´s equations, for both the lossy and lossless case.

For the lossless transmission line, the characteristic impedance is described as:

$$Z_0 = \frac{L}{C} \tag{10}$$

For the lossy transmission line:

$$Z_0 = \frac{R + j\omega L}{G + j\omega C} \tag{11}$$

If a transmission line is terminated with a load equivalent to the characteristic impedance, the transmission line is "matched". By matching the transmission line, signal reflections are prevented and all power reaches the other end of the transmission line. [10]

3.1.6 Wave Propagation

An electromagnetic wave is described by the solution of the wave equation:

$$V(x,t) = f_1(\omega t - kx) + f_2(\omega t + kx) \tag{12}$$

Where f_1 and f_2 are two arbitrary voltage functions traveling in opposite directions. k is the wavenumber in (rad/m). Since the current wave is related to voltage via the characteristic impedance of the medium, the following equation can be established [10]:

$$I(x,t) = \frac{V(x,t)}{Z_0} \tag{13}$$

As mentioned above, in transmission lines voltage and current are considered as wave-fronts propagating through a medium. As they propagate with a velocity equal to some fraction of light speed, wavefronts can be dilated, attenuated and deformed as they encounter discontinuities in the medium. The propagation constant of a transmission line is:

$$\gamma = \alpha + j\beta = \sqrt{(R + j\omega L)(G + j\omega C)} \tag{14}$$

where α is the attenuation constant in [nepers/m] and β is the phase constant which represents the change in phase per unit distance, it is given in [rad/m].

The propagation speed can be derived from the telegrapher´s equations, for the lossless transmission line:

$$v = \frac{1}{\sqrt{LC}} \tag{15}$$

For the lossy transmission line, the propagation velocity is:

$$v = \frac{1}{\sqrt{(R + j\omega L)(G + j\omega C)}} \tag{16}$$

The velocity factor of a signal, is the velocity at which an electromagnetic signal propagates through a medium in relation to how fast an identical signal travels through vacuum. The velocity factor is expressed as a percentage of the signal velocity through vacuum. In a coaxial cable, the velocity factor is related to the dielectric constant of the insulator ϵ. Generally, a coaxial cable is considered to have a velocity factor in between 65%-86%. XLPE-insulation is considered to have a velocity factor of 65.9% while Air Space Polyethylene has a velocity factor 84 %. [15]

It is clear from eq 16, that a signal which contains several frequency components, such as a square wave will distort as it propagates throughout the medium. This occurs due to the fact that the propagation velocity is dependent on frequency, and is called dispersion. [10]

The semiconducting layers of the coaxial cable are considered to act as short circuits. It was shown by K.Steinbrich that for frequencies $< 6MHz$ there is no noteworthy effect on attenuation or propagation velocity change caused by the semiconducting layers. [9]

When a wave-front encounters an impedance discontinuity on the transmission line that is different from the characteristic impedance of the transmission line, a reflected signal will be generated which will travel in the opposite direction of the incidental wave. If only a fraction of the incidental wave is reflected, the remaining incidental wave-front will refract through the discontinuity with a partly decreased energy content. This phenomenon is described with the reflection coefficient Γ:

$$\Gamma = \frac{Z_L - Z_0}{Z_L + Z_0} \tag{17}$$

where Z_L is the load impedance and Z_0 is the source impedance. The reflection coefficient is valid between $-1 \leq \Gamma \leq 1$, where -1 represents a short circuit discontinuity and 1 an open circuit discontinuity. [10]

3.1.7 Electrical Field of a Coaxial Cable

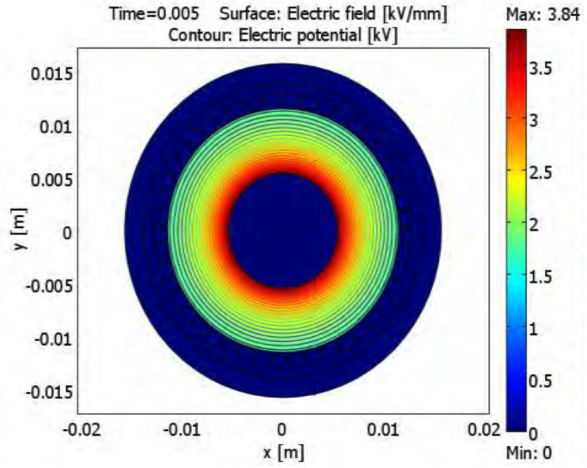

Figure 10: Equipotential electrical field distribution of a shielded coaxial cable. ©[2012] IEEE [18]

The electric field for a shielded coaxial cable is entirely confined within the insulation material of the cable, between conductor and sheath. The scalar value of the electric field is equal to the derivative of the voltage:

$$E = \nabla V \tag{18}$$

As can be seen in fig 10 and can be derived from equation 16, the voltage stress posed on the insulation is at it's largest close to the edge of the center conductor.10 The cable simulated in fig 10, does not feature a semi-conducting layer such as layer 2 in fig 7. The semi-conducting layer is applied to mitigate the very high electrical field and lower the voltage stress on the insulation. [18]

3.1.8 Transmission Line Shielding

Not all transmission line cables in Safegate's AFL-systems around the world are shielded, different airports have different strategies. For some airports, cost is the deciding factor and shielded cables are an unnecessary capital cost. Other airports are more careful and know that unshielded cables in HV-systems pose a significant risk to system availability and operating costs. Even if a transmission line is shielded, the isolation transformers still remain unshielded, resulting in a broken shield loop.

Shielding a cable means to confine the electrical field to the insulation of the cable, this is done to obtain a symmetric radial distribution of the electrical field and thus, obtaining a symmetrical electrical stress on the insulation. This is done by encapsulating the insulator of the transmission line in a conductive screen, this screen is then grounded at each end and at every cable splice. For shorter cable segments, only grounding at one end can be satisfactory. A symmetric distribution of electrical stress minimizes the possibility of surface discharges, as well as shock and fire hazards. According to the Okonite Company [17], shielding should be considered for all single conductor cables above 2kV.

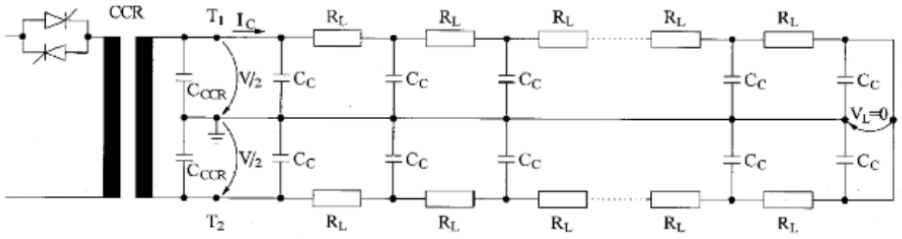

Figure 11: Circuit equivalent of a shielded cable. [16]

As mentioned above, in a shielded cable the entire electrical field is radially distributed along the insulation. This is because the potential of the grounded sheath is very close to 0V along the entire cable if it is grounded regularly at splices and interconnections. As can be seen in fig 11, the distributed capacitance C_c to ground is constant along the length of the transmission line.

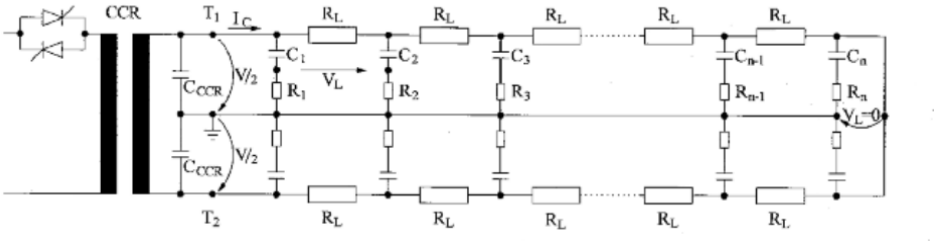

Figure 12: Circuit equivalent of an unshielded cable. [16]

In an unshielded cable, the matter becomes a lot more unpredictable. As can be seen in fig 12, the impedance to ground is made up of local earth resistance $R_1...R_n$ and local cable capacitance $C_1...C_n$. The "ground" in the unshielded case is an earth line that runs along the length of the transmission line. The voltage which the insulation material is subjected to depends on the resistance and capacitance to earth. Therefore, depending on if the surrounding environment is humid or dry, the voltage stress on the insulation will vary. If the environment quickly changes from dry to humid or vice versa in a short geographical span, a voltage will build up along the insulation material. Variations in voltage stress on the insulator can pose serious safety risks. The potential of electrical trees developing in the insulator also increases, especially if the cable is wet or dirty. [16]

3.2 Current Transformers

The isolation transformer that connects the individual light to the series circuit are current transformers (CT), generally of toroidal shape but H-cores are used at airports as well. The toroidal shape minimizes leakage inductance as well as cross-talk between transformers. The transformers are electrically unshielded, but some models can be grounded on the secondary side. In order to withstand weathering effects and chemical resistance, the CT:s are completely encapsulated.

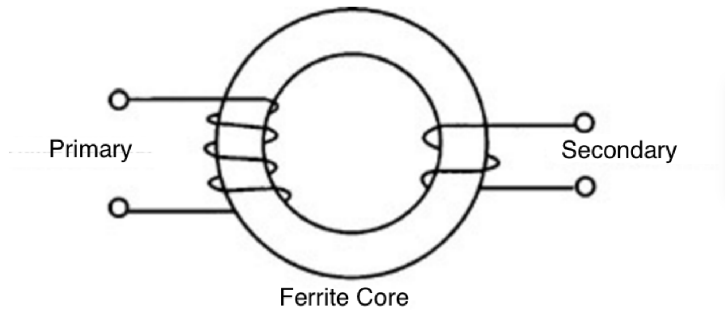

Figure 13: Schematic of a toroidal shaped transformer.

A current transformer is not very different from a regular VT (voltage transformer), but instead of maintaining and transforming voltage, a CT transforms current. What differentiates the two transformer types is that a CT generally holds more turns in each winding [19]. This means that a CT should never operate with an open secondary winding. Since the CT will try to maintain a current through the secondary, secondary winding voltages can rise to dangerous levels. This can occur when light fixtures break and produces an open secondary circuit.

The output current for a CT:

$$I_S = I_P \frac{N_p}{N_s} \tag{19}$$

3.2.1 Equivalent Circuit

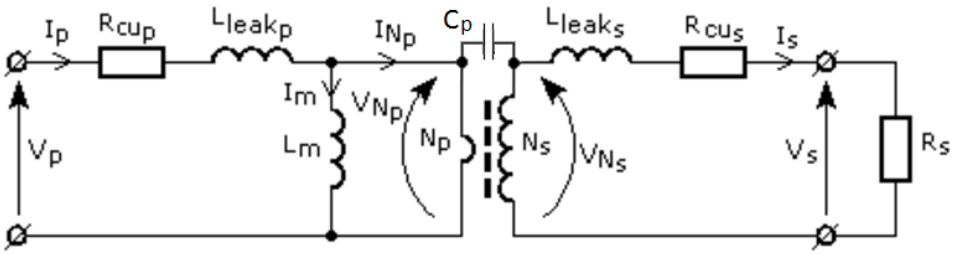

Figure 14: Circuit equivalent of a current transformer.

The equivalent circuit of a CT is very similar to that of a voltage transformer. In fig 14, it is visible that leakage and magnetizing inductance is represented as inductors in series and in parallel with the ideal transformer. The leakage inductance represents energy stored in non-magnetic regions between windings, this is due to the fact that there is some imperfect flux coupling in the physical geometry. [21]

Between the windings, the inter-winding capacitance is represented with C_p. Ohmic losses are represented as resistors in series with the remaining circuit. Considering the number of turns in a CT and the dimension of the iron core, the electrical length and ohmic losses will be significant [19]. In practice, there also exists a turn-to-turn capacitance that will bypass the transformer core at very high frequencies, but this capacitance is on the order of femtofarads and will not effect the frequency response within the bandwidth that is of interest in this study and is therefore neglected. [App B.1]

3.2.2 Frequency Response & Wave Propagation

A transformer acts as a band-pass filter in terms of it's frequency response. A transformer will not allow DC to pass through from primary to secondary, and will attenuate high frequency components. At some high frequency, C_p will resonate and couple the primary and secondary windings.

Since the CT:s are connected in series in AFL-systems, the frequency response through the CT primary is of interest. A transformer mirrors the load on the secondary onto the primary side. Therefore, at power frequency the transformer impedance seen from the primary should be the light fixture load. Additional attenuation will occur at higher frequencies where transformer operation is not optimized. [21]

Considering that the EFLA CT:s have sizable cores and approximately 100 turns per winding, the electrical length of the CT:s is not neglectable, especially when there can be upwards of 100 CT:s on one series circuit. The propagation parameters of the transformers is also different from that of the coaxial transmission line. Since a transformer is a complex network of distributed inductances and parasitic capacitances, the theoretical propagation velocity is unknown. (Section 7.2).

3.2.3 CT Saturation

An equivalent circuit model assumes a constant core permeability and that the following relationship is linear

$$B_c = \mu_c H_c \tag{20}$$

In practice, a transformer core can be magnetically saturated. When saturation occurs, the permeability of the core is reduced to that of air. This happens when the imposed magnetic field H can not increase the magnetization of the core. Therefore, the increase in internal flux density stagnates, and B flattens out. [14]:

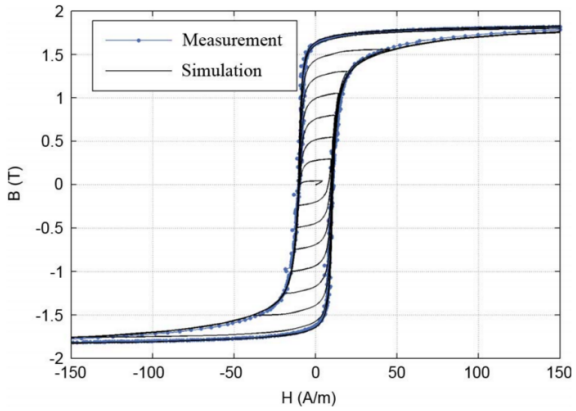

Figure 15: Major & minor hysteresis loop for a standard CT. ©[2011] IEEE [22]

An inductor or transformer has a maximum volt-second rating which describes the saturation limit. [27]

$$\frac{V_{peak}}{N} < B_{sat}\omega A_{core} \tag{21}$$

3.3 Electrical Faults

In an AFL-system fault event, there are 3 consecutive states of operation.

1. Pre-Fault Steady State
2. Fault Transient State
3. Post-Fault Steady State

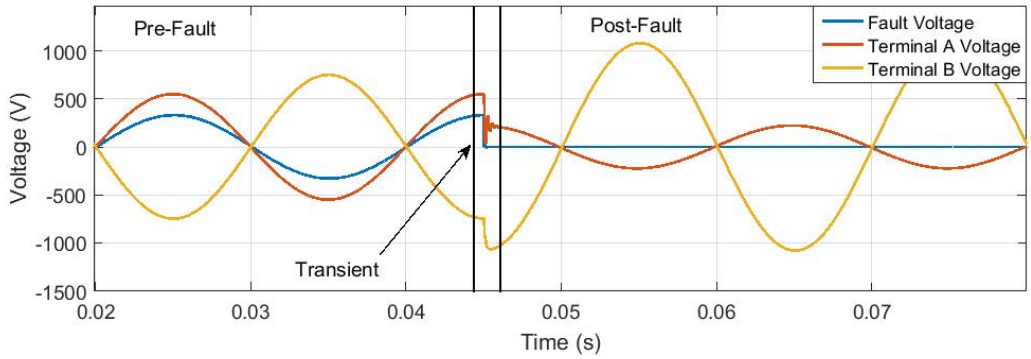

Figure 16: Illustration of fault states of a bolted ground fault, with a current source.

Before a fault, the system is in normal steady state operation. When a fault occurs and the system enter the transient fault state, a voltage impulse is generated at the fault location and steady state is disturbed, the energy stored in the distributed L and C parameters of the transmission line starts to oscillate. Eventually, the oscillations die out and we obtain the post fault steady state, where the system has adjusted to the parameters of the new faulted circuit.

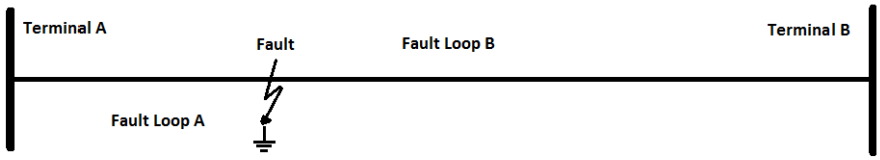

Figure 17: Schematic of post fault state.

The post fault steady state parameters will be decided by the location of the fault. When a fault occurs, two fault loops will be obtained. One loop from terminal A to fault, and another from terminal B to fault. As can be seen in fig 16, $V_a << V_b$. Which means that the fault is significantly closer to terminal A than to terminal B.

A fault in an electrical transmission system can have a number of different causes, these can be completely external or depend on the electrical operation. Electrical faults can be described as a spark gap in parallel with a nonlinear resistance appearing in a cable segment. The fault resistance is nonlinear, and can be voltage dependent. But, for fault location techniques a basic linear fault model will suffice. [24] The fault can either be categorized as a series fault where the core conductor is subjected to a unwanted discontinuity, or a ground fault (shunt fault) where core conductor and the concentric shield establishes a low resistance path. In practice, an electrical fault can also be a combination of a shunt and series event. [23]

Generally for overhead lines, faults can disappear by themselves since the arc can self-extinguish, this is usually not the case for underground cables. When the insulation suffers a breakdown, a low resistance path is formed between conductor core and sheath (conductive shield). This produces a ground fault, which can either stay as a ground fault or develop into a series fault. A series fault is developed if the cable is completely burned apart. In order for a ground fault to be established in an underground system, insulation has to break down, either due to mechanical or electrical disturbances.

Insulation can suffer breakdowns for a number of reasons. When insulation is subjected to electrical stress, voids and impurities in the insulation material can give rise to a phenomenon known as electrical treeing which can start to propagate in the insulation until it causes a fault. If moisture or water is present, another phenomenon known as water treeing can start to degrade insulation quality, even under low electrical stress. Mechanical intrusion can also cause a fault, this can be due to improper handling of the cable during construction of the AFL-system or even due to rodents eating through the cable.

Given that the cable is energized at fault inception, a fault event will generate fault waves that will travel from the fault location towards the terminals of the transmission system. The fault wave is generated due to the instantaneous change of voltage and current at the moment of fault. [25]

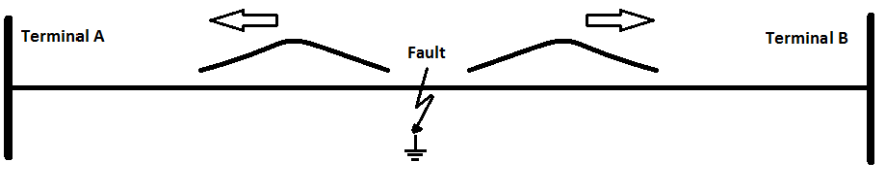

Figure 18: Illustration of fault waves.

3.3.1 Ground Faults

When insulation has degraded to the point of breakdown, there are 3 possible fault scenarios. Either a short circuit develops, this can be due to mechanical damage that has forced conductor and sheath into contact, or a carbon-metal bridge has formed between the two layers providing a fault resistance $< 5\Omega$ due to burnt cable insulation. The insulation can also evaporate and provide a gaseous low resistance path between conductor and sheath. A fault with resistance $< 5\Omega$ is referred to as a bolted fault. [23] In the case of an AFL-system where the source is a CCR, the source will eventually adjust to the post fault steady state and produce a 6.6A output current.

Critical ground faults which affect flight operations at airports are very unusual, these occur a few times a year. A fault of this magnitude would be in the same order as bolted faults. The majority of ground faults are rather small, usually in the order of a few $100k\Omega$. Smaller faults do not affect daily operations, but can potentially develop into a critical fault and therefore affect flight operations in the future. [1]

3.3.2 Series Faults

A series fault in a coaxial cable will occur when the core conductor is severed. In order for this to happen in a coaxial cable, a ground fault must first occur where core and sheath is in contact first. The transformation time from ground to series fault, can vary significantly. Causes for series faults can be mechanical damage where the sheath and/or conductor has been severed, electrical causes include ground faults which have been allowed to blow apart the entire coaxial cable. [23]

[1] Source: Interview with Richard Thulin at Arlanda airport.

In splices and connectors, a series fault can occur without first undergoing a ground fault event. Water intrusion and faulty splice connections can cause the connector surfaces to oxidize. Aluminum and copper are two conductors whose oxidized surface has a higher resistance than the base metal. Therefore in faulty splices where the quality of the oxidization-inhibitors has been compromised, contact-resistance can be significantly higher. [28]

In an AFL-system, a series fault is considered more dangerous than a ground fault. During a ground fault, voltage will be adjusted down in order for the CCR to output 6.6A. But, when a series fault occurs, the CCR will have to increase voltage in order to maintain rated current output. This will produce dangerous excess voltage on the series circuit.

3.3.3 Intermittent Faults

An intermittent electrical fault is a fault which is not permanent, but which occurs periodically or seemingly sporadic. This can be due to partial insulation breakdown at peak voltages, or splice glitching. A partially faulty splice could suffer from glitching due to water or moist intrusion or due to mechanical fatigue. The electrical manifestation of a intermittent fault can vary significantly depending on the type. If a splice is mechanically fatigued, the fault will not show unless it is mechanically stressed. In an AFL-system for instance, this is possible if an aircraft is taking of or landing and thus producing substantial vibration in the area surrounding the runway.

3.3.4 Fault Inception Angle

The fault inception angle is the angle at which a fault occurs ($0 < \varphi_{fault} < 2\pi$), and is of high importance when analyzing and discussing the potential of different fault location techniques. In OHL-systems a fault is entirely independent of the fault inception angle, since faults are caused by exterior events such as lightning strikes or falling trees. In underground transmission lines, internal cable faults are caused by electrical stress, meaning that a coaxial cable fault is statistically more likely to occur close to peak voltages. According to Flytkjaer Jensen and data from Energinet.dk, all faults caused by internal cable failure occurs with a maximum deviation of 25° from peak voltage. [25] Although, since AFL-systems are not completely buried, rather inserted into cable ducts between manholes, the system is still vulnerable to external causes of failure. For instance, rodents and water or moisture intrusion. The size of the fault waves generated by the fault, is entirely dependent of the fault inception angle. If a fault occurs when the momentary voltage at the fault location is 0V, no fault waves will be generated.

4 Method

The scale of a master thesis requires a planned methodology to accomplish the specifications of the project. The chosen methodology for this master thesis is "Product Design and Development", fifth edition by Karl T. Ulrich and Steven D. Eppinger [26] who are well known authors of many product development books and papers. The methodology consists of identifying customer needs, in this case it is the personnel on the airports, then concept generation takes place, followed up with concept evaluation and concept selection which in this case results in a scoring matrix which can be seen later in chapter 8.5.

A number of IEEE reports has been studied and the basis of this master thesis will be formed from reports about fault location on power cables and grids, since fault location on AFL systems with impedances along the transmission line is a newly pioneered area. The research also included a visit to Arlanda Airport, where maintenance staff was interviewed, and TDR was tested on a few cable systems.

4.1 Project Plan

The project plan has been divided in five different phases. The project started with a literature study, where the problems and all possible methods were identified. This phase was followed up with an evaluation of the identified methods. Some testing and documenting was done in parallel with the evaluation but extra time was also planned for this. Writing report, preparing presentation and come up with ideas how the methods can be integrated in the already existing system was the final matter of the project. A Gantt schematic of the project plan is shown below.

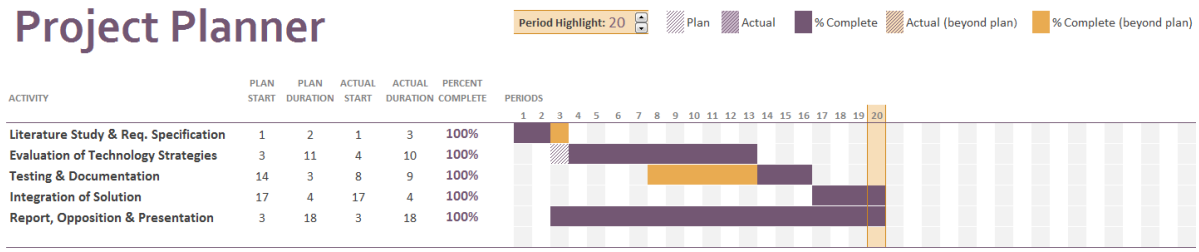

Figure 19: Initial Gantt schematic of the project plan

4.2 Tools

During the project different computer tools for simulation and calculations were used. To estimate attenuation in transmission lines and transformer frequency response LTSpice [42] was used. LTSpice was also used when simulating faults on the series circuit. For post processing, the data obtained from LTSpice simulations was imported into Matlab where all the calculation were made.

4.3 Specification & Evaluation

The fault location and SoH technologies were evaluated using a concept generation methodology by Karl T. Ulrich and Steven D. Eppinger. Utilizing a concept scoring matrix, all of the possible technologies can be compared in relation to a number of selection criterias that has been deemed important for an AFL-application. These criterias were obtained in a literature study and in several interviews and discussions at Safegate. The criterias cover technical aspects of the application, as well as operational and economic criterias.

4.4 Method Validation

The basic models of the system is built up with segments of transmission lines and transformers in a certain order of choice. The simulation depend on how the parameters of these different elements are decided. Measurements of a XLPE-cable has been made by ADB-Safegate in their lab and the parameters for the transmission line in the simulations are verified with these measurements. Some data regarding current transformers have also been made. However, frequency response has not been measurable with existing equipment in the lab, although attempts have been made with amplifiers and a regular signal generator. A model for the transformers has been established in LTspice, but the frequency response has therefore not been validated with real measurements. Although, the obtained results are within the limit of expected values.

Since it is problematic to actually test and introduce electrical faults on real AFL-systems, simulation tools is of importance in this study. Testing was performed on components and systems where testing equipment was available. For the traveling wave method and impedance based methods a real electrical fault was not tested for safety reasons. A commercial TDR on the other hand has been lent from an external company to evaluate the TDR method. The state of health methods require external more advanced equipment that could analyze the treeing and other impurities in the cables, but these were not tested either due to the limited time and available equipment.

5 Fault Location Strategies

Fault location systems have been in use in standard electrical transmission systems for decades. FL-systems play an important role in regard to power continuity, reliability and power quality. Since an electrical fault in general cause mechanical damage, fast fault localization enables efficient equipment repairs and sometimes even makes it possible to utilize pre-emptive maintenance. The importance and interest of FL-systems have recently grown due to technical and economic advances in low-cost DAQ and computation systems. [24]

In the present day, there are a multitude of different fault location technologies in use, all of which are developed for the standard commercial grid. These technologies can be categorized into offline and online methods. Online methods consists of two types of methods, impedance-based and traveling wave based methods. An online method works autonomously to approximate a fault using DAQ-systems and signal processing. The signal processing involved, can be more or less advanced. With the recent rise of artificial neural networks (ANN) and fuzzy logic, fault location has been identified as a possible application. Offline methods include time domain reflectometry (TDR), high voltage pulse surging and visual inspection. These methods are considered to be very accurate, but extremely time consuming and requires extensive personnel training. [25]

The relative error obtained from a fault location method can be written as follows:

$$error(\%) = \frac{d - d_{exact}}{l} * 100\% \tag{22}$$

where, d is the fault location obtained from the FL-algorithm, d_{exact} represents the actual fault location and l is the total electrical length of the transmission line.

The general roots of fault location errors which applies for all fault location methods are incorrect fault classification and insufficient or inaccurate data assumptions. Usually, the total transmission line length is only known with some error, or transmission line parameters are effected by outer factors such as weather and soil resistivity. [23]

The fault location method can not affect or disturb ongoing operation on the series circuit. In order for it to be backward compatible with previous Safegate solutions it can not require ASP communication between fixtures since older series circuits does not provide this feature. Therefore the online methods have been limited to utilizing the terminals of the CCR.

5.1 Impedance Based Methods

In electrical grids today, there are one- and two-ended impedance methods in use today. One ended methods are used in situations when both terminals are not in the same geographical position, and communication is needed between the two to utilize two-ended methods.

Impedance based FL is structured so that one can sample voltage and current phasors at one or both terminals. The obtained data is then inserted into algorithms that produce an approximated fault location based on circuit equations. Since these algorithms utilize circuit parameters, a substantial amount of data has to be known about the transmission line including line parameters and distance approximations.

An impedance based fault locator requires a phasor measurement unit (PMU) in order for terminal currents and voltages to be measured at power frequency and calculates an estimated fault location.

The algorithms requires phase-to-ground voltages and phase currents at the terminals. [29]

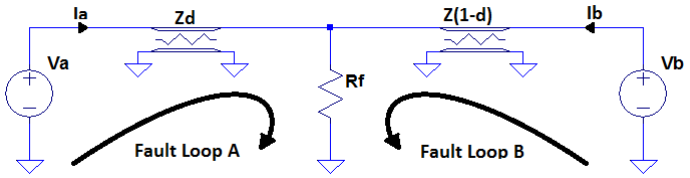

Figure 20: Fault loop schematic of a ground fault.

As mentioned in section 3.4, when a ground fault occurs in a transmission line, two fault loops are obtained, one from each terminal. The fault loop seen from terminal A can be described with the following KVL-equation:

$$0 = V_a - dZI_a - R_f I_f \tag{23}$$

Where Z is the distributed line impedance p.u, d is the distance p.u and I_f is the fault current. If one measures the impedance at terminal A in a fault event using current and voltage phasors, a value of the apparent impedance from source to fault is obtained.

$$Z_{fa} = \frac{V_a}{I_a} = Zd + R_f \frac{I_f}{I_a} \tag{24}$$

However, it is not obvious that the fault impedance will be entirely resistive, if $\frac{I_f}{I_a}$ in the equation above is a complex number, the fault impedance will include a capacitive or inductive component. This reactive component can induce errors into the fault location estimation, this phenomenon is called "the reactance effect". [29]

As can be seen in the equation above, the fault loop impedance is a definitive measure of the fault loop length. However, the fault impedance is unknown, so this can not come to any practical use unless the fault impedance is either very small or equal to zero. [24]

For the remainder of this section, two impedance based fault location algorithms will be presented:

- Reactance method (one ended)
- Synchronized & un-synchronized phasor method (two ended)
- Voltage magnitude profile for non-homogeneous systems (two-ended)

The reactance method measures the impedance from source to fault, utilizes the fact that the ratio of reactance to fault and the total reactance of the line is proportional to the distance to fault.

$$d = \frac{Im(V_a/I_a)}{Im(Z)} \tag{25}$$

By only utilizing the reactive component of impedance, the method is able to compensate for fault resistance. If $\frac{I_f}{I_a}$ is complex, a considerable reactance error will be introduced, since the reactance effect affects the apparent line reactance to fault.

The synchronized/un-synchronized phasor method is a two ended method, which exploits the fact that data can be used from both terminals of the transmission system. By utilizing KVL from terminals A

and B to fault, the following statement can be obtained.

$$\begin{cases} 0 = V_f + ZdI_a - V_a \\ 0 = V_f + Z(1-d)I_b - V_b \end{cases} \tag{26}$$

In the equation above, where all terms are phasors except the distance to fault d in p.u from terminal A, which is a scalar. By subtracting one equation with the other, the fault voltage can be eliminated. if we solve for d we will get:

$$d = \frac{V_a - V_b + ZI_b}{Z(I_a + I_b)} \tag{27}$$

According to IEEE, this FL algorithm provides a way to find the fault location by using post-fault phasor data. Although, if the measurements are unsynchronized, this requires the system to have reached steady state, i.e that the fault resistance is constant. If the fault impedance is time varying, this will lead to different magnitudes and phase angles at the terminals. Therefore, synchronized phasor measurements will provide all four phasors (voltage and current at both terminals) at a specific time stamp, which will correspond to one specific fault impedance. Otherwise, errors are introduced and accuracy is compromised. [29]

The methods described above are mainly applicable to homogeneous transmission line systems. The algorithms will have to be altered if they are to be used on an AFL-system.

In metropolitan areas, transmission lines are usually a combination of OHL- and underground-lines, a so called hybrid transmission line. In order to cope with non-homogeneous lines, Gong et al. developed a two ended impedance based FL methodology which utilizes current and voltage measurements at the terminals along with characteristics of the TL to establish a voltage profile from each terminal and thus find the fault location at the intersect of those two curves. [39]

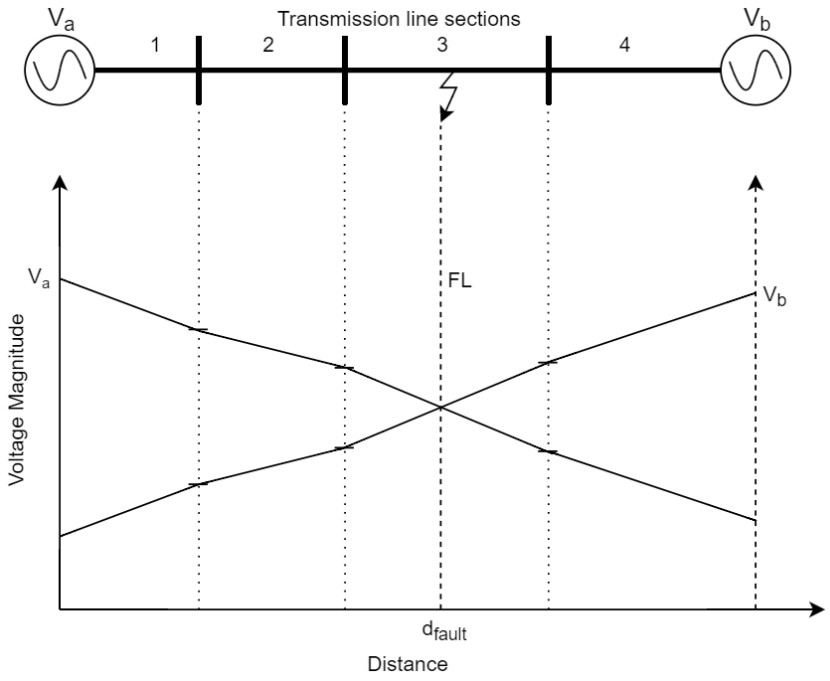

Figure 21: Voltage profile of a fault hybrid line.

5.2 Time Domain Reflectometry

Time domain reflectometry (TDR) is a fault location method, which transmits low-voltage pulses with short time duration into the cable and analyzes the reflections coming back to the reflectometer. It is essential that the cable is shielded, since the method requires a conductor and a sheath of equal electrical length. The pulse is often a short square wave with a low voltage of about 20V. As the pulse travels through the cable it will be reflected due to deviations from the characteristic impedance of the cable. Visible impedance discontinuities can consist of cable ends, splices, transformers and cable faults. An open end will only reflect the wave but a shorted end or ground fault will reflect and inverted pulse (figure 23).

When a pulse is transmitted into the cable the distance between cable opening and the discontinuity or irregularity can be determined from a reflection-time display. The display shows the transmitted and all the reflected pulses at the time when they arrive back to the TDR. An example can be seen in figure 22.

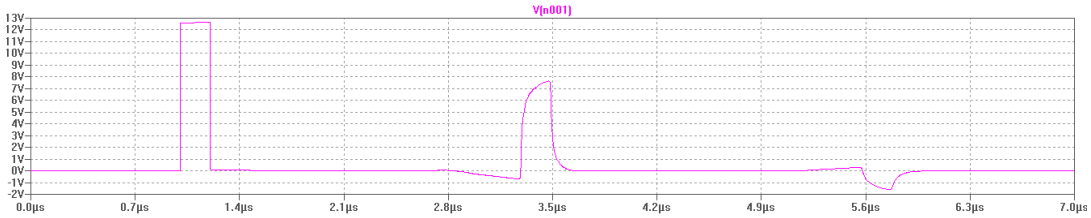

Figure 22: Simulation of how the pulse is transmitted into a cable with an open end. The pulse is transmitted at time 1µs and reflected from the open end at 3.2µs.

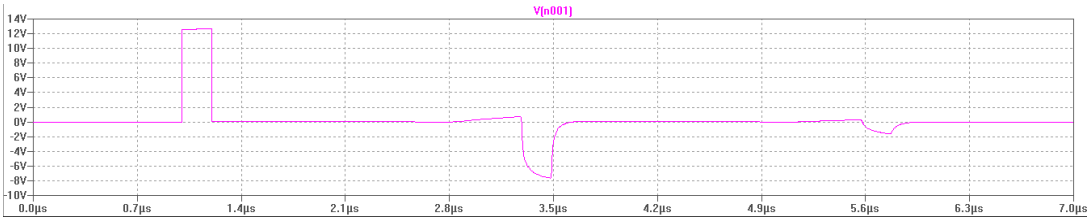

Figure 23: Simulation of how the pulse is transmitted into a cable with an shorted end. The pulse is transmitted at time 1µs and reflected and inverted from the shorted end at 3.2µs.

With only a TDR, it is not possible to locate ground faults with resistance values greater than ten times the characteristic impedance of the cable or intermittent cable faults [29]. Therefore, high resistance ground faults may become problematic to locate. Furthermore, due to high frequency attenuation, any reflections obtained from long distances will be severely attenuated.

Main factors influencing fault location accuracy are:

- The length of the cable
- Incorrect approximation of velocity factor
- Excessive reflections from unwanted impedance discontinuities

5.3 High Voltage Pulse Surging

High voltage pulse surge (HVPS), also called capacitive discharge or thumping, is a method as the name implies transmitting a high-voltage pulse into the system. The pulse itself will introduce a large potential over the fault on the cable in order to generate an arc in between the gap of the fault (either conductor-conductor or to conductor-earth). That arc will generate energy into its surroundings in form of sound waves and electro-magnetic waves that can be heard or detected by electronic sensors or even the human ear.

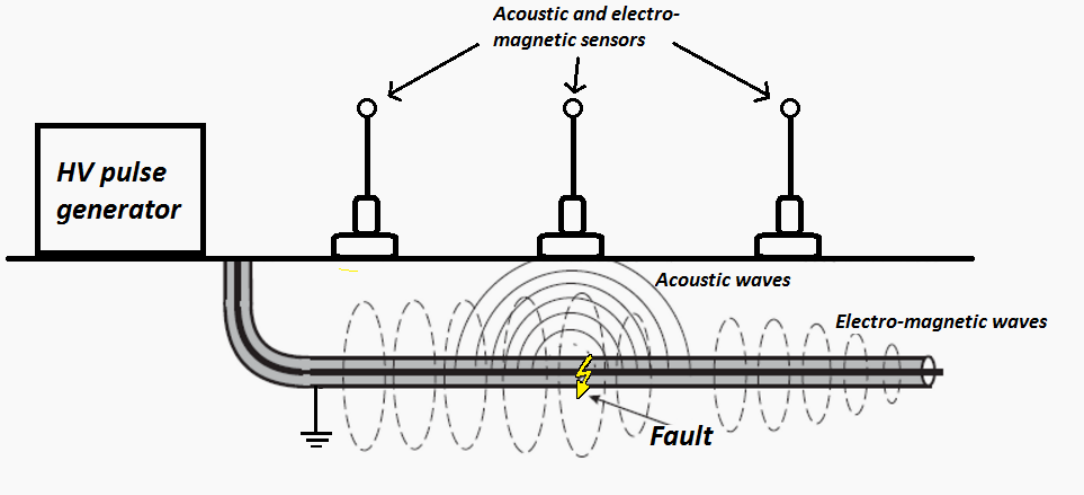

Figure 24: When sending in the HV pulse the fault will generate both electro-magnetic and acoustic waves that can be detected with sensors.

5.4 Traveling Wave Methods

In order to overcome the limitations of traditional fault location technologies, traveling wave based methods have been adopted for use in the electrical grid in recent years. The method exploits the correlation between backward- and forward-propagating waves in a medium. When a fault event occurs in a transmission line, if the inception angle is different from 0, a fault wave will be initiated in both directions of the transmission line. Ideally, this fault wave is a perfect square wave containing a multitude of frequency components. Due to the high propagation velocity and frequency content of the fault wave, high sampling frequency is of utmost importance. The recent improvements in DAQ and communication systems have allowed for extremely high sampling rates and processing of large amounts of data, which have made traveling wave methods more relevant in recent years. Traveling wave methods are considered to be more accurate and less dependent on system parameters than traditional FL-methods, but implementation is more costly.

In a homogeneous medium, the fault wave travels at some fraction of light speed, in a coaxial cable the propagation velocity is determined by the distributed line parameters (section 3.2.6). As the wave travels through the medium, it is subjected to attenuation and thus, the wave energy decreases. When the fault wave encounters an impedance discontinuity, it is reflected and refracted according to the reflection coefficient of the discontinuity. [24]

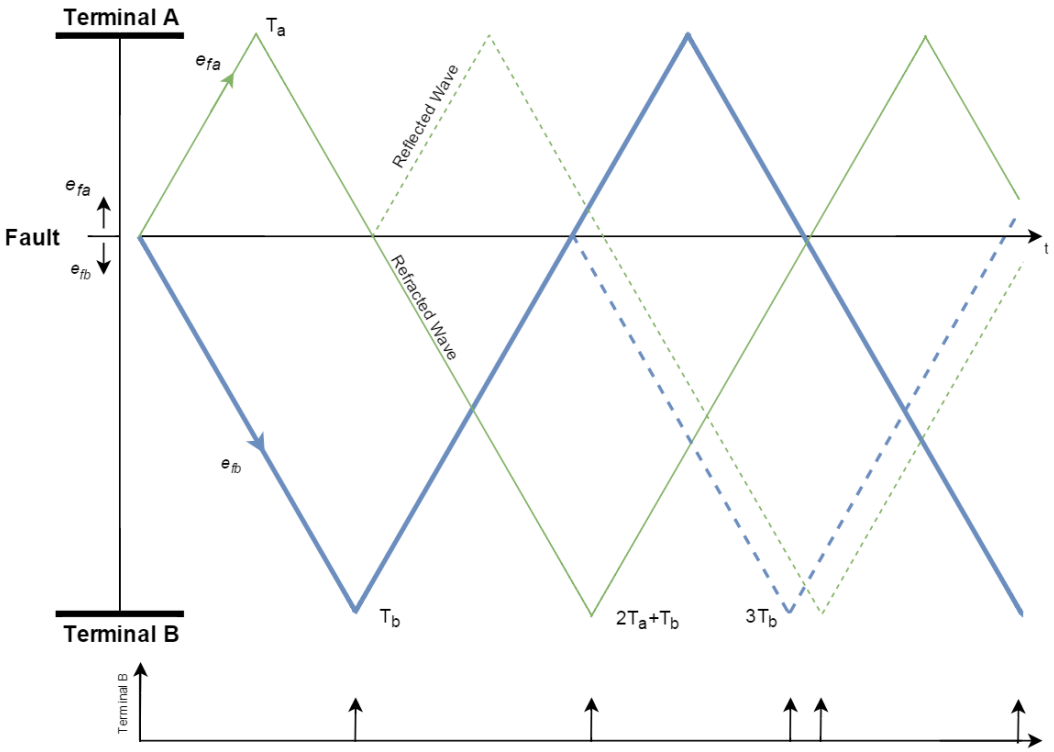

Figure 25: Lattice diagram of traveling wave in a homogeneous medium generated from a ground fault.

As can be seen in the lattice diagram in fig 25, the fault waves travel towards the terminals, reflects and refracts at the discontinuities. If the total line length (l) is known, the fault location d_{fault} can be calculated in [m] from terminal A for a one ended method.

$$d_{fault} = \frac{l}{2} + \frac{cV_f \Delta t_a}{2} \tag{28}$$

where c is the light speed in vacuum, V_f is the velocity factor of the medium. Δt_a is the time difference between the incidental wave at terminal A and the first reflection. For a two ended method:

$$d_{fault} = \frac{l}{2} - cV_f(t_b - t_a) \tag{29}$$

t_a and t_b are the respective arrival times of the traveling waves at terminal A and B.

Traveling wave-technologies are generally categorized according to their mode of operation or design: Types A, B, C, D and E. Type A, utilizes a one ended implementation where the incidental and fault wave is observed as well as the wave reflected from the opposite terminal. Although, type A can be problematic if there are multiple discontinuities on the line, since it can be difficult to distinguish the different wave fronts from each other. Type D on the other hand, utilizes a two ended implementation, where the incidental waves at both terminals are recorded. This eliminates the problem of distinguishing multiple reflections from each other since only the "first" transient is required to determine the fault location. In standard grid systems, the two ended method requires accurate time tagging at both terminals (done via GPS) and a communication system to bring the data to a centralized computing device. Type C is an active one ended method, which sends a pulse into the transmission line and records the reflection response of the system. This method is also known as TDR, which is treated as a separate

method in this study (section 3.5.2). Type E is a one ended method that records the transients produced when the transmission line is re-energized when the circuit breakers at the terminals are closed. Traveling wave equipment that is used today, runs simultaneously in type A and D. If two ended methods are used, it is only a matter of detecting the fault waves. For systems with a large amount of attenuation, the fault waves can be attenuated to the point where measurement equipment can not detect the waves. [29]

The accuracy of a traveling wave FL-method is influenced by a number of factors. Firstly, sampling rate. The sampling frequency of the measurement equipment is directly correlated to the error of the transient detection. If a device samples at 1 MHz, the maximum detection error for a 2 terminal TW FL will occur when the incidental wave at each terminal is detected exactly 1 sample apart. Therefore, if we assume that $V_f = 0.62$, the maximum error will be 86m [25, p.127]. Furthermore, propagation velocity for very high frequency signals are slightly frequency dependent. According to C.K Flytkjaer Jensen, a wave evaluated at $1MHz$, induces an error of 6m for a 25km cable and 12m for a 50km transmission line. Therefore, a constant propagation velocity can be assumed for the transmission lines in this study. [25, p.107]

GPS-based traveling wave FL systems suffer in accuracy due to the uncertainty of the GPS time tagging. Measurement transducers can also give errors if they are saturated or for any other reason fail to reproduce the transient waveforms. One problem that can result in incorrect fault alarms can be incorrect wave detection, this is due to the fact that there can be other sources of waves which the FL system can not distinguish from an actual fault. In order to counter this problem one can utilize advanced signal processing to learn the transient signature of that specific system. [29]

5.5 Wavelet Transform

The Wavelet transform (WLT), is a mathematical transform which allows for time-frequency analysis. The uncertainty principle states that a high time resolution will result in a low frequency resolution and vice versa. Unlike the Fourier transform where a window of constant size is used, the WLT utilizes a variable window sizes to overcome the uncertainty principle. [25, p.171] The WLT has recently gained attention in power engineering due to the possible uses within transient signal and analysis, voltage distortion analysis, power quality analysis and monitoring, and power system protection. Although, the WLT is applicable in any scenario where non-stationary signals and transients are of interest. [24, ch:4.5.2]

The wavelet transform on the signal $s(t)$ is defined as follows:

$$C(a,b) = \int_{-\infty}^{\infty} s(t) \frac{1}{\sqrt{a}} \psi^* \left(\frac{t-b}{a} \right) \mathrm{d}t. \tag{30}$$

Where a and b is the scale and time shifting factors. ψ^* is the time shifted and scaled mother wavelet $\psi(t)$. A discretization of the WLT can be described as:

$$C(a, iT_s) = T_s \frac{1}{\sqrt{|a|}} \sum_{n=0}^{N-1} \left[\psi^* \left(\frac{nT_s - iT_s}{a} \right) s(nT_s) \right] \tag{31}$$

Where N is the total number of samples, i is an integer describing the number samples the daughter wavelet ψ^* is shifted in time. T_s is the sampling time.

Whereas the Fourier transform breaks a signal up into sine waves at different frequencies, the WLT

divides the signal $s(t)$ into a multitude of shifted and scaled versions of the original wavelet (mother wavelet). [25, p.172]

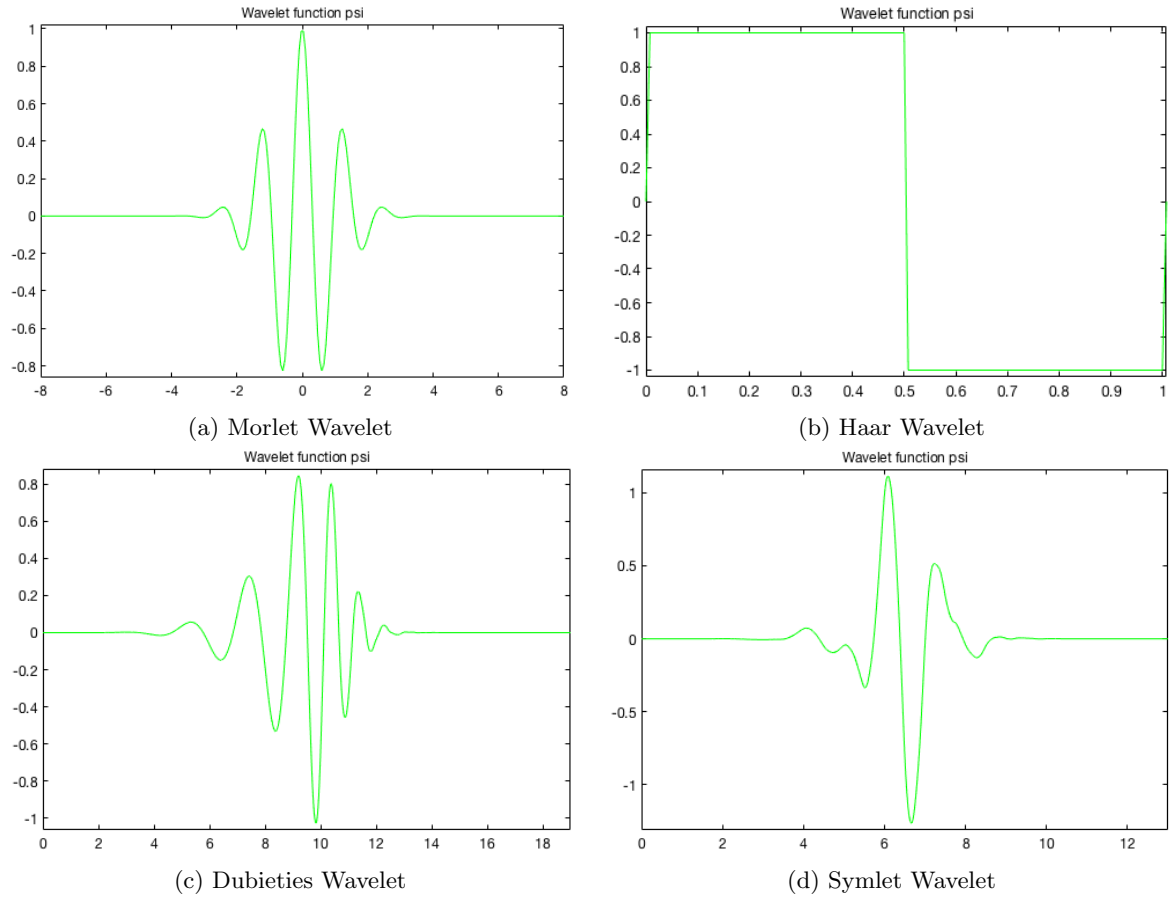

(a) Morlet Wavelet

(b) Haar Wavelet

(c) Dubieties Wavelet

(d) Symlet Wavelet

Figure 26: Four of the more popular wavelets used in transient analysis.

The center frequency of a wavelet, is stated as "the frequency at which the modulus of the Fourier components of the mother wavelet is maximized" [25, p.173]. This means that the center frequency captures the dominant oscillation for that specific wavelet. By adjusting the scale (time window) of the wavelet, different frequency bands can be captured. This allows one to decompose the original signal into several signal components at different frequency bands.

Generally speaking, low scales containing high frequencies are considered to be more accurate but can be affected by noise. This means that transients which do not originate from the fault can muddle the result. High scales containing low frequencies which is less accurate, can be sensitive to power frequency, therefore fault transient characteristics may be lost. Dispersion effects may also influence the arrival time of fault waves. [30]

Considering the discussion above, Zhang [30] recommends utilizing high scales to detect the fault and it's approximate location, then applying a low scale high frequency decomposition to extract fault information and more precise fault location data.

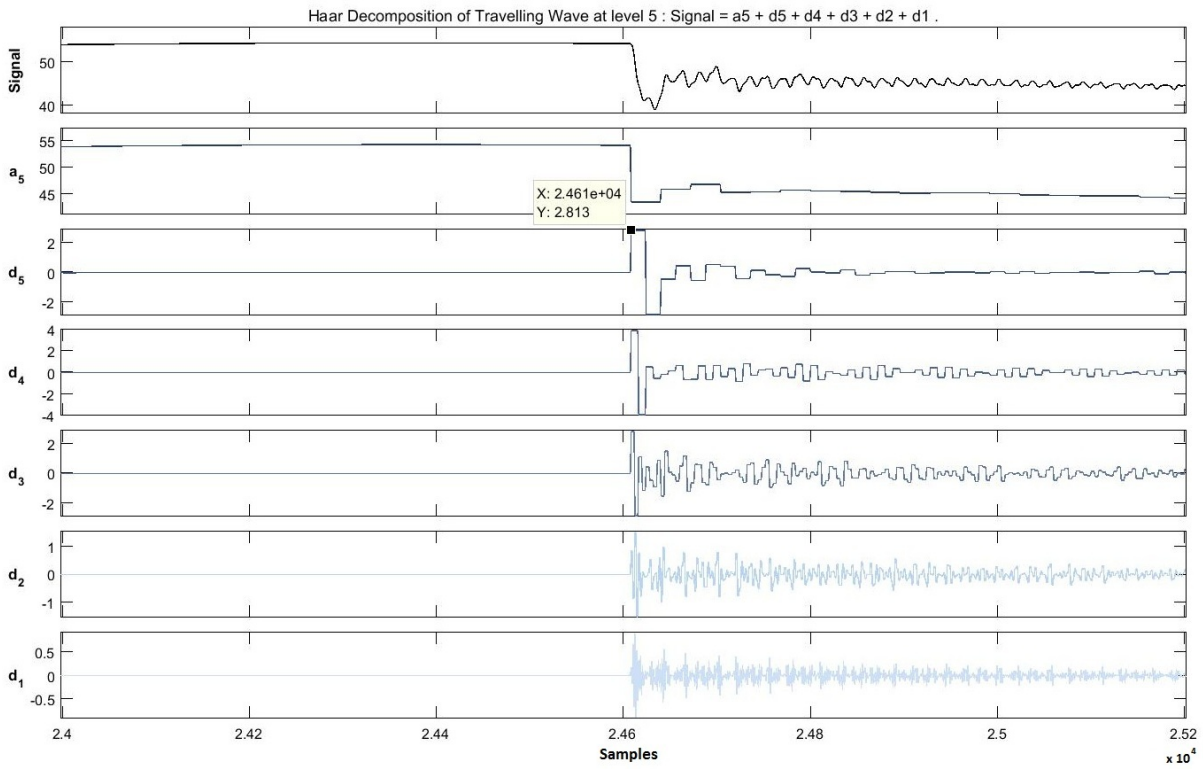

Figure 27: Voltage fault wave, haar Wavelet Decomposition at different scales. $F_s = 1MHz$

In fig 27, A voltage fault wave is displayed as "signal". The signal is then decomposed into coefficients of each scale. As can be seen, each decomposition coefficient captures a frequency band. Coefficient a_5 captures the overall trend while d_1 and d_2 encompass the very high frequency behavior. The Haar wavelet, whose psi function is a step function from 1 to -1 (fig 26b) can be seen in the figure above. This is especially visible in coefficient a_5 and d_5 where each progression in the coefficients is discrete.

The result in fig 27 shows that it is possible to obtain high time resolution of fault waves, given that the sampling frequency is sufficient. Although, in a noisy environment where several random transient occur, additional signal processing is required to distinguish between signals which do not originate from faults and thus isolate the fault waves. The "signature" of the system has to be learned.

5.6 Artificial Neural Networks & Fuzzy Logic

Artificial neural networks (ANN) and fuzzy logic (FLog) are examples of soft computing, where precision and certainty are not the goals. Research within soft computing is an effort to mimic intelligence and allow for decision making and pattern recognition which would not be possible using hard computing. The qualities that have been of interest regarding the mimicry of intelligence is mainly the ability to make rational decisions, adapting to missing data and accumulating experience over a longer horizon of time. Conventionally, one can use hysteresis and threshold values to monitor a process and make that it operates "within limits". In more complex systems and scenarios, fault indicators can become ambiguous and thus obstruct fault detection using conventional techniques. Fault location on power networks has been identified as a possible application of AI where accuracy and efficiency of FL processes can be significantly improved.

Unlike Boolean logic, fuzzy logic provides a framework for determining relations between events and objects based upon ambiguous, imprecise or noisy information. The main idea with FLog is that nothing is "false" or "true". No well defined boundaries exist for the application, and can therefore partly be false and true to some degree. It's application in FL algorithms is therefore of interest to the research community. In a fault event, there is an amount of information which can not be known in all scenarios, such as fault resistances and measurements can not always reproduce all possible characteristics of such an event. Furthermore, observation possibilities are limited due to the difference in geographical position and the number of observable parameters are restricted to terminal voltage and currents. [24, p.361-365]

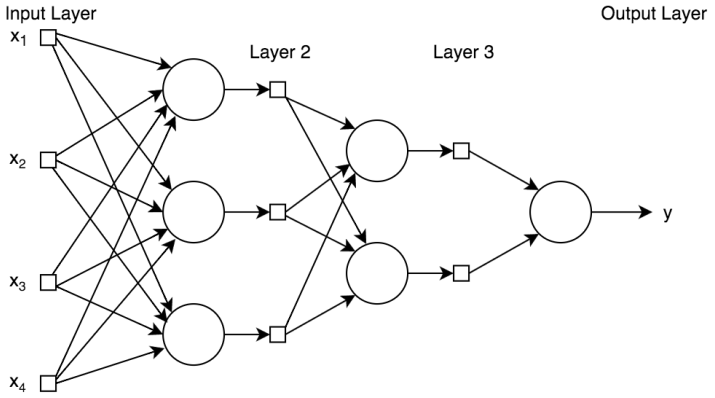

Figure 28: Multi-layer feed forward ANN architecture

ANNs are a structure of layers comprised of "neurons" which are interconnected. Each neuron performs an operation on the data it is fed from the input or previous neuron and then feeds it forward. ANNs mimic intelligence in the manner that it is trained by using previous scenarios to achieve a desired output, and therefore relies on previous experience.

Engadget reported in June of 2015 that AI researchers had used the video game Super Mario to train an ANN. In this case, the desired output was to maximize a "fitness level" that increased as the video game character progressed to the right, and the inputs were the pixels of the video game. As the "learning iterations" progressed, the AI found the right combinations of inputs to achieve the desired outcome, it was not aware of the video game in any way [31]. The same method of thinking can be applied to fault location algorithms. By designating a desired result, and showing an ANN data of fault events and allowing the ANN to accumulate experience from previous examples it is possible to utilize this method in real applications. [24, ch:9.2]

Although, training an ANN for use in FL algorithms requires large amounts of reliable data. This data is not always available, and if data from simulations is used, there is a possibility for insufficient model assumptions which will impact algorithm performance.

6 State of Health

Power cables suffer from degradation over time. Degradation is caused from so called "ageing mechanisms". These mechanisms can cause intrinsic or extrinsic ageing, intrinsic degradation is an irreversible in the material properties of the insulation and affects a large part of the material. Extrinsic degradation however, results in localized alterations in the insulation. This type of ageing can be defects or voids in the insulating material which originates from manufacturing, transport or installation.

Table 2: Ageing factors for cable insulation. [32, p.15]

Electrical	**Thermal**	**Mechanical**	**Environmental**
Voltage Level	Maximum Temp.	Bending	Gases
Frequency	High/Low Ambient Temp.	Vibration	Water/Humidity
Current	Temp. Gradient	Torsion	Corrosive Chemicals
	Temp. Cycling	Compression	Radiation
		Tension	Lubricants

Electrical factors can enable mechanisms such as treeing, dielectric losses and capacitance as well as overheating, this can lead to increased losses, thermal runaway and ageing. Thermal stress includes very high or low temperatures, as well as fast temperature changes. This can lead to thermal expansion & shrinkage, which in turn, can cause mechanical stress and ruptures. Loss of adhesion and internal material separation can cause effects such as partial discharge and accelerated propagation of electrical trees. Water and moisture intrusion as well as chemical contamination is also a source of electrical and thermal losses, and can lead to failure over time. The primary ageing factor for extruded cables such as XLPE coaxial power cables is electrical. [32]

Reliability concerns do not only regard cable insulation but also connectors and cable splices. Cable splices and connectors are especially sensitive to thermal fluctuations and extreme temperatures. In order to maintain a low ohmic contact resistance between conductors, there has to be proper mechanical contact. With large temperature swings and thermal cycling stress relaxation is affected, which in turn influences mechanical stability [36]. If a connector is fatigued or incorrectly sealed, water and moisture intrusion can become a major problem causing unwanted ground faults.

6.1 Electric Trees

Water trees are a structure of accumulated masses of precipitates of liquid water within the polymer insulation material. Water trees influence the local dielectric properties of the insulation, compromising the uniformity of the electric field distribution [33]. Water trees that grow from voids within the insulation material are called bow-tie trees, while water trees initiated at material interfaces is referred to as streamer trees. Water trees do not cause failure by themselves, but provide initiation sites for electrical trees due to electric field disturbances. [33]

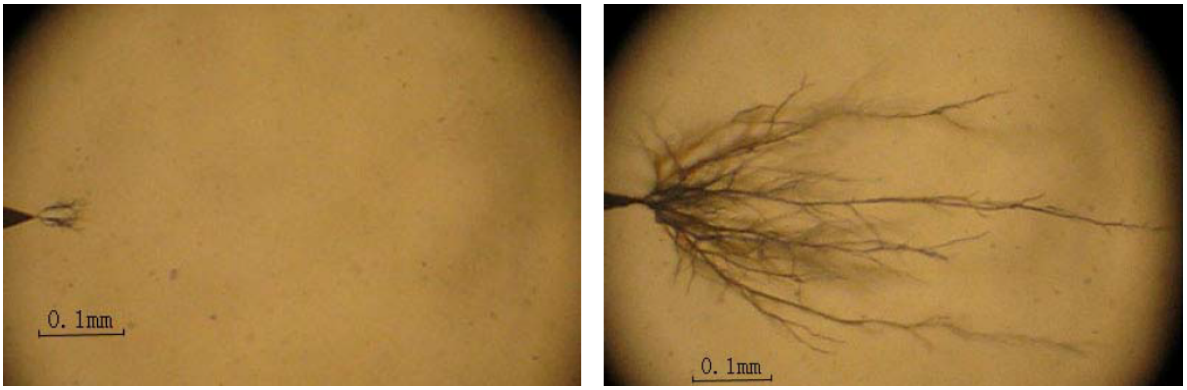

Figure 29: Propagation of electrical trees in XLPE insulation ©[2012] IEEE [34]

An electrical tree is a pattern of impurities in an electrical insulator which can cause cable failure. Unlike water trees, electrical trees can propagate relatively fast and will accelerate as it grows. Once it has initiated, the tree will propagate due to partial discharges inside the established impurities and channels. The main cause of treeing is electrical voltage stress and as they propagate, the electrical field is distorted causing further treeing. As the branches of the tree breaks the insulation it is carbonized, transforming it into a semiconductor channel. Finally, the tree branches will establish a carbon bridge between conductor and sheath, leading to cable failure. [35, p.3]

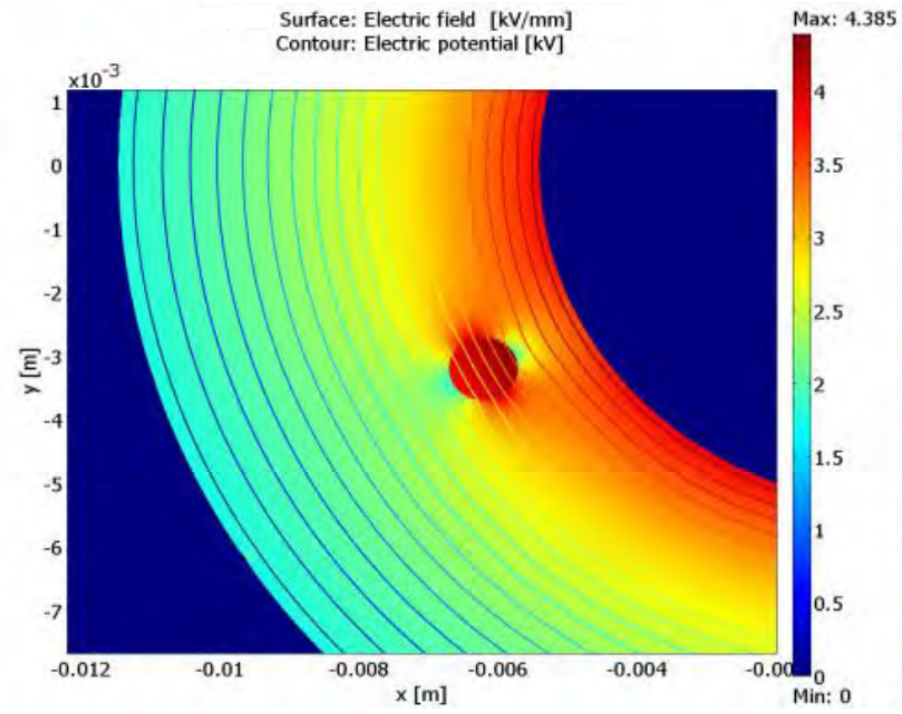

Figure 30: Effect on electrical field due to void-defect in an XLPE coaxial cable. ©[2012] IEEE [18]

In fig 30, a small void defect is presented. As was mentioned above, the void distorts the electrical field distribution causing local maximas and minimas. Local maximas and large fluctuations in the electrical field increases the likelihood of electrical trees developing.

6.2 Partial Discharge

Partial Discharge (PD) is a dielectric discharge in the solid electrical insulation of the transmission cable under high or medium voltage stress. It occurs statistically distributed in gas, liquid and solid medium, due to irregularities in the cable insulation as in fig 31. To mention a few these irregularities can be voids, material separation, fillers and electrical trees.[32, ch:6.1]. There are multiple sources of PD, a cable can be faulty from the production line, or it can develop voids and other defects during operation in normal or abnormal conditions.

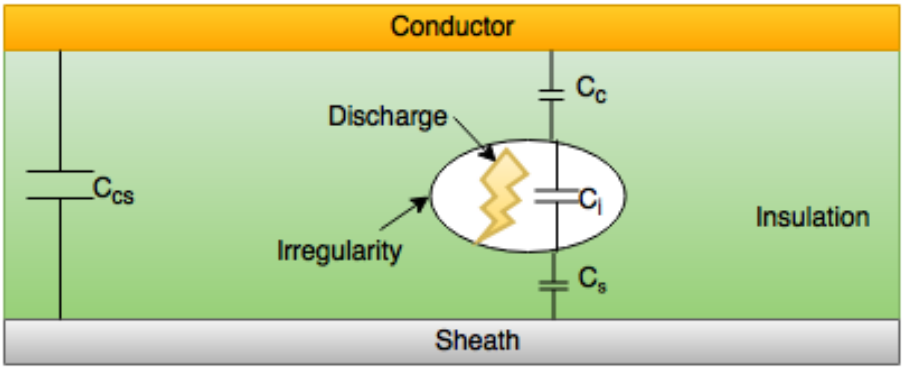

Figure 31: An example of an irregularity in the cable insulation which causes a partial discharge. Can be compared with figure 30.

The effects of PD within high voltage cables and equipment can be very serious, ultimately leading to complete failure. It is therefore of interest to locate and replace cables that are defect due to treeing etc. The PD initiation depends on several different factors, such as location, size, shape and medium of the irregularity.

Partial discharge can be compared with the Corona discharge phenomenon which emits a glowing light in the air around the sharp edges of an object with medium or high potential. Corona discharge will occur when the strength of the electric field around a conductor is high enough to form a conductive region, but not high enough to cause arcing or electrical breakdown to nearby objects. Partial discharge however is not visible within the solid insulation of the cable and is therefore not possible to detect visually.

Partial discharge gives rise to symmetric narrow pulses that can be measured in the conductor, these can be modeled as Gaussian. Pulse width is approximately in the range of tens of nanoseconds. PD pulses can be symmetric or asymmetric, in the latter case the pulse can be modeled as a sum of Gaussian pulses. In long distance power cables, a fitting bandwidth for PD detection is about 20 MHz. As insulation degradation proceeds, the number of occurrences per period increases. [37]

Since PD is a intermittently occurring phenomenon, it has to be treated as a statistical quantity. With every half period, there is a large variation in the number of and magnitudes of the discharges that occur as voltage is applied. Since PD is a measure of voltage stress, the number of occurrences increases with applied voltage magnitude. [32]

6.3 Tan δ

The dissipation factor *tan* δ is a measure of the insulation quality in a transmission line. In a perfect shielded transmission line the conductor will be separated from the sheath by the insulation and the insulation current should ideally lead with 90°. The insulation can however never be 100% pure and due to ageing of the insulation impurities like dirt and moisture enter into it. These impurities and irregularities provide conductive pathways for the current, and thus there will also be a real component of the insulation current. If the real current between conductor and sheath increases, on a segment of a transmission line, a loss factor *tan* δ will be introduced. By sending a low frequency wave into the cable and measure the phase shift from the current and voltage the quality of the cable can be analyzed. We can for simplicity assume that an ideal transmission line is approaching the properties of a perfect capacitor between conductor and sheath. Impurities will then change this equivalent circuit to a capacitance in parallel with a resistance.

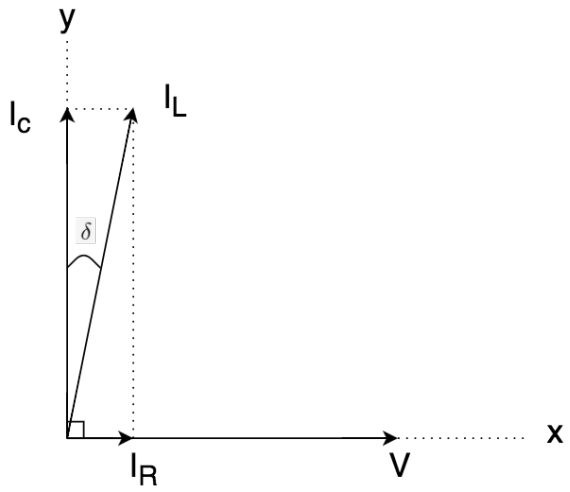

Figure 32: Vector Diagram of non-ideal capacitive insulation current.

6.4 SoH Diagnostics

Monitoring SoH of power systems in order to perform preemptive maintenance is of great interest to the power industry. There exists a multitude of available methods fit for this purpose. This section will discuss a few of the more popular ones regarding underground extruded cable systems. The only SoH online diagnostics tool found in the literature is online PD measurements. Pulses emitted from the PD location propagate along the transmission lines at some fraction of light speed. These pulses can be measured (voltage or current) using high frequency DAQ-systems. However, for long transmission lines attenuation become an issue due to the very high frequency content and low amplitude of PD pulses. Furthermore, electrical online PD measurements are extremely sensitive to exterior noise. [37]

Offline methods include dielectric spectroscopy, where the loss factor tan δ is analyzed over a certain frequency span. This allows for detection and characterization of insulation quality and possibly the presence of water trees. Although, if this is done on unshielded cables, there is a possibility of stray currents posing a problem. [38] Non electrical diagnostic methods can be performed using optical microscopy where individual trees are observed and analyzed. This allows for an in depth analysis into tree characteristics and contaminant level. Chemical analysis to analyze contaminants or simple visual inspection can also be performed. [32]

7 Simulations

Considering the scale and safety issues of introducing real faults on a series circuit in order to obtain data on various fault conditions, no extensive fault testing could be performed. Instead, simulations of larger circuits were performed in LTspice.

7.1 Transmission Line Model

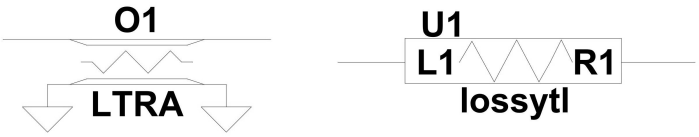

Figure 33: ltline(left) & telegrapher(right) transmission line models.

The TL parameters below were calculated according to the equations in section 4.1.2 using geometric and material data from the EUPEN cable shown in fig 7.

Table 3: Transmission line parameters, EUPEN Cable.

Resistance $[m\Omega/m]$	**Inductance** $[\mu H/m]$	**Capacitance** $[pF/m]$	**Conductance** $[nS/m]$
2	0.24	124	0.5

From the parameters in the table above, propagation factor and characteristic impedance can be obtained using the equations in sections 3.1.5 and 3.1.6. For high frequencies, we can assume that $R << j\omega L$ and $G << j\omega C$ [40]. This will provide us with:

$$V_f = 0.6116 \tag{32}$$

$$Z_0 = 43.95\Omega \tag{33}$$

In the LTspice library, there are two standard types of transmission line components (ltline). A lossy and a lossless transmission line. These two components are based on a signal-delay and lumped LC or RLGC circuit as was presented in section 3.1.2.

As discussed in section 3.1.4, the telegrapher´s equations offer a way to model the dynamics of transmission lines with differential equations. The circuit equivalent LTspice implementation can be found in fig 34. The component description of the telegrapher's based TL component can be found in appendix A.1. The lossytl-component also includes frequency dependent R, G and L due to the skin effect.

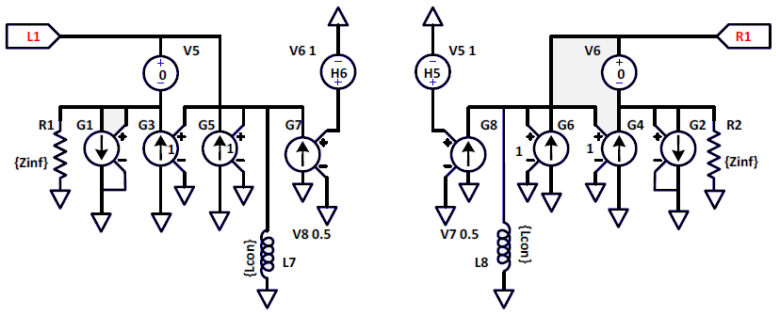

Figure 34: Equivalent circuit, lossy TL based on telegrapher´s equations

In order to compare the performance of the ltline and telegrapher TL models, a simple attenuation simulation was executed in LTspice. A transient analysis was also performed to compare signal propagation parameters of the two TL models.

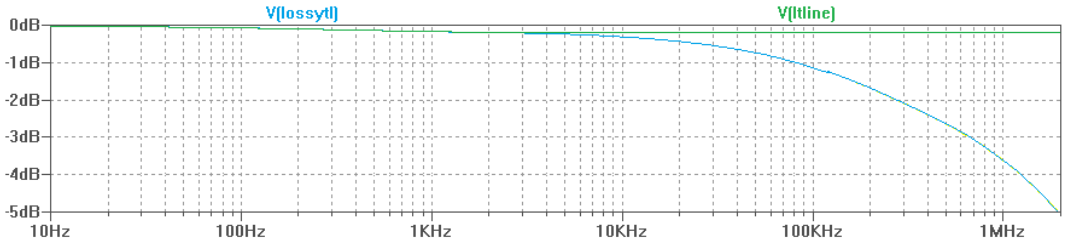

Figure 35: Transmission line attenuation, 1km.

It was found that the ltline component was only able to accurately model a coaxial cable below approximately $10kHz$. At higher frequencies, attenuation does not increase for the ltline TL, while the lossytl component behaves as expected for higher frequencies.

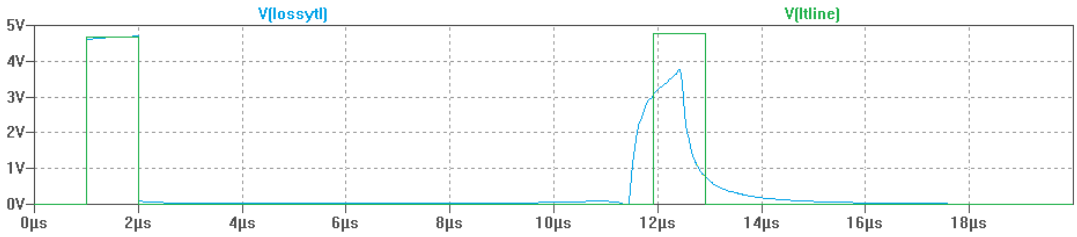

Figure 36: Transient analysis, on 1km TL with open end.

As can be seen in the figure above, the ltline model does not cause any noteworthy dispersion or attenuation. The reflected signal is almost identical to the emitted wave, ltline also has a constant $V_f = 61.22\%$. Lossytl on the other hand, subjects the emitted wave to both dispersion and severe attenuation. It is also visible that different frequency components of the emitted square wave have different propagation velocities, but on average lossytl has a $V_f = 62\%$. However, for the large scale transient simulations performed in this study, mainly ltline was used in order to reduce simulation execution times. The inaccuracy due to transmission line attenuation was deemed negligible in comparison to CT attenuation considering that the maximum series circuit length that was simulated was 2583m. For AC analysis and smaller transient analysis such as TDR simulations, lossytl was used in order to capture attenuation and dispersion phenomena more accurately.

7.2 Current Transformer Model

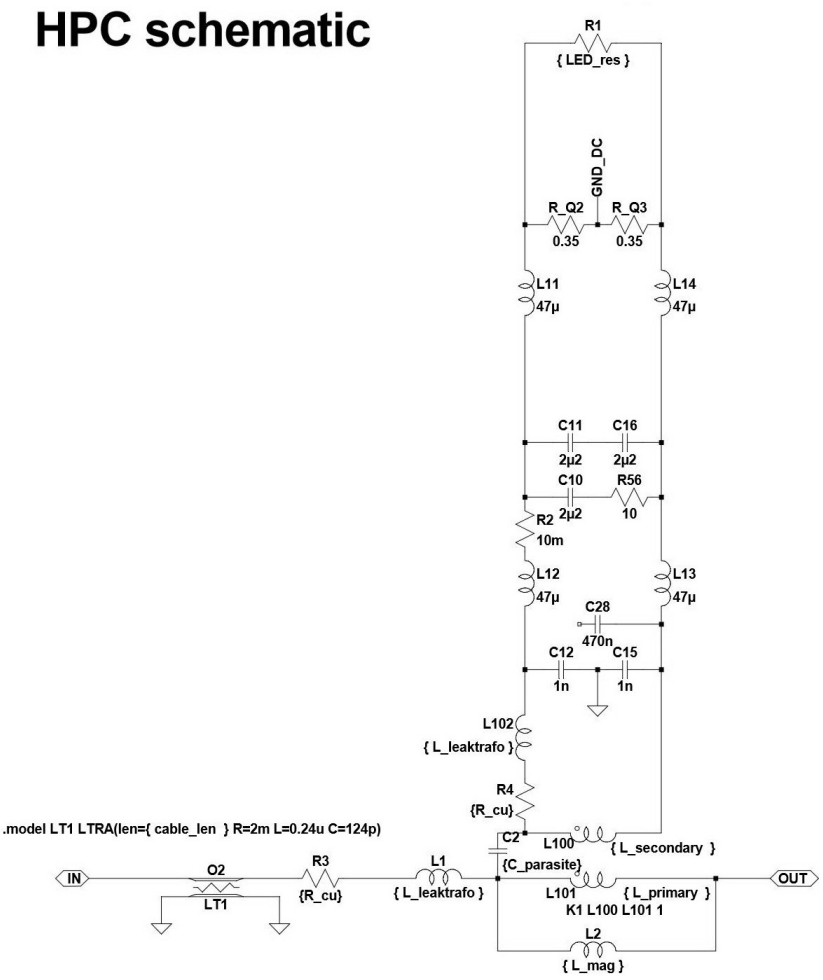

Figure 37: Current transformer and load model

The CT model is based on an equivalent circuit model, where the frequency response of the current transformer and load is represented. As is displayed in the figure above, each HPC component consists of a transmission line in series with a CT load, these HPC:s will then be placed out in series to form a series circuit.

The CT is modeled using resistances, leakage and magnetization inductors and a parasitic capacitance. The interturn capacitance was found to be in the order of femtofarads and was therefore neglected [App B.1]. Connected to the secondary of the CT is a simplified circuit of a $\approx 60W$ LED light fixture.

What is not captured in the model is the electrical length and propagation velocity of the CT. According to measurements done in the Safegate lab, the electrical length of the EFLA 641 is approximately 19.79m. If a traveling wave type FL algorithm is to be implemented in practice, this will have to be accounted for in order to avoid error introductions into the FL algorithm.

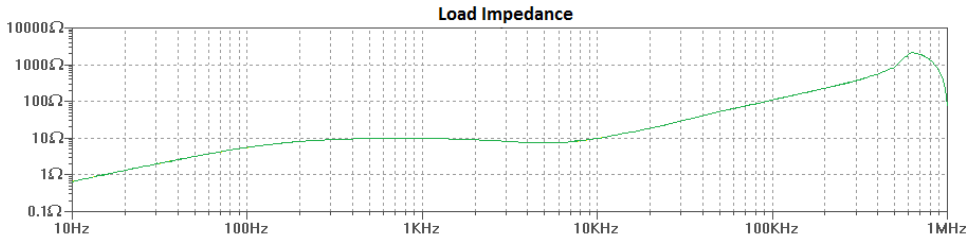

Figure 38: Load Impedance $|Z|$, AC analysis. Efla 651.

The perceived attenuation of a transformer is due to reflections, which occur due to the fact that the transformer poses as a impedance discontinuity on the series circuit, causes high frequency waves to reflect and effectively attenuate wave propagation on the series circuit. The amount of reflected energy is described by the reflection coefficient in section 3.1.6. Fig 38 displays the frequency dependent impedance of a HPC component which is simulated on the series circuit. It is obvious that very high frequency content will be severely attenuated due to CT reflections.

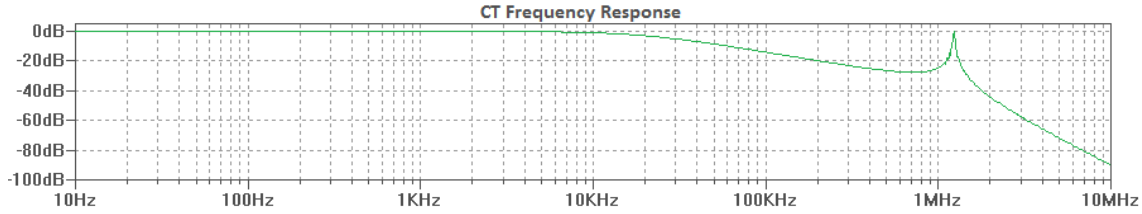

Figure 39: CT frequency response, primary-secondary winding. Efla 641.

The frequency response of the transformer (prim-sec), which is based on an equivalent circuit shows the transfer function for the Efla 641 CT. As one can see in the figure above, lower frequencies are not attenuated since no saturation effects are captured with the equivalent circuit model.

The data which the HPC component is based on was obtained from the EFLA website [20] and from measurements made by Peter Körner at Safegate [App B.2]. As can be seen in the table below, parameter values for all transformers is not available. Performing frequency response and impedance measurements for all the transformers of interest would have been ideal. But due to the fact that special equipment such as high power signal generators or signal generator amplifiers would have been needed for transformers of this size, it has not been possible to perform these tests within the timeframe of this study. Only the Efla 641 and 651 have been used in simulations.

Table 4: Transformer Data

Model	$C_{parasitic}$	L_{prim}	L_{sec}	L_{mag}	L_{leak}	R_{cu}
Efla 531 - 30/45W	$51pF$	$64.8mH$	$62.7mH$	-	-	-
Efla 541 - 100W	$85pF$	$30.8mH$	$30.3mH$	-	-	-
Efla 561 - 300W	$99pF$	$44.7mH$	$44.1mH$	-	-	-
Efla 641 - 100W	$209pF$	$14.9mH$	$14.7mH$	$14mH$	$40\mu H$	$1m\Omega$
Efla 651 - 200W	$233pF$	$14.7mH$	$14.5mH$	$25mH$	$60\mu H$	$1m\Omega$
Amerace - 30/45W	$49pF$	$11.3mH$	$10.8mH$	-	-	-
Amerace - 300W	$78pF$	$64.8mH$	$62.7mH$	-	-	-

7.3 Series Circuit Models

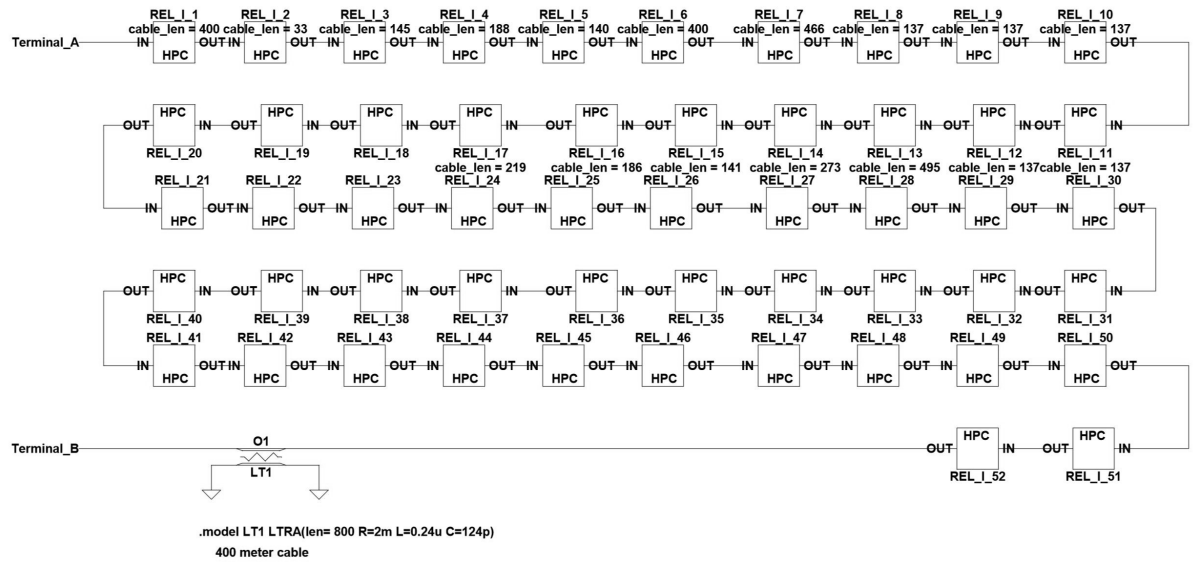

Figure 40: Series circuit of a European airport in LTspice.

The series circuit that was implemented in LTspice, is based on a blueprint from an existing circuit at a European airport, which will be referred to as "the airport" in the future. This circuit consists of 52 transformers and 11570m of coaxial cable. The data acquired from all simulations is sampled from the "terminal A"- and "terminal B"-nodes. The idea with large scale series circuit simulations is to subject the system to various fault conditions, acquire data from terminals A and B, and effectively perform impedance based and traveling wave FL in Matlab to evaluate the potential of these techniques.

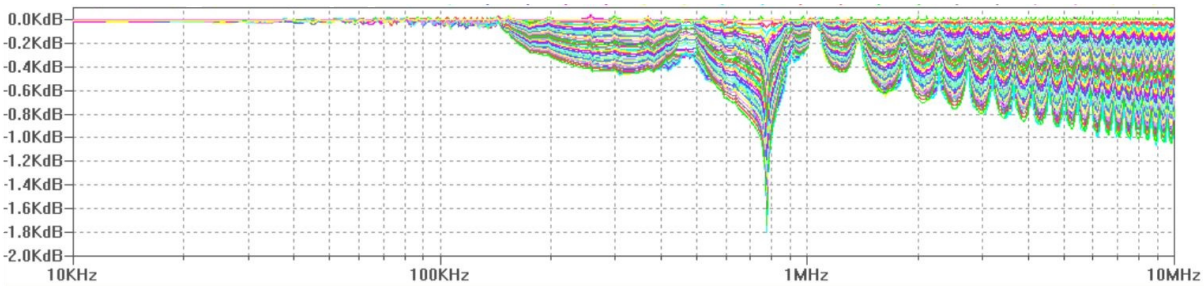

Figure 41: AC analysis, airport series circuit.

In fig 41, the frequency response at the input of all transformers on the airport circuit is displayed. One can see that above $\approx 110kHz$, attenuation increases significantly and becomes very location specific. The initial intention was to simulate the entire series circuit, but in order to reduce execution time of transient simulations, the size was reduced down to 1/5 of the original size. Simulating high frequency transients in transmission line systems is computationally demanding, and initially lead to extreme execution times. By reducing the size of the circuit, simulation duration was reduced from 18-20 hours to approximately 4-5 hours.

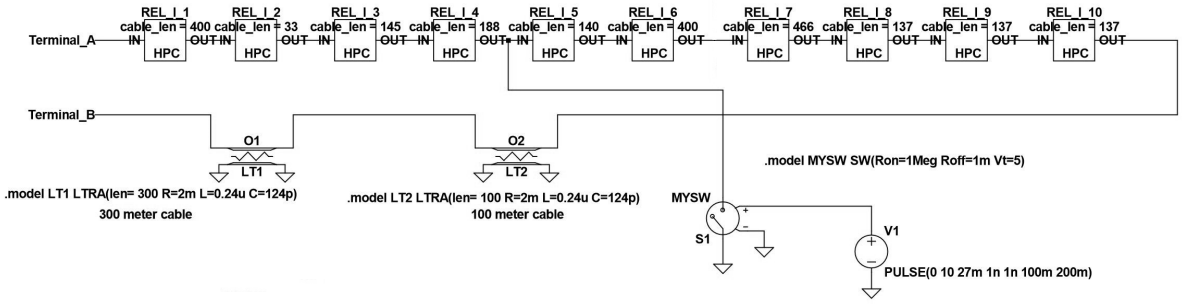

Figure 42: 1/5 of the airport series circuit, with fault switch in LTspice.

The reduced segment of the airport circuit, includes 10 transformers and 2583m of transmission line. In order to simulate a fault, a simple resistive switch(MYSW) to ground was implemented, MYSW is actuated by a square wave voltage source.

This fault configuration allows for quick and easy adjustment of fault conditions such as location, resistance and inception angle. The fault resistance in the performed simulations is modeled as a constant resistance.

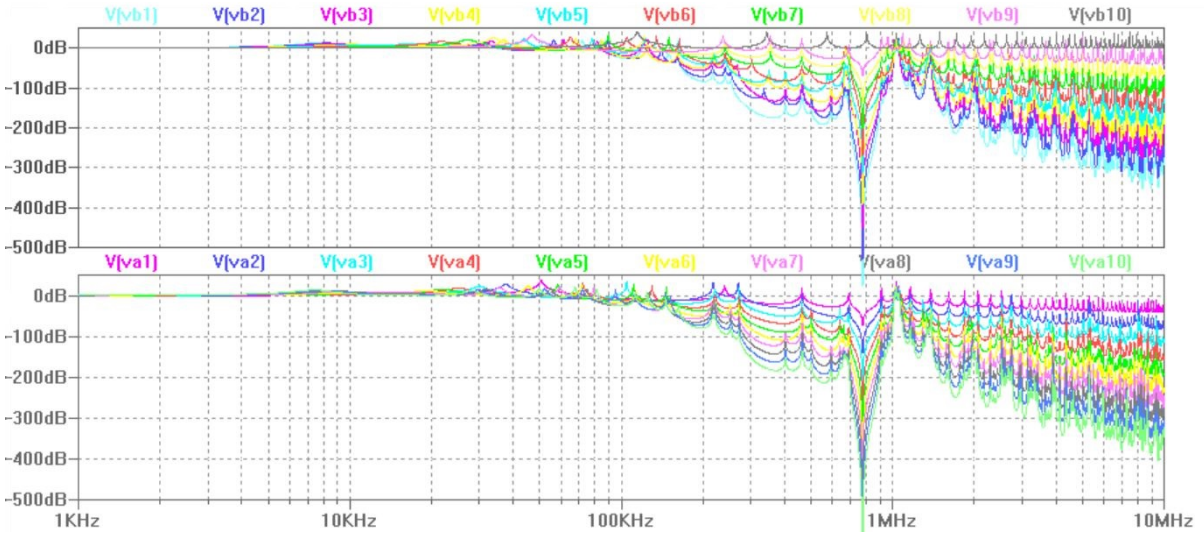

Figure 43: AC Analysis airport series circuit, Terminal A(bottom) and B(top).

In the figure above, the attenuation from each node of the small airport circuit to each terminal is displayed. One can see that node 1 (1 transformer from terminal A) is significantly attenuated at terminal B and very little at terminal A, and vice versa for node 10.

The LTspice simulations do not include any PLC or CCR thyristor firing delays, the effect of these elements are introduced in Matlab. The complete LTspice simulation schematic is available in app A.2.

8 Results & Discussion

In this chapter, the results of this study will be presented. Firstly, performance of traveling wave, TDR and impedance based methods on the series circuit will be examined. The main issues and strengths for these methods will also be discussed. The results of the concept evaluation and scoring will be presented in the last part of the chapter. Methods such as HV pulse surging, visual inspection, Tan δ and partial discharge have not yielded any simulated or tested results and will only be mentioned in the concept evaluation and scoring section of this chapter.

8.1 Traveling Wave

As mentioned in previous chapters, traveling wave FL utilizes the wave emitted from a fault when the voltage instantaneously drops at the moment of fault. This wave is recorded at the terminals of the circuit, and can be used to perform online fault location.

The traveling wave equipment would be connected to the "terminals" of the substation, after filtering components such as the SCI, SCF and also after the SCM. This has to be done in order to not unintentionally affect the high frequency content of the waves generated at the fault.

While traveling wave is promising due to the fact that it requires less system specific data and is highly accurate in standard grid systems, there are a number of dependencies and potential problems will be addressed in this section. Traveling wave is capable of detecting intermittent faults and series faults, but the results in this section mainly concerns various ground faults.

8.1.1 1 & 2 Terminal Measurements

As illustrated by the lattice diagram in fig 25, an instantaneous fault will produce two fault waves traveling in opposite directions. By measuring the time between the incidental wave from the fault and the reflected wave from the opposite terminal, the fault location can be obtained. However, this is only to any practical use where the line is homogeneous and the two terminals A and B are in separate geographical locations. In the AFL case, both terminals are in the same location, making 2 terminal setups more attainable since no time-syncing equipment is required and there are several impedance discontinuities on the circuit.

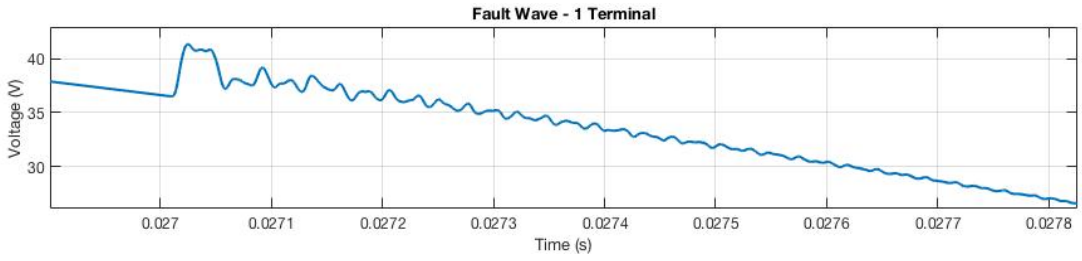

Figure 44: Simulated fault wave recorded at terminal A of the airport circuit.

In the figure above, the incidental wave is clearly visible shortly after the $27ms$ time stamp. Following the incidental wave, there are a number of reflections originating from transformer, fault and terminal reflections. Distinguishing between different types of reflections is significantly problematic.

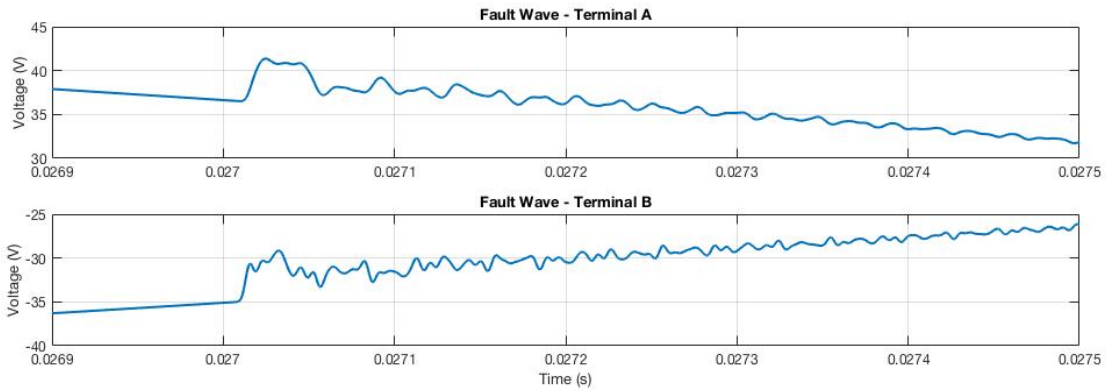

Figure 45: Simulated fault wave recorded at terminal A & B of the airport circuit. ($f_s = 1MHz$)

In fig 45, we can observe the voltage waves generated by a bolted ground fault. A fault of this nature generates a square wave at the fault location, the figure above shows that the fault wave is subjected to dispersion, reflections and refractions. But, since only the incidental wave has to be time stamped, multiple terminal measurements radically simplify the procedure. The only issue then, is the matter of detecting and accurately time stamping the transient. Therefore, 2 terminal TW is strongly recommended.

8.1.2 Sampling Frequency

The accuracy of the traveling wave technology is strictly dependent of sampling frequency. A 2 terminal transient detection system will have a theoretical sampling error described by the following equation:

$$e_s = \frac{V_f c(\Delta t_a - \Delta t_b)}{2} \tag{34}$$

where Δt_a and Δt_b represent the delays between the exact arrival of the wave and the instance of sampling. This means that the worst case scenario occurs when one terminal correctly samples the incidental wave $\Delta t = 0$ and the other terminal delays the wave exactly 1 sample $\Delta t = \frac{1}{f_s}$. [25, p.127] In order to be of any practical use, sampling frequency must exceed $f_s = 1MHz$. At $1MHz$, the worst case sampling error is $86m$, while a $10MHz$ sampling frequency provides $9.2m$.

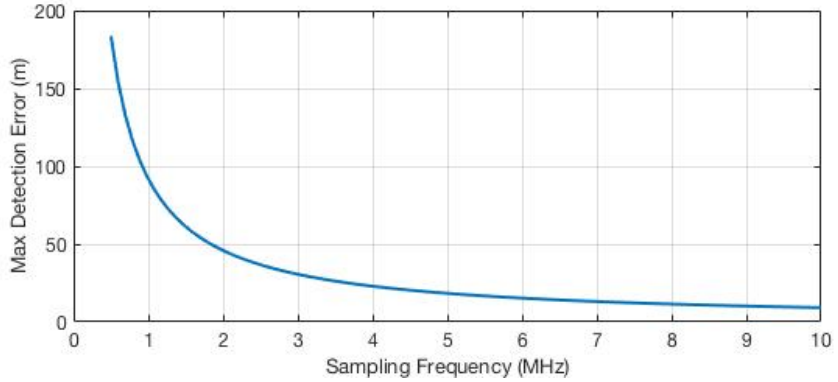

Figure 46: Worst case traveling wave FL error due to sampling frequency.

8.1.3 Algorithm Implementation

Before the traveling wave methodology can be evaluated and tested, the actual algorithm for performing traveling wave based fault location will be presented in this section. In the two prior sections 8.1.1 and 8.1.2, the benefit of multi terminal measurements and the effects of sampling frequency were presented. When performing traveling wave based FL, we therefore utilize voltage measurements at both terminals of the "substation" and a constant sampling frequency of $f_s = 1MHz$.

Since LTspice utilizes a variable step-size solver, the data obtained from transient simulations was first re-sampled to a uniform sampling frequency of $f_s = 1MHz$ using the Matlab "resample" command. Furthermore, the obtained data was fed into the Wavelet transform where the Haar wavelet was used. The Haar wavelet consists of a step function which is suitable for transient detection (see fig 26b) [41, p.137]. To ease implementation, Matlab's "Wavelet Toolbox" was used for the Wavelet implementation.

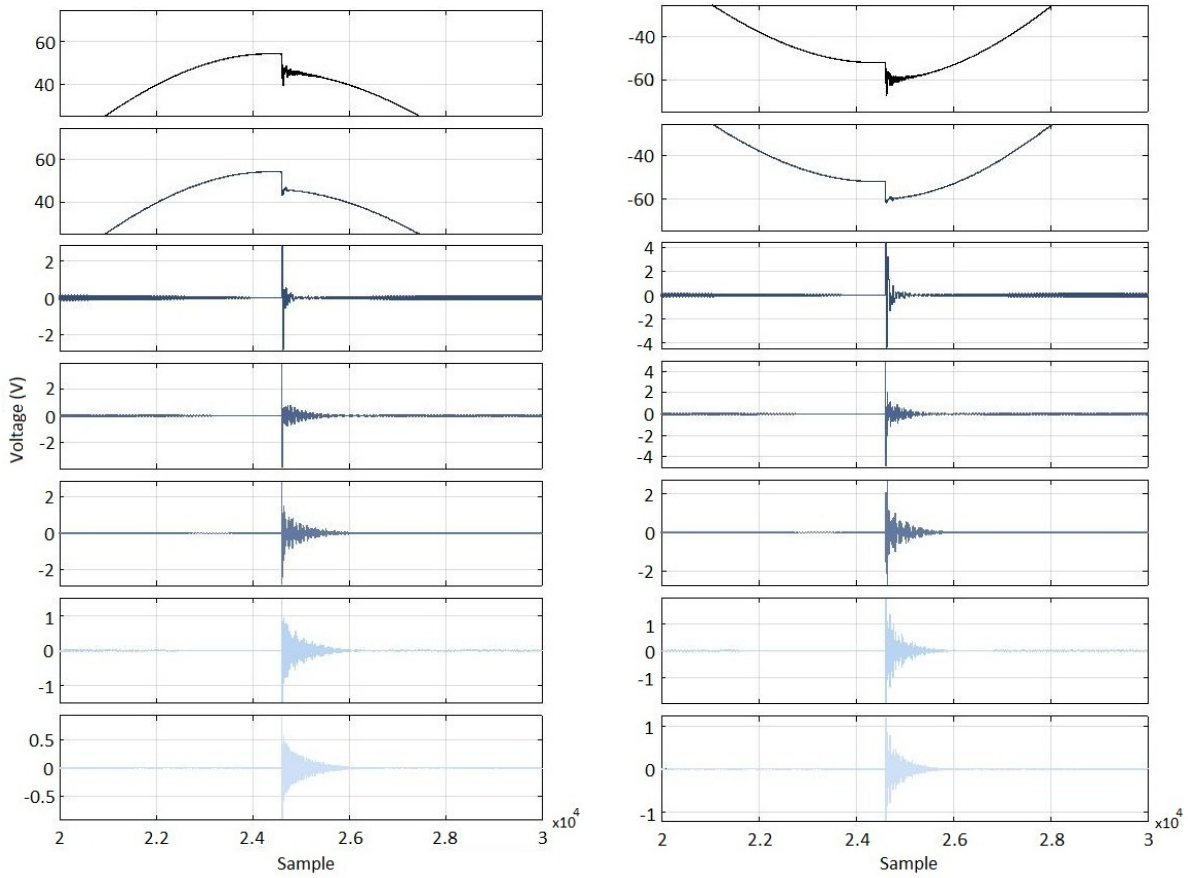

(a) Voltage - Terminal A

(b) Voltage - Terminal B

Figure 47: Wavelet Transform, Haar level 5 decomposition.

Once the data was implemented into the Matlab environment, an effort to identify the particular sample where the incidental wave hits the terminals was made. The initial idea was to set a threshold limit which can identify a "fault state", but due to differences in fault wave magnitude for different fault conditions this proved to be an insufficient method. Since a majority of the fault conditions are unknown at the time of the fault, it is problematic to anticipate the fault wave magnitude and frequency content. Therefore, the sample or interval of possible samples was found manually through observations. Finally, equation 29 was applied to obtain a distance to fault.

8.1.4 Effect of Impedance Discontinuities & Attenuation on Traveling waves

In order to properly evaluate the voltage and current inputs recorded at the terminals, understanding reflection and attenuation on the series circuit is critical. Therefore, a pulse test was performed in LTspice to evaluate high frequency behaviour of the transformer.

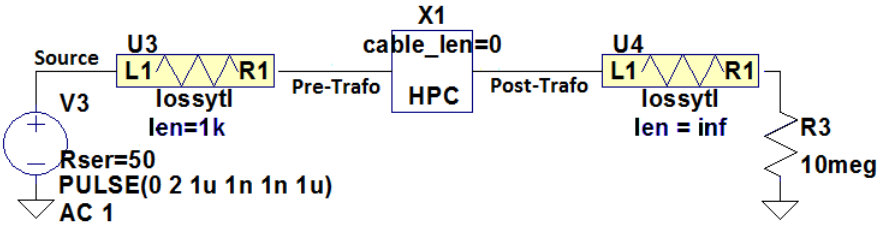

Figure 48: High frequency pulse test setup in LTspice.

The test setup featured a voltage pulse source, connected to a $1km$ TL. A transformer of interest was then connected in series and finally connected to a line of "infinite" length. The setup was subjected to a 1 μs voltage pulse of $1V$ and the transient response was observed.

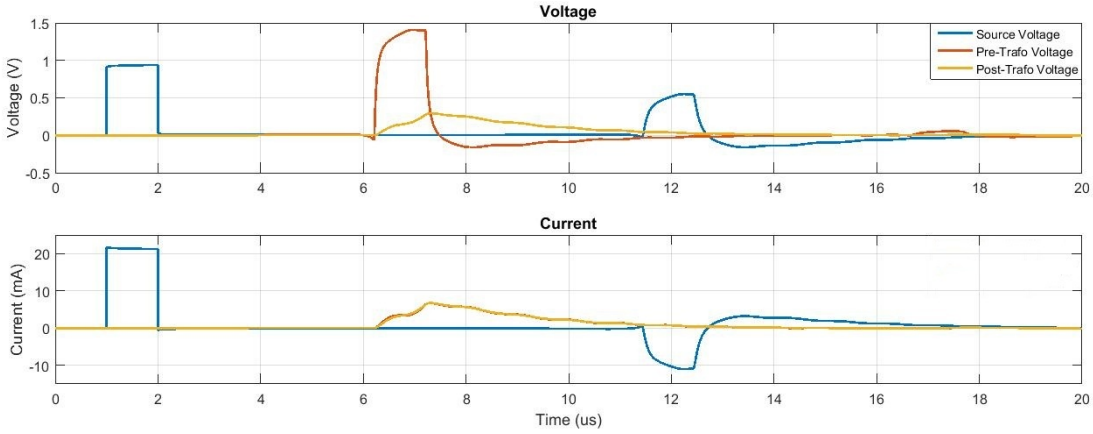

Figure 49: Efla 641 reflection and refraction of a $1\mu s$ pulse.

In fig 49, both voltage and current pulse propagation is visible at different locations in the test circuit displayed in fig 48. It is obvious that a majority of the emitted voltage pulse is reflected at the "pre-trafo" node. Since the transformer poses as a discontinuity with an impedance $>> Z_0$ of the transmission line, the wave is reflected with the same polarity as the incidental wave, which can be seen as an increase in pulse amplitude at the "pre-trafo" node.

The refracted voltage pulse however, consists of the pulse energy remaining after reflection. As can be seen in the "post-trafo" node of the voltage plot. The refracted wave suffers from extreme dispersion and energy loss and is thus effectively subjected to a loss in high frequency signal content. The current pulse on the other hand, can not penetrate the transformer windings due to the inductive nature of the windings. The pulse then sees this as an "open end". This can also be seen if one compares with the reflected voltage pulse. The "pre-trafo" reflection almost doubles in amplitude while the current waveform is extinguished at the transformer input. It is therefore recommended to primarily use voltage waveforms as a basis for capturing fault waves. The length of the pulse in the case presented above is $1\mu s$, which is an effective frequency of $1MHz$, if compared to the expected frequency behavior of a series

circuit as presented in fig 40 and 42, it is expected that frequency components in the MHz range will suffer from attenuation and dispersion.

To examine how signals with lower frequency content propagates through the transformer, pulses with longer lengths were simulated, TL length to transformer was increased to keep the pulses from merging together as pulse length was increased.

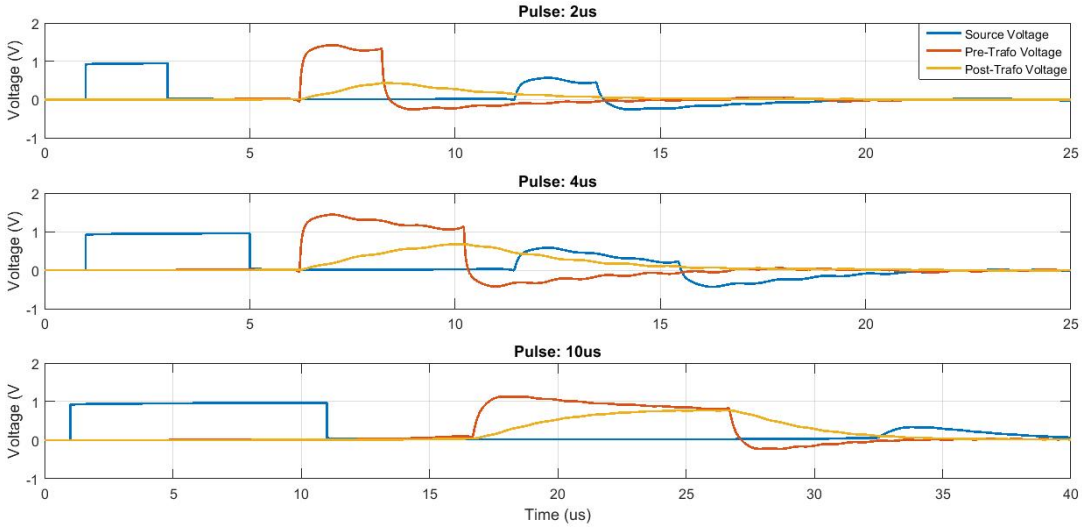

Figure 50: Efla 641 reflection and refraction at different pulse lengths.

The figure above features pulse lengths of $2\mu s$, $4\mu s$ and $10\mu s$, corresponding to frequencies of $500kHz$, $250kHz$ and $100kHz$. If the refracted graphs (post-trafo) are compared to the reflected waves (pre-trafo) it is apparent that the amplitude of the refracted wave in relation to the reflection increases as frequency decreases, thus allowing more of the incidental wave through the discontinuity. These results are expected considering fig 38. However, the refracted wave is still severely dispersed at all tested frequencies.

While the transformer is responsible for a very large portion of the high frequency attenuation, the transmission also contributes with a distance dependent attenuation. If we refer back to fig 35 and 36, it is obvious that the amount of dispersion and attenuation is significantly lower in the transmission line (/km) than in the transformer. For longer series circuits with TL lengths of up to 20km, it is possible that TL attenuation may become significant in relation to transformer attenuation.

As mentioned in section 7.2, the electrical length of each transformer is not included in the simulations. In order to find the approximate electrical length of a transformer, a CT of model ELFA 651 was disassembled in the lab.

Table 5: CT dimensions. (EFLA 641)

	Inner D [cm]	**Outer D [cm]**	**Height [cm]**	**N [ ]**	**Conductor D [mm]**
Iron Core	6.0	11.7	4.8	-	-
Prim. Winding	6.0	11.9	5.0	127	1.6
Sec. Winding	5.0	12.5	6.0	126	1.6

As the transformer is of a toroidal shape, the electrical length of the primary conductor is easily calculated as 19.79m. This means that for every transformer a traveling wave encounters, it travels 19.79m with a propagation velocity different from that of the transmission line. Therefore in practice, the propagation velocity through a CT is unknown. Thus, an error of unknown magnitude will be introduced for every transformer the fault wave passes through. Although, if the propagation velocity is known this can be accounted for.

8.1.5 Fault Conditions

Fault conditions are of importance due to the fact that these parameters can affect the size of the observed fault wave. The fault wave at the terminals is decided by a combination of attenuation- and fault condition parameters. It is therefore of interest to investigate the actual effect of these fault conditions on traveling wave method. In the literature review, there was a number of fault conditions of interest that were identified:

- Inception angle
- Fault resistance magnitude
- Location

In order to gain an understanding of how these affect traveling wave results, a number of transient simulations were executed in LTspice on the small airport series circuit shown in fig 42.

In appendix C.1, raw data obtained from the terminals is presented. The waveforms were obtained from several simulations where a $1m\Omega$ ground fault was induced $906m$ from terminal A at various inception angles. Even at a first glance, it is obvious that fault inception angle significantly affects the size of the observed waves.

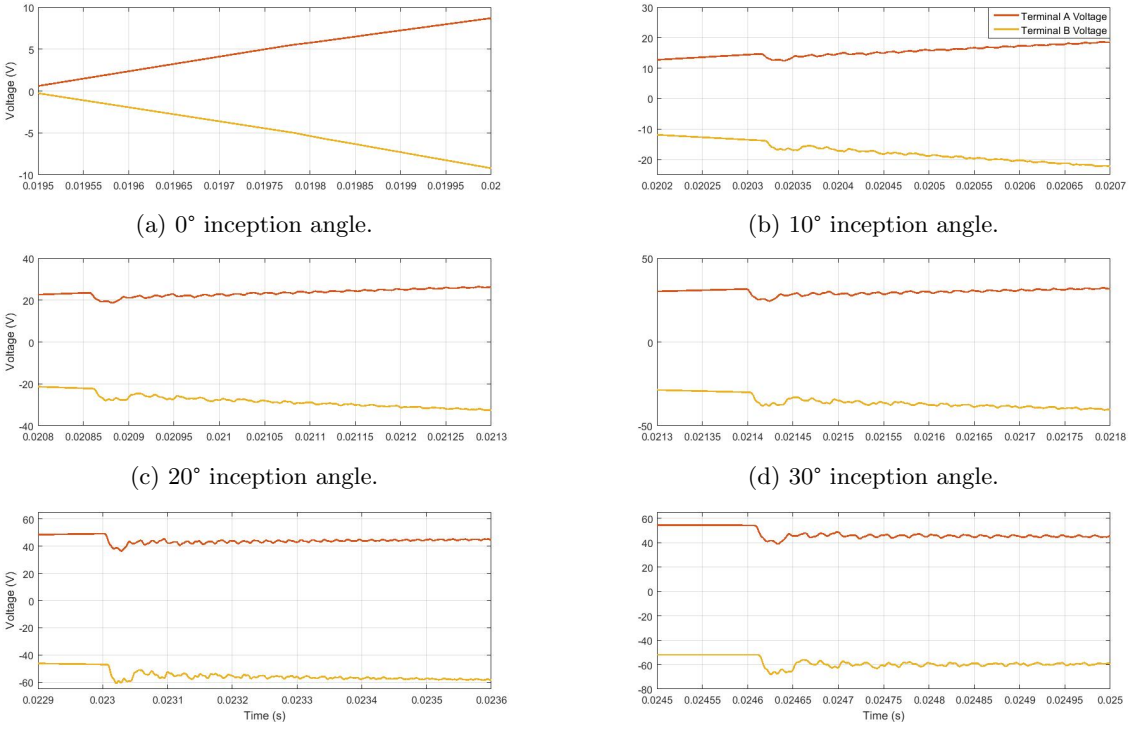

(a) 0° inception angle.

(b) 10° inception angle.

(c) 20° inception angle.

(d) 30° inception angle.

(e) 60° inception angle.

(f) 90° inception angle.

Figure 51: Fault inception angle, terminal A and B fault wave from the airport transient simulations.

Table 6: Incidental Wave magnitude.

Inception Angle (degrees)	0°	10°	20°	30°	60°	90°
Terminal A (V)	0	2.03	4.23	6.29	11.12	13.10
Terminal B (V)	0	3.02	5.62	8.15	13.88	16.00

From the acquired data, it is obvious that the magnitude of the incidental wave increases with inception angle. As long as the wave is detectable, FL will not be affected. The required magnitude of the observed wave to detect a fault transient is decided by the signal-to-noise ratio of the system.

Fault resistance can greatly vary for different fault types. The effect of this was simulated in the small airport series circuit, where a ground fault was induced at $t = 27ms$ and $906m$ from terminal A.

In fig 52, The effect of a varying fault resistance is displayed. It is obvious that both magnitude and frequency content of the fault wave is affected by R_f. As R_f increases, the discrepancy between pre-fault and post-fault steady state decreases, thus generating a smaller wave or none at all. It is visible that for $R_f \geq 1k\Omega$, no fault wave is generated. Although, worth to note is that the voltage at the fault location is very low, approximately $6V$. A higher voltage at the time of fault will produce fault waves even for higher fault resistances.

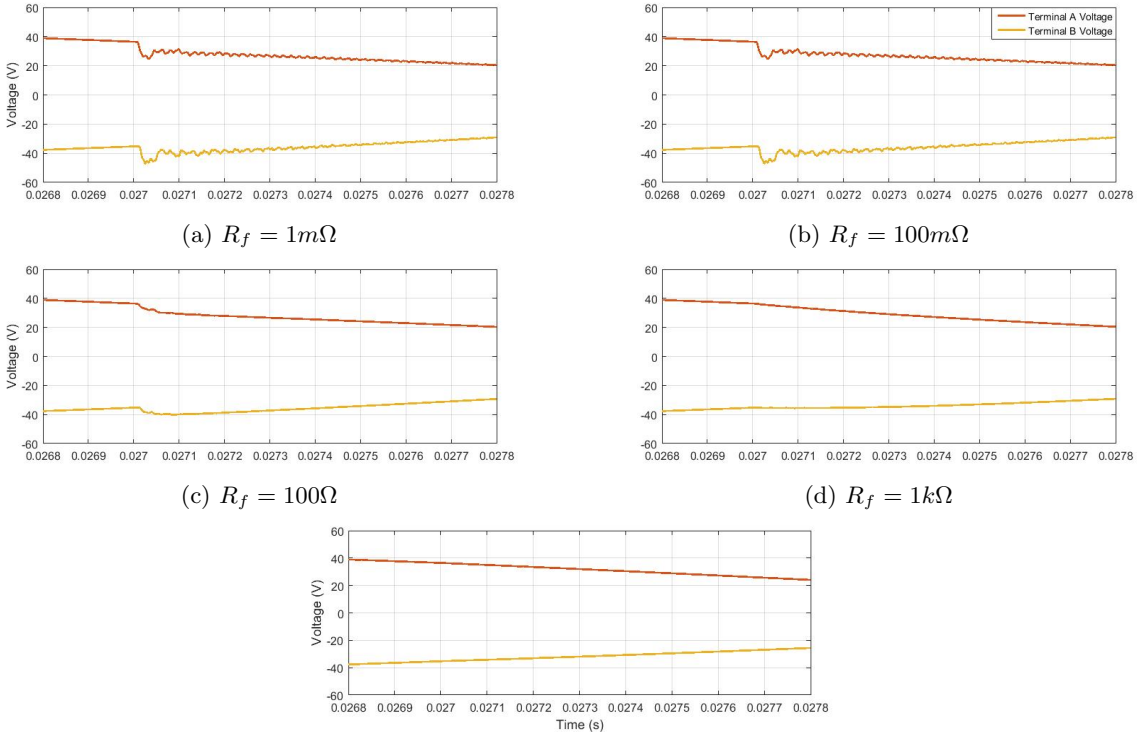

(a) $R_f = 1m\Omega$

(b) $R_f = 100m\Omega$

(c) $R_f = 100\Omega$

(d) $R_f = 1k\Omega$

(e) $R_f = 10k\Omega$

Figure 52: Fault resistance, recorded fault wave from airport transient simulations, $1m\Omega < R_f < 10k\Omega$.

As mentioned above, the wave emitted from the fault location depends on voltage magnitude at the time of fault and fault resistance. Since a series consists of only 1 source, there exists a point on the series circuit where the voltage is always 0. A point where the impedance towards terminals A and B "cancels out". If a fault occurs at this point, no fault wave will be generated. As one moves from the terminal towards this point, the voltage will decrease. Therefore, fault wave magnitude is also highly dependent of fault location. Furthermore, fault location also effect the amount of attenuation the fault wave is

subjected to. If a fault occurs very close to terminal A, the wave traveling towards terminal B will be significantly more attenuated when measured at terminal B than at A.

In order to evaluate how fault location influences traveling wave performance, a $R_f = 1m\Omega$ ground fault was induced at $t = 27ms$.

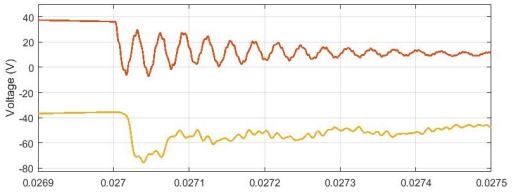

(a) $d_{fault} = 433m$ from terminal A.

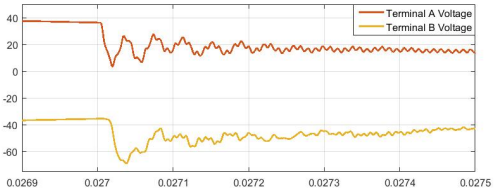

(b) $d_{fault} = 578m$ from terminal A.

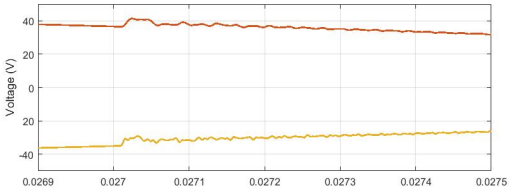

(c) $d_{fault} = 1306m$ from terminal A.

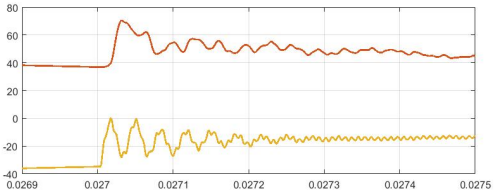

(d) $d_{fault} = 1909m$ from terminal A.

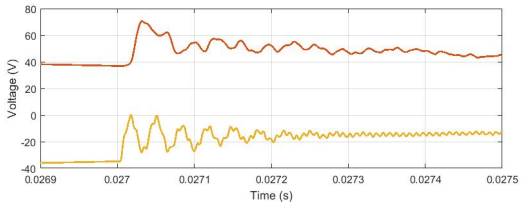

(e) $d_{fault} = 2046m$ from terminal A.

Figure 53: Fault location, recorded fault waves from the airport.

From the retrieved waveform data, it is obvious that fault location both influences the magnitude of the observed fault waves at each terminal and the frequency content. In terms of magnitude, fig 53c suffers from extremely low wave magnitudes. This is as was previously discussed in this section due to the low fault voltage at the fault location. Voltage decreases as one get's closer to the impedance midpoint on the series circuit, at $d_{fault} = 1306$ it is nearly zero.

In fig 53a and 53e, the effect of attenuation is apparent. In the referred figures, the difference in traveled distance for each fault wave is at it's maximum for the airport circuit. In fig 53a the fault wave has traveled 433m to terminal A and 2150 to terminal B. Apart from the difference in arrival times for the two waves, it is visible that the wave in terminal B has suffered from dispersion and has been effectively "smoothed out". When the incidental wave suffers from excessive dispersion, it will be harder to detect the exact arrival sample of the wave, this can affect accuracy since only an interval of possible arrival samples can be determined.

8.1.6 Noise and Transient Analysis

A major challenge with TW in an AFL-system is distinguishing different transients from each other and being able to reliably observe when the system is in a fault state. This section will therefore perform TW-based fault location and examine the effect of the following phenomena on the wavelet transform:

- White noise.
- CCR thyristor
- PLC

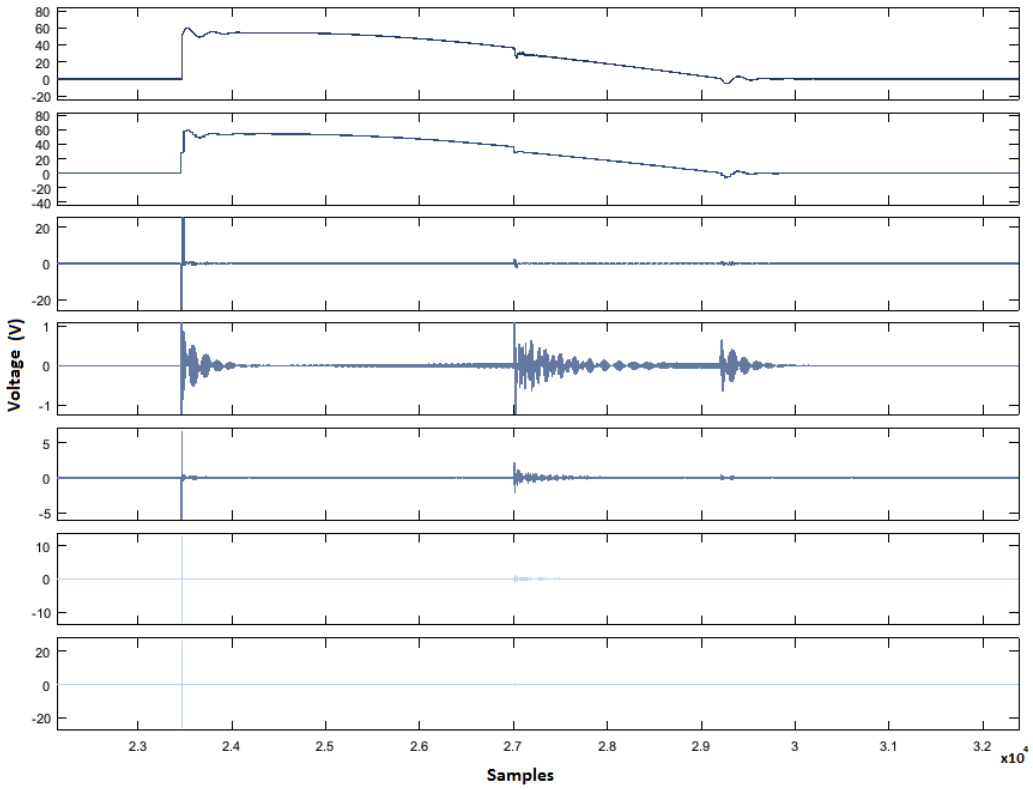

Figure 54: Level 5 Haar decomposition of fig 81a with CCR firing delay.

In the figure above, the effect of thyristor cutting has been introduced into the waveform. When chopping the waveform, the CCR produces a sinusoidal resonance around $3800Hz$ for a few periods before dying out. In fig 54, 3 transients are visible in the wavelet transform, 2 of which are due to the chopped up waveform. The transient at sample: $2.7x10^4$ is caused by a ground fault. One can see how the frequency content of the fault transient is a lot more "noisy" and appears clearly in several scales. CCR oscillations however, are uniform in frequency content and easier to distinguish. The fault wave generated by the fault in the figure above is small in relation to the thyristor effects. But still, the wavelet transform can accurately detect and reconstruct the transient.

While the thyristor chopping is a transient phenomenon, noise and PLC will litter the frequency spectrum continuously, and make the detection of small transients more challenging.

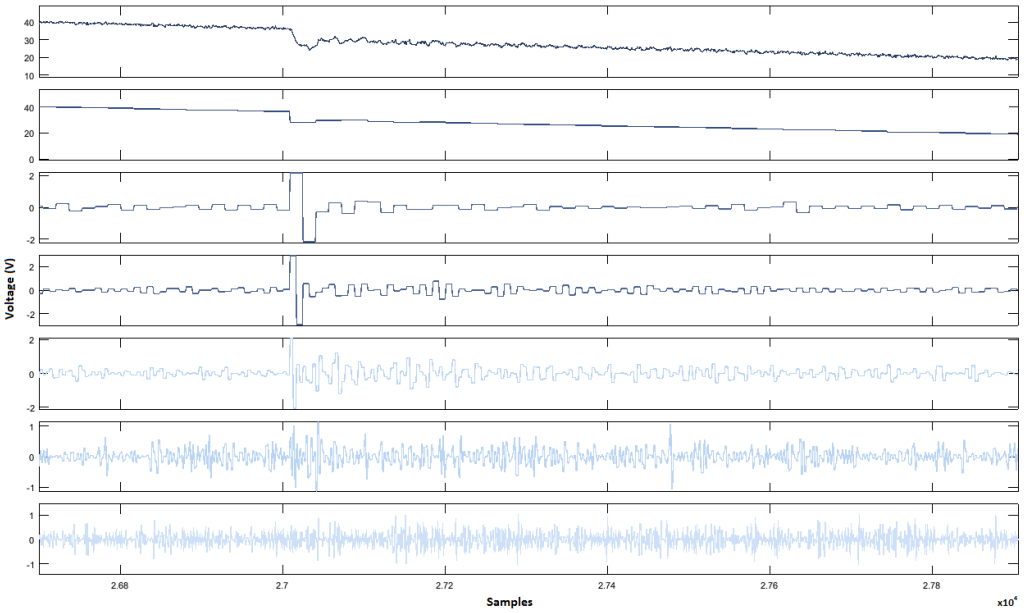

Figure 55: Level 5 Haar decomposition of fig 81a with 0.25W white Gaussian noise.

In the figure above, $0.25W$ white noise has been introduced into the waveform obtained from the LTspice simulation. It is obvious that the noise influences the low scales the most (high frequency). Ideally one wants to use the high frequency components for the most accurate fault localization. Although, the noise in the figure above is simulated, real-life signals will still contain some high frequency noise.

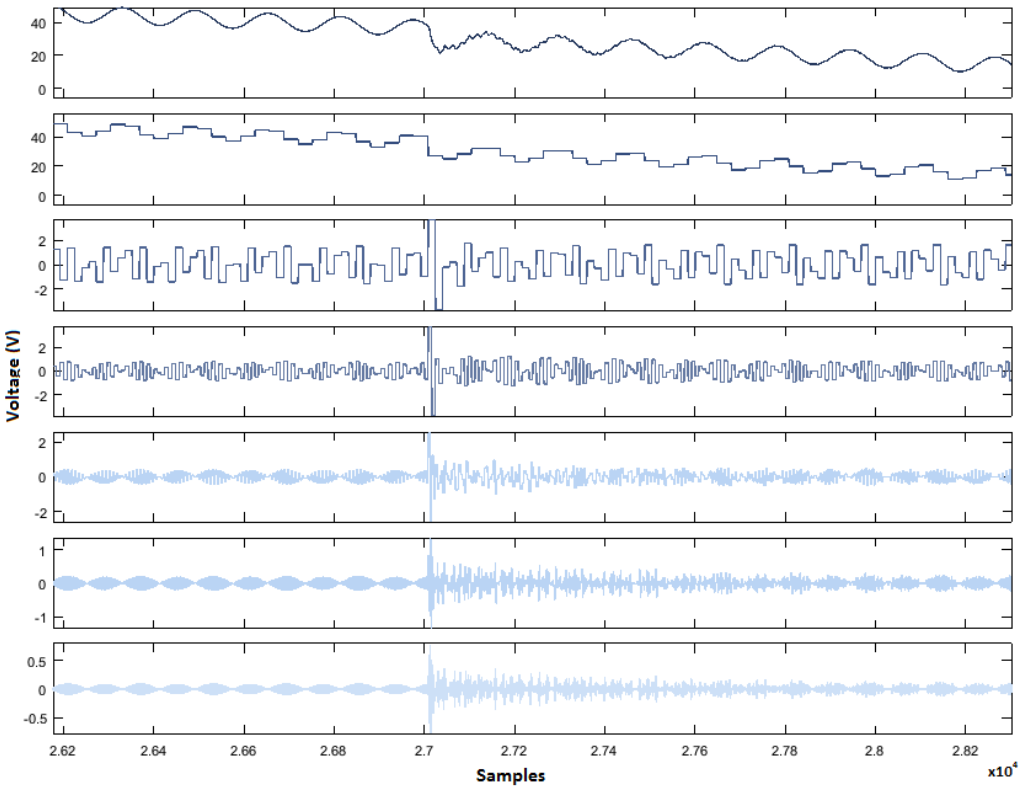

Figure 56: Level 5 Haar decomposition of fig 81a with communication overlay.

The power line communication is modulated in the spectrum $2 - 20kHz$, in fig 56 communication has been simulated by introducing a sinusoidal wave in this frequency range, which is sufficient to observe the effect of the PLC on a transmission line level. In fig 56, the PLC is visible in all scales. Although, due to the isolated frequency content of the communication signal it is easy to observe the fault wave.

Table 7: Fault Location, traveling wave arrival samples.

Fault Location (m)	$433m$	$578m$	$1306m$	$1909m$	$2046m$
Arrival Sample - Terminal A	27005	27005	27013	27009	27012-27014
Arrival Sample - Terminal B	27007-27011	27009-27011	27011	27005	27005

The data in table 7 were obtained from fig 82, the arrival times of the fault waves were obtained arbitrarily in a visual manner. Obtaining the exact arrival sample of a wave was in some cases difficult due to large amounts of dispersion at high frequencies, instead an interval of possible arrival samples was taken. This proved to be a problem when the fault took place close to one of the terminals, where one fault wave has to travel across the entire series circuit to reach the opposing terminal. Unfortunately, the airport series circuit is only 2583m long and therefore circuits longer than the airport circuit will face even more dispersion and high frequency attenuation.

Table 8: Fault Location, traveling wave FL algorithm results.

Fault Location (m)	$433m$	$578m$	$1306m$	$1909m$	$2046m$
Fault: (d_{approx})	558.26	374.96	1658.1	2024.7	2758.0
Error (m)	125.26	-203.04	352.1	115.7	712

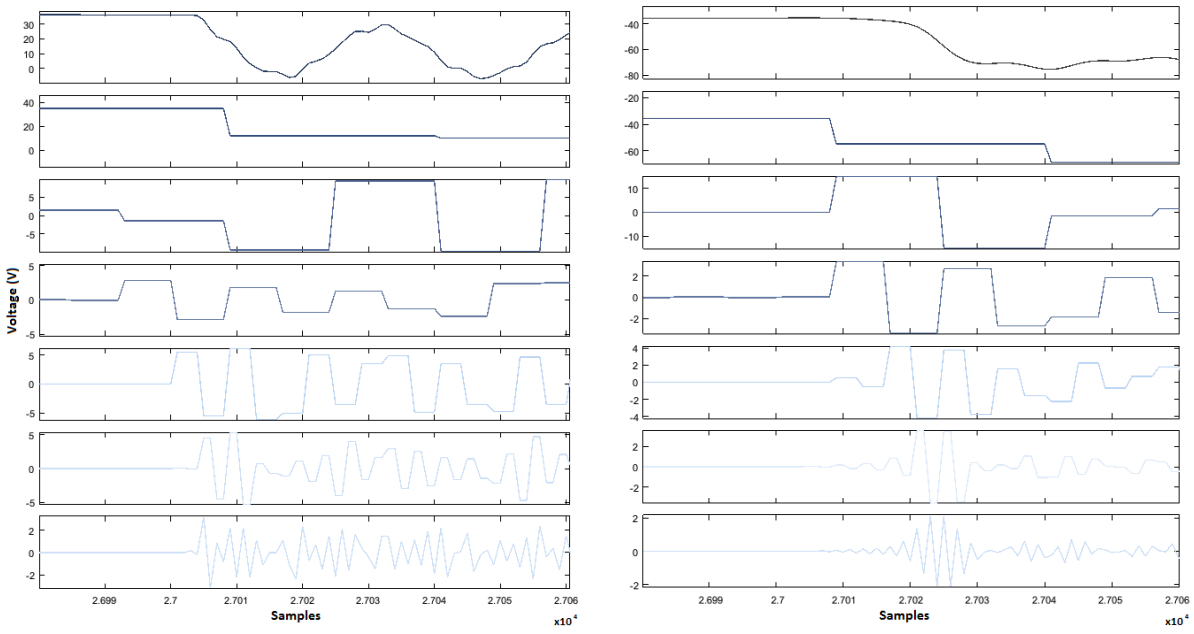

(a) Voltage - Terminal A

(b) Voltage - Terminal B

Figure 57: Haar level 5 decomposition of ground fault at $d = 433m$, $f_s = 1MHz$.

In the figure above, one can observe the difference between the incidental waves at each terminal. The wave at terminal B is significantly more dispersed than terminal A.

8.2 Impedance based methods

In the section 5.1, 3 impedance based algorithms were presented. However, only the voltage profile-based methodology is appropriate for non-homogeneous systems. Therefore, the reactance method and synchronized and unsynchronized phasor method will be omitted from the study. The voltage profile method can only locate ground faults, since it requires a fault loop from each terminal in order to function. Furthermore, intermittent faults do not produce any sustaining changes in the fault loop and therefore, impedance based methods are not applicable.

The voltage profile method utilizes current and voltage measurements either from the CCR or on the "terminals" of the substation. As long as all impedances are accounted for in order to establish the correct voltage profile. Generally impedance based methods require more system specific data than other methods, and the voltage profile method is no exception. Since the fault location is derived from approximations of circuit parameters, accurate estimations of component parameters and circuit distances are especially important. As a consequence of this, the accuracy of impedance based FL is dependent on the total length of the circuit. Since circuit parameters are always approximated to some degree, the approximation error of the parameter will be amplified when multiplied with the distance of the circuit. A longer distance will induce a larger error.

8.2.1 Algorithm Implementation

The algorithm used to estimate the voltage profile of an AFL-circuit only requires voltage measurements since the CCR produces a constant current. Although, in reality the CCR does not have instant feedback control which means that at a fault event, the instantaneous current will likely diverge from the set value. The CCR can only correct the value at the next period. The current source in the LTspice simulations is significantly better at maintaining the set value, but for the purpose of this study, the results are sufficient.

The algorithm developed in Matlab, assumes $6.6A$-peak and utilizes the voltage peak values recorded from terminals A and B of the reduced airport circuit. The TL and CT voltages at $50Hz$ and $6.6A$-peak had been separately obtained in LTspice and then implemented into the algorithm. According to terminal voltages, TL lengths and number of CT:s a voltage profile is established from each terminal. The intersect of these curves represent the fault location. Since the analysis was made on pure sine waves, both peak values or rms values can be used, as long as one is consistent. In an actual setting where a CCR is used as power source, rms values will be required to accurately portray voltage profiles when the the voltage waveform is not entirely sinusoidal.

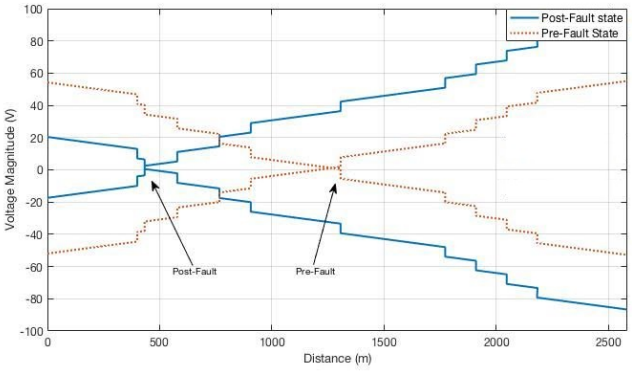

Figure 58: Voltage profile example of the airport circuit, pre- and post-fault states.

A few issues with this method are worth to discuss. Firstly, this method require knowledge of light fixture states and thus communication in order to accurately represent the voltage drop of specific CT:s. Furthermore, the occurrence of CT saturation will influence the profile, therefore this phenomenon needs to be detected, located and it's effect on the voltage profile has to be accounted for in the algorithm. Finally, the curves from each terminal will always intersect at some point. Thus, if a fault occurs at the point where the curves already intersect pre-fault it will go undetected. The voltage profile method must be accompanied by a separate detection system.

8.2.2 Fault Conditions

This section presents the results obtained in fig 80, 81 and 82, where the performance of the voltage profile method will be evaluated in regard to fault inception angle, fault resistance and fault location.

For inception angle evaluation fault parameters were set to $R_f = 1m\Omega$ and $d_{actual} = 906m$. The same data was used in section 8.1.5 for traveling wave.

Table 9: Fault Inception Angle, voltage phasor magnitude.

Inception Angle (degrees)	**Fault State**	0°	10°	20°	30°	60°	90°
Terminal A (V)	**Pre**	58.18	58.19	58.19	58.19	58.19	58.19
	Post	46.05	46.07	46.07	46.07	46.06	46.96
Terminal B (V)	**Pre**	55.40	55.40	55.40	55.40	55.40	55.40
	Post	60.29	60.29	60.29	60.29	60.28	61.19

The data presented in the table above consists of pre- and post-fault voltages of terminals A and B. It is obvious that post-fault voltages do not change significantly with fault inception angle, which is to be expected due to post-fault voltages being independent of fault inception angle.

Table 10: Fault Inception Angle, FL algorithm results. Fault: $d_{actual} = 906m$.

Inception Angle (degrees)	0°	10°	20°	30°	60°	90°
Fault: (d_{approx})	908.1	908.1	908.1	908.1	908.7	908.4
Error (m)	2.1	2.1	2.1	2.1	2.7	2.4

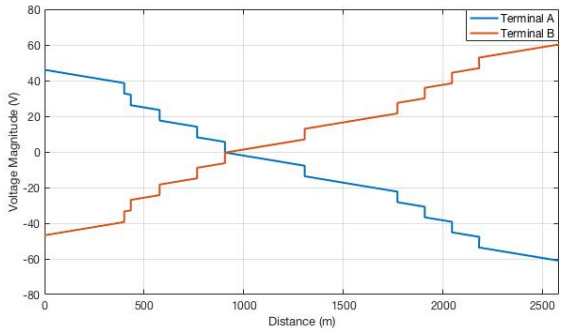

Figure 59: Fault inception angle 0°, voltage profile of the airport circuit

Table 11: Fault Resistance, voltage phasor magnitude. $t_fault = 27ms$.

Fault Resistance (Ω)	**Fault State**	$1m\Omega$	$100m\Omega$	100Ω	$1k\Omega$	$10k\Omega$
Terminal A (V)	**Pre**	54.30	54.30	54.31	54.31	54.31
	Post	48.00	48.01	48.02	48.24	52.64
Terminal B (V)	**Pre**	52.02	52.02	52.02	52.03	52.02
	Post	62.21	62.21	62.20	62.02	57.87

Table 12: Fault Resistance, FL algorithm results. Fault: $d_{actual} = 906m$.

Fault Resistance (Ω)	$1m\Omega$	$100m\Omega$	100Ω	$1k\Omega$	$10k\Omega$
Fault: (d_{approx})	908.9	909.2	909.7	920.5	1149.5
Error (m)	2.9	3.2	3.7	14.5	243.9

The effect of an increasing fault resistance is apparent, it does affect accuracy of the method. According to the data in table 11, the difference between pre- and post-fault voltages decreases with increasing R_f. This can be explained by the fact that a high fault resistance causes a smaller disruption of the pre-fault steady state operation and an error is introduced. As was mentioned in the previous section, the curves will always intersect at some point, even if pre-fault voltages are used as an input into the algorithm. Therefore, with a very high R_f the fault intersect of the curves will be shifted towards the pre-fault intersect.

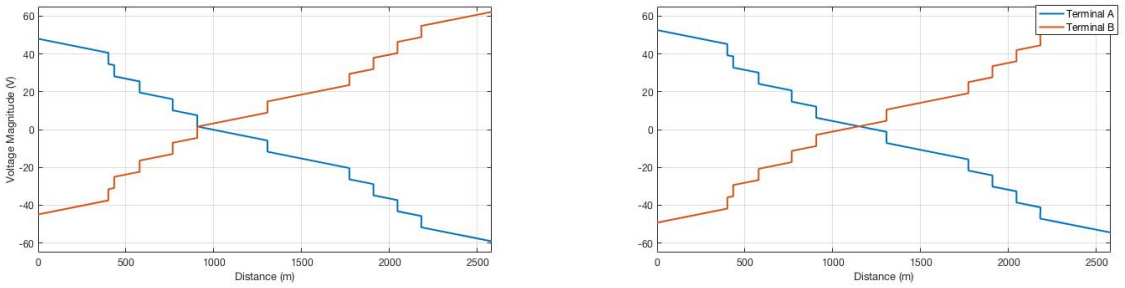

(a) $R_f = 1m\Omega$ (b) $R_f = 10k\Omega$

Figure 60: Fault resistance dependency, voltage profile of the airport circuit.

In fig 60, the discrepancy in FL approximation between $R_f = 1m\Omega$ and $R_f = 10k\Omega$ is displayed. The pre-fault intersect for the data presented above occurs at $d = 1306m$.

When the performance of the method was evaluated in relation to fault location, a $R_f = 1m\Omega$ fault was initiated at $t = 27ms$ at different locations on the series circuit.

Table 13: Fault Location, voltage phasor magnitude.

Fault Location (m)	**Fault State**	$433m$	$578m$	$1306m$	$1909m$	$2046m$
Terminal A (V)	**Pre**	54.25	54.29	54.43	54.43	54.54
	Post	20.40	29.43	61.60	85.26	85.23
Terminal B (V)	**Pre**	55.14	55.20	51.90	51.76	51.79
	Post	89.7	80.77	48.57	24.94	24.94

Table 14: Fault Location, FL algorithm results.

Fault Location (m)	$433m$	$578m$	$1306m$	$1909m$	$2046m$
Fault: (d_{approx})	433.1	578.1	1324.0	1960.8	1960.8
Error (m)	0.1	0.1	18.0	51.8	-85.2

In the presented data, it is visible that as the fault location varies, so does the magnitude of the terminal voltages. This is to be expected as the lengths of the fault loops from terminal to fault changes.

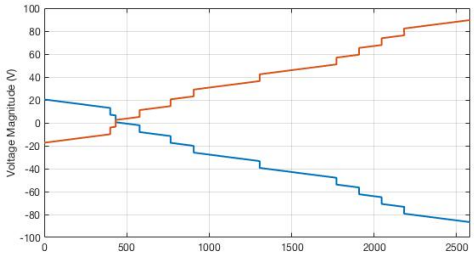

(a) $d_{actual} = 433m$ from terminal A.

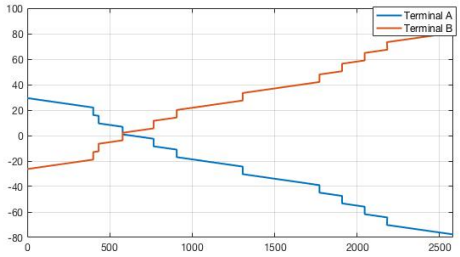

(b) $d_{actual} = 578m$ from terminal A.

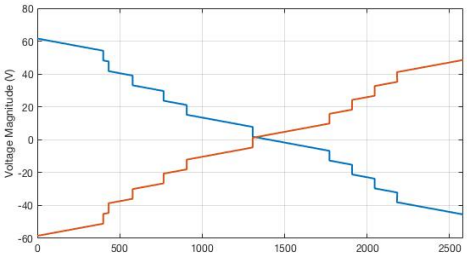

(c) $d_{actual} = 1306m$ from terminal A.

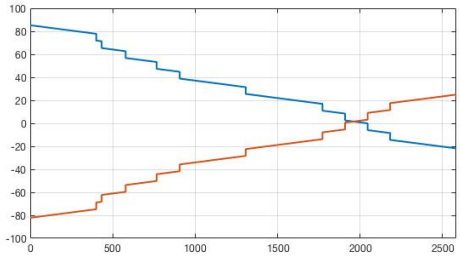

(d) $d_{actual} = 1909m$ from terminal A.

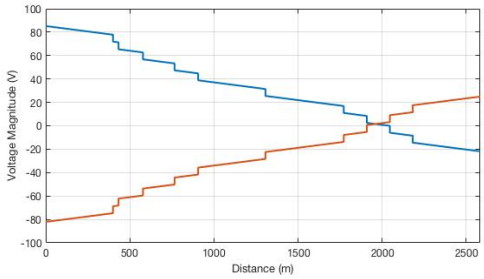

(e) $d_{actual} = 2046m$ from terminal A.

Figure 61: Fault location, voltage profile of airport circuit.

The results presented in table 14 shows an error that increases as the distance to terminal A grows. The cause of this error is unknown, the fact that an error is introduced close to terminal B indicates that one of the voltage profiles is incorrectly constructed close to terminal B. But since the voltage profile from terminal B is a mere inversion of voltage profile A, this would introduce errors close to both terminals A and B. In general, the profile method provides accurate fault location for small fault resistances and is independent of fault inception angle, a maximum error of 3.2% for low resistance ground faults in a simulated setting on the airport circuit is obtained. Although, in practice where circuit parameters might not be uniform along the circuit further errors will be introduced. Aged cables will influence accuracy of the method since TL parameters can degrade over time and depending on the local environment of certain cable segments, some segments can age faster than others resulting in varying circuit parameters.

8.3 Time Domain Reflectometry

The Megger TDR is able to produce $20V$ with pulse lengths between $2\mu s$ and $2ns$, which provides an effective range of a few meters up to $20km$. It is possible to adjust velocity factor and characteristic impedance to optimize the TDR equipment for specific cable systems.

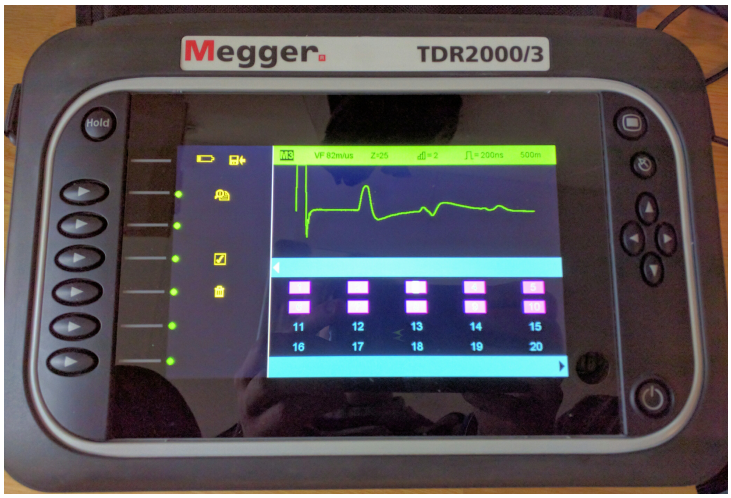

Figure 62: Megger TDR.

Since the TDR does not requires high voltage equipment it has been tested both in a simulated environment as well as with a real commercial TDR (Megger TDR2000/3). The lab cable length was validated in order to adjust the velocity factor of the TDR equipment. The velocity factor is specific for different cable types, and has to be validated prior to performing fault location with TDR. Three different setups has been evaluated. Measurements on a transmission line without, with one and with two transformers.

8.3.1 Transmission line

The figures below show the results from simulated and tested pulses being transmitted into the cable with open and shorted ends of the cable. This is done to verify the TDR-theory presented in section 5.2 and will be useful when continuing with extended TDR-measurements with impedance discontinuities along the transmission line. The two graphs below shows LTspice results when transmitting a pulse through the cable with open and shorted cable end.

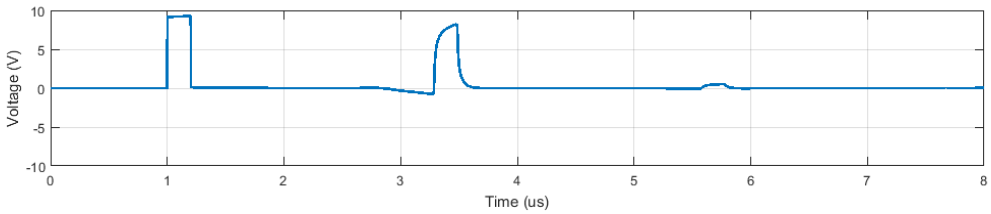

Figure 63: LTSpice simulation of an open coaxial cable at 219m.

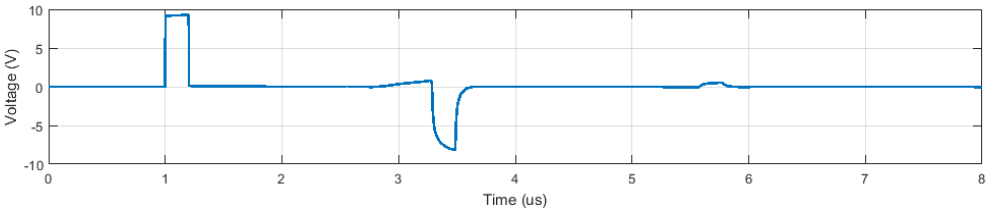

Figure 64: LTSpice simulation of an shorted coaxial cable at 219m.

The same tests were performed on the real XLPE-cable in the Safegate lab. These tests were performed with the commercial TDR and the results were as expected nearly the same as the simulated results. The real cable consisted of two cables segments (109.5m each) jointed together. The "bump" in the middle of the figures below is the small reflection of energy from the joint of the cable segments.

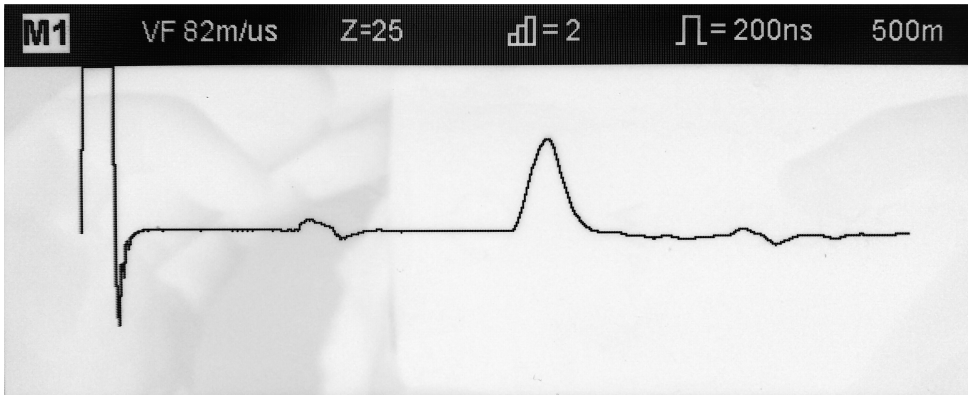

Figure 65: Open coaxial cable at 219m with two jointed cables (109.5m each).

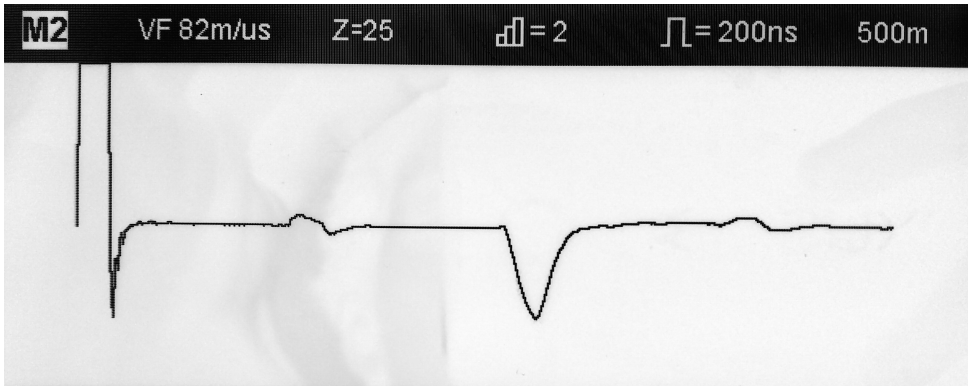

Figure 66: Shorted coaxial cable at 219m with two jointed cables (109.5m each).

The results in both the simulation and the tests on the real cable confirms the theory of TDR. The wave pulse gives a minor reflection at the splice shown at 109.5m and was reflected with the same polarity when the the pulse reached the open end of the cable. A shorted end produced a reflection with inverted polarity.

8.3.2 Effect of impedance discontinuities on TDR

In the figures below, results obtained from both LTspice and lab tests where TDR has been applied to a cable system with CT:s placed along the cable. Since the main purpose of TDR is to measure impedance discontinuities, it is of interest to study how the current transformer affect TDR performance.

The two figures 68 and 69 shows the results from the LTSpice simulation with one transformer with shorted and open secondary side respectively. Similar results are achieved when using the commercial TDR on two shielded transmission lines (XLPE-cable 109.5m each) and one transformer (EFLA KR641, 100W) between the both transmission cables. These results can be seen in figure 70 and 71. The test- and simulation-setup is presented in 67.

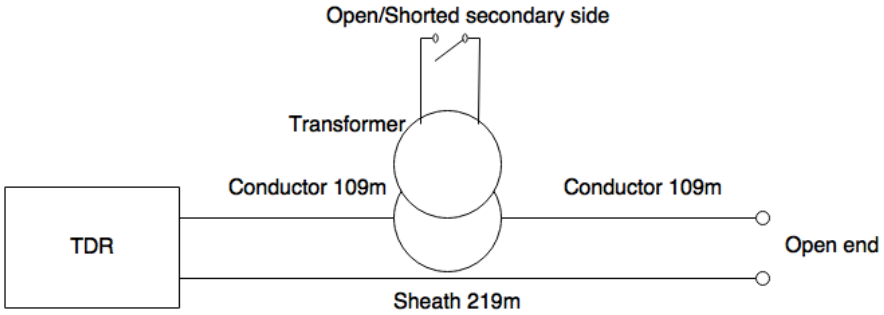

Figure 67: A basic sketch of the setup in the tests with one transformer.

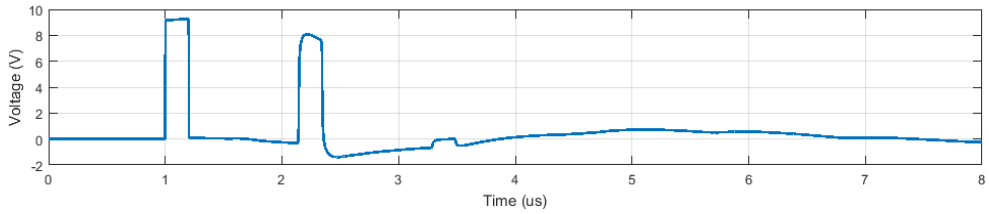

Figure 68: LTSpice simulation of an open coaxial cable at 219m and a transformer halfway on the transmission line with shorted secondary side.

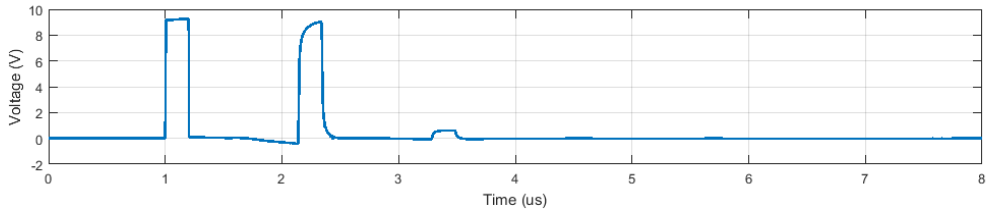

Figure 69: LTSpice simulation of an open coaxial cable at 219m and a transformer halfway on the transmission line with open secondary side.

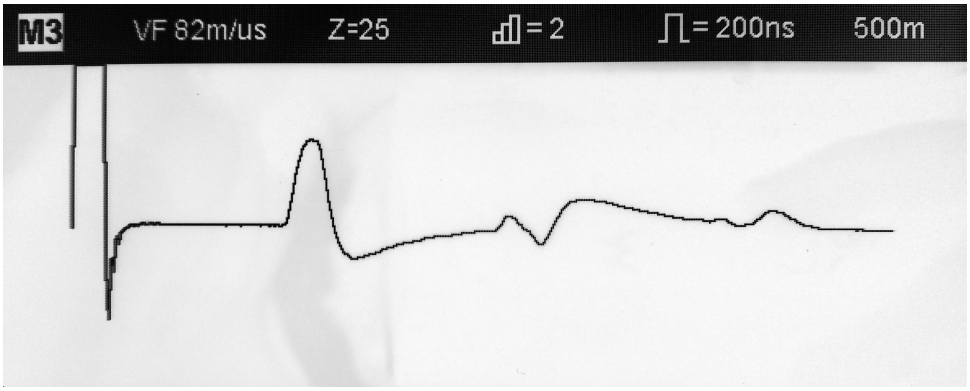

Figure 70: Open coaxial cable at 219m and a transformer halfway on the transmission line with shorted secondary side.

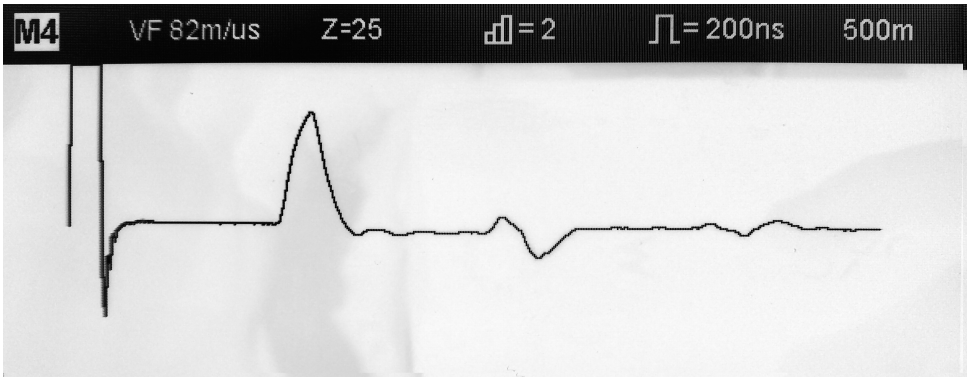

Figure 71: Open coaxial cable at 219m and a transformer halfway on the transmission line with open secondary side.

The majority of the pulse energy is reflected at the in all results. The difference between a shorted and open secondary winding of the CT is only manifested with a slightly sharper peak on the reflection for an open winding and a negative overshoot for a shorted secondary. The bumps which are visible after the main reflection is correlated to the secondary pulse reflection on the transformer.

The tests performed with two transformer on cable were done to verify that only a small part of the pulse energy is transmitted through the transformers. The setup is shown in fig 72.

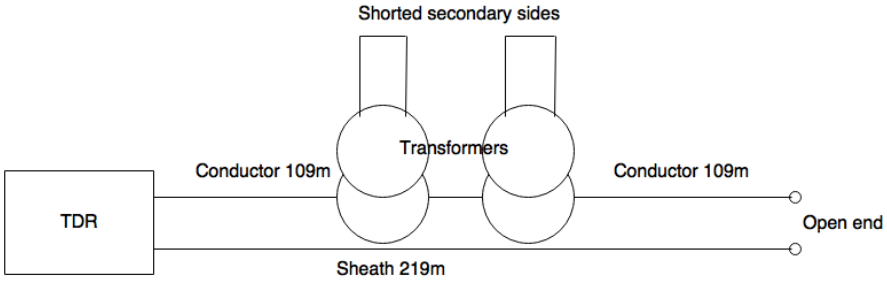

Figure 72: A basic schedule of the setup in the tests with two transformers.

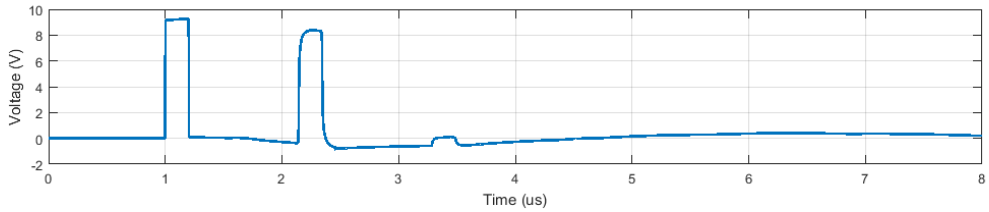

Figure 73: LTSpice simulation of an open coaxial cable at 219m and two transformers halfway on the transmission line with shorted secondary sides.

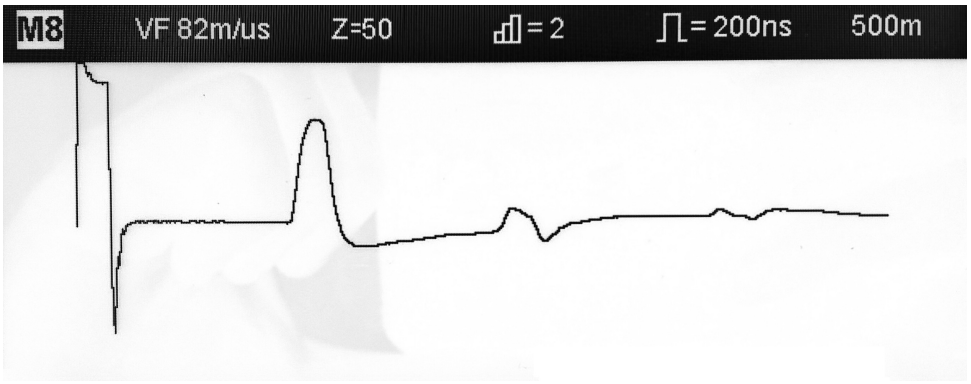

Figure 74: Open coaxial cable at 219m and two transformers halfway on the transmission line with shorted secondary sides.

As can be seen in simulations and tests above, the pulse energy of the transmitted waves is mostly reflected on the transformers and only a small discrepancy between open and shorted secondary CT windings can be seen in the waveforms. The energy of the pulse is however so greatly reduced that this method is of no use if a fault happens beyond the first transformer of the AFL and one wants to measure only from one place on the system. The TDR method is however very accurate if a fault occurs between the measurement location and the next transformer of the series circuit. If the distance between measurement location and the first transformer is known, not only detection of a fault will be possible but also a fairly accurate localization of the fault. Although, TDR measurements must be done from every single man hole and the distance between transformers has to be known to detect and localize faults with TDR.

8.4 Arlanda Customer Case

As a part of the study, Arlanda Airport was visited. At Arlanda, the electrical maintenance team was interviewed and some TDR tests were performed on a few cable systems. The main purpose of the visit was to understand the routines, procedures and problems that occur at airfields.

Safegate has worked alongside Arlanda for many years providing airside equipment such as docking systems and AFL-systems. At Arlanda there are three runways along with attached taxiways. The airfield contains approximately 190 series circuits averaging 7km in length, where the longest series circuit is 12km.

8.4.1 Operative Study

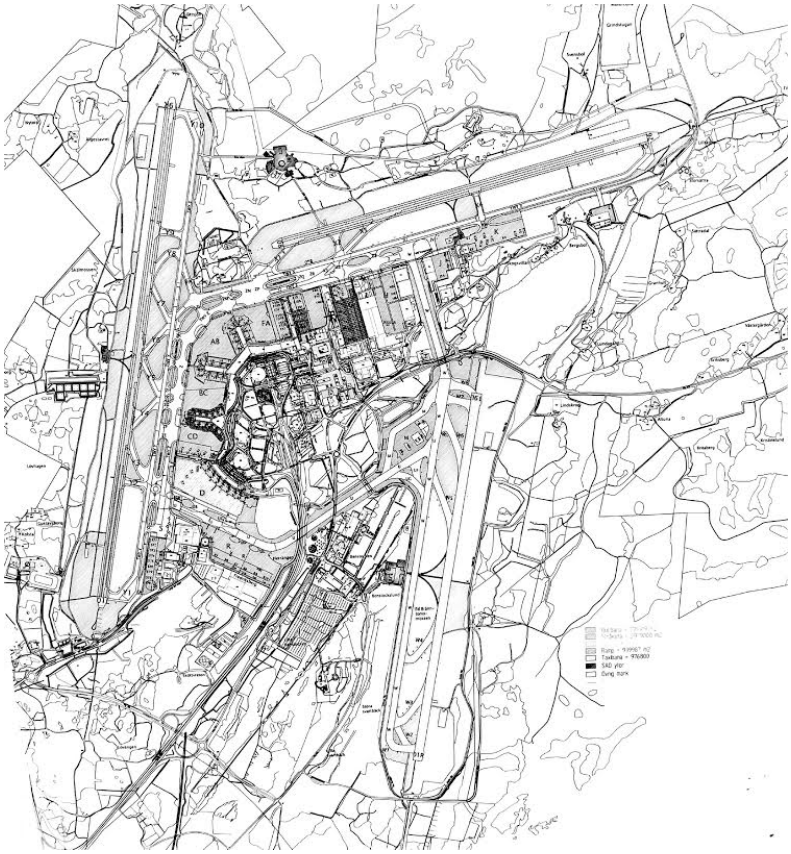

Figure 75: Geographical map of Arlanda airport

The electrical maintenance team works mainly preemptively in order to prevent failures that affect flight operations. Many of the electrical faults occurring at Arlanda are high resistance ground faults which do not affect flight operations. These can be in the range of $M\Omega$ down to a few $k\Omega$. To date, the pre-emptive maintenance mainly consists of locating these high resistance faults using an isolation tester and a "divide and conquer"-methodology and repairing them before a low resistance path is established between conductor and sheath. This FL-methodology is very time consuming and personnel-intensive.

The main cause of cable system failure for Arlanda are faulty splices and connectors where moisture and water have penetrated the mantle of the cable. At some specific areas, where cable installations are particularly exposed some cables are shown signs of water intrusion into the cable sheath itself. Furthermore, interviews with maintenance at Arlanda showed that these intermittent high resistance ground faults are extremely weather dependent and also sensitive to certain chemical compounds used on the airfield. One of these chemical compounds which is especially detrimental to splices and connectors is called potassium acetate. This compound is used as a deicer for airplanes and runways during winter. Along with acting as an effective deicer, this compound also lowers the surface tension of water allowing it to easily penetrate cable sheaths, splices and connectors. This poses a problem for SoH methods, since ground faults mostly occur when cable systems are exposed to chemicals, water or moisture, the SoH measurements have to be performed when the system is exposed. Performing an SoH evaluation in dry conditions is not representative for wet conditions.

8.4.2 TDR Tests

Regarding the TDR tests performed at Arlanda, these were performed at substation K70 at which a high resistance ground fault had been found using the isolation tester. According to the isolation tester equipment, this specific ground fault was at $220k\Omega$.

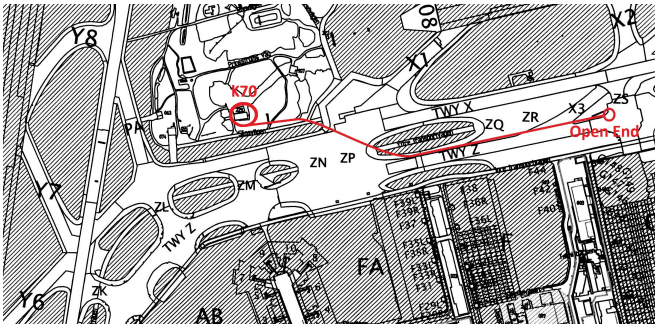

Figure 76: Faulty cable segment tested from K70 sub station. Approximately $l = 2km$.

The cable was disconnected from it's first transformer and then measured with TDR from the substation (fig: 76). The results of this measurement can be seen below.

Figure 77: TDR-Result, K70 signal.

In fig 77, we see the outgoing and reflected pulse. Due to the long distance, the reflected pulse is significantly lower in amplitude. There are also some small perturbations between sent and received pulse.

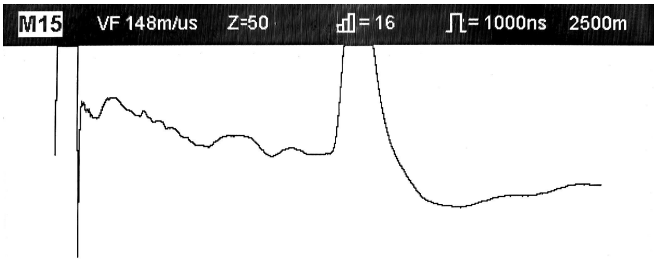

Figure 78: TDR-Result, K70 amplified signal.

Since it was known that this specific cable had a high resistance ground fault, such as a faulty connector or splice it was of interest to amplify the signal between sent and received pulse, this is visible in fig 78. As one can see in the figure, there are several events taking place between the two major pulses. Although, due to the number of events in the signal at very low amplitude, it is difficult to determine a specific fault location.

8.5 Concept Evaluation & Scoring

From the concept generation phase, all obtained methods have been evaluated and scored according to a number of factors and metrics. The importance of each metric have been evaluated and been given a weight factor, which symbolizes the importance of the metric. All scoring of a method is relative to the other methods in the study. Therefore, a "1" does not mean that a method is bad at a certain metric, only that it is worse than the other methods.

8.5.1 Concept Scoring for Fault Location Methods

In table 15 all fault locating methods has been scored according to their capability to fulfill requirements for a certain metric. This score is multiplied with the weight factor and added to the total score of the method. If a metric is not applicable on one method a "-" is used and no points are added to the total score. The total added score for each method is shown in the last row of the table below. Since the methods can have a different number of "non applicable"-fields, the maximum score of each method can be different. Although, the scoring is not meant to provide a definitive answer to which method that is the "best" one. It is only supposed to provide an indication.

An interesting consequence of the scoring table available on the next page, is that visual inspection which is the SoH- and FL-method used today has received very high points. Visual inspection along with isolation testing is a very accurate method of FL which is independent of a lot of factors, this makes it a very dependable method. The disadvantage of visual inspection, is that it is very time- and personnel-intensive. The maintenance crew at Arlanda, spent a lot of their time on FL and according to them, it is also difficult to pinpoint a fault. And as is shown in table 15, the scoring matrix does not reflect the required time and personnel well enough.

The technical metrics that are of most importance in this study are fault sensitivity, sensitivity to impedance discontinuities and primary loop length. These are also the metrics that really set the methods apart. As was mentioned previously in the study, the main problem for the traveling wave method is the high frequency attenuation and dispersion from the transformers. Even for a small segment of the airport circuit with 10 transformers, there was significant high frequency dispersion which was problematic when determining the exact arrival sample of the fault waves. The impedance based voltage profile method gains a higher score in "sensitivity impedance discontinuity" since it overcomes the attenuation problem by utilizing phasor measurements and circuit parameters as a basis for performing fault location. On the other hand, voltage profiling requires accurate circuit modeling in order to reconstruct the voltage along the circuit, and is sensitive to local variations in circuit parameters that can not be modeled.

Voltage profiling is also capable of detecting and locating (with a sizable error) high resistance faults where no traveling waves are emitted from the fault location. This gives the voltage profile method a significant advantage over traveling wave for short series circuits, which is reflected in the concept scoring.

TDR is capable of locating very large differences in impedance on a cable, but for large ground fault resistances the method falls short. TDR is also troublesome since an entire series circuit can not be analyzed from the CCR terminals, no TDR pulse can penetrate the transformer windings. Therefore, TDR requires a maintenance crew to analyze individual cable segments between transformers and does not solve the operative issues of current fault location methods.

Table 15: Concept scoring matrix - Fault location methods

Metrics / Methods	**Weight factor**	**Traveling wave**	**Impedance based algorithms**	**TDR**	**HV pulse surge**	**Visual inspection**
Technical specifications						
1-Terminal Measurement	1	1	1	-	-	-
2-Terminal Measurement	1	3	3	-	-	-
Measure Voltage (terminal)	2	3	3	3	3	2
Measure Current (terminal)	2	1	3	3	3	2
Require Ext. Sensors	3	3	3	3	1	3
Requires High Sampling Rate	2	1	3	3	2	3
Ground Fault Sensitivity	5	1	2	1	1	3
Series Fault Sensitivity	5	3	1	3	1	3
Secondary Winding Fault Sensitivity	3	1	1	1	-	1
Intermittent Fault Sensitivity	5	2	1	1	2	1
Noise Sensitivity	3	1	3	2	3	3
Performance on Shielded Cables	5	3	3	3	3	3
Performance on Unshielded Cables	4	1	3	1	3	3
Sensitivity to impedance discontinuity	5	1	2	1	2	3
Sensitivity to Primary Loop Length	5	1	1	3	2	3
Can perform FL and SoH	2	1	1	2	2	2
Requires complementary method	3	3	3	2	1	2
Requires extra data about primary loop	4	2	1	2	3	3
Fault Inception Angle Sensitivity	1	1	3	3	3	3
Operational specifications						
Requires personnel training	3	3	3	1	1	1
Time to Perform Task for Personnel	5	3	3	2	1	1
Number of people of required	5	3	3	2	1	1
Online Operation	3	3	3	1	1	1
Offline Operation	2	1	1	3	1	1
Cost specifications						
R&D-cost	1	1	2	3	3	3
Equipment cost	1	1	1	2	2	3
Operational cost	3	3	1	1	1	1
Commercial Equipment Available	2	2	1	3	3	3
Total Score		173	189	167	149	185

8.5.2 Concept Scoring for State of Health Methods

A similar evaluation has been done for the State of health methods. Some of the metrics from table 15 can however be ignored, as they are considered as non applicable for the SoH-methods. A smaller concept scoring matrix for the state of health methods is shown in table 16.

Table 16: Concept scoring matrix - State of health methods

Metrics / Methods	**Weight factor**	**Tan δ**	**Partial discharge**
Technical specifications			
Requires High Sampling Rate	2	-	1
Noise Sensitivity	3	3	1
Performance on Shielded Cables	5	3	3
Performance on Unshielded Cables	4	1	3
Requires extra data about primary loop	4	3	3
Operational specifications			
Requires personnel training	3	2	2
Time to Perform Task for Personnel	5	1	1
Nbr of people of required	5	2	2
Online Operation	3	1	1
Offline Operation	2	3	3
Cost specifications			
R&D-cost	1	3	1
Equipment cost	1	2	1
Operational cost	3	2	1
Commercial Equipment Available	2	3	3
Total Score		87	85

The SoH methods have both received very similar concept scores. None of them are fit for online operation, PD is extremely sensitive to noise and Tan δ does not need to be performed often enough for an online implementation to be meaningful. Therefore a maintenance routine has to be built around the methods in order for them to be useful. The methods provide similar information using different electrical phenomena, both provide a benchmark on electrical insulation quality for a conductor. Both methods are complex, relatively expensive and time-consuming to perform. Although there exist commercial solutions for both Tan δ and PD, which removes the need for R&D.

SoH methods are not only meaningful for airport maintenance crews, they can also be used by Safegate engineers during commissioning of new series circuits in order to benchmark if existing series circuit cable systems are in sufficient condition so that ASP operations and other features can be ensured.

9 Conclusions & Future Work

The goal of this study was to perform a technical and operative feasibility study of fault location and SoH methods on airfield series circuits. The basis of the study was formed from a literature study of conventional fault location and SoH technologies, these methods were then applied and evaluated for a series circuit system. Due to design constraints such as backward compatibility and operation without PLC, the online methods were limited to utilizing CCR terminals.

AFL-systems differ from conventional grid systems. Firstly, a CCR will provide a different source behaviour than a source in a conventional grid. Furthermore, a series circuit consists of transformers as distributed loads along the circuit. Therefore, the effect of these system differences had to be evaluated for the methods of interest. Finally, the use of manholes transformer connections and splices allow for more frequent water and moisture intrusion than in a conventional grid, which makes the cable system more vulnerable than if the system would be completely buried.

Since there is no standardized series circuit configuration, different airports use a multitude of different cable and transformer manufacturers and since layout differs between airports transformer placement and series circuit lengths can differ significantly. It is therefore difficult to determine if a method can perform well on all circuits. Initially, the online methods TW and voltage profiling looked very promising, since they overcome the time- and personnel-issue of current FL methods. Unfortunately, the problems with high frequency attenuation, dispersion and high ground fault resistances are not solved. TW based fault location suffers from dispersion problems even for very short circuits with few transformers, larger series circuits will attenuate and disperse any fault waves even more making them harder to detect and localize in time. Impedance based voltage profiling however, does not utilize any high frequency signal components and thus, is not affected by attenuation and dispersion limitations. Although, voltage profiling is also sensitive to high ground fault resistances which introduces errors in the fault location algorithm. The performance of voltage profiling will also decrease with series circuit length since the FL error originates from the approximation circuit parameters and local variations in said parameters.

Due to the fact that FL with HV pulse discharging may cause furtherm damage to equipment, the only offline method of interest was TDR. TDR has had great success in conventional grid systems. Even if TDR FL is very time and personnel intensive, a method which can localize any potential faults (series or ground) on a given cable segment is an improvement to current FL routines. It was found that TDR provides very accurate fault location for large ground and series faults, although since the majority of faults consists of high resistance paths to ground, it was very difficult to utilize TDR to locate these. Since TDR is a qualitative analysis of signal reflections it requires a significant amount of experience to operate reliably.

Developing preemptive maintenance routines is of interest if availability is to be enhanced in the coming years. Therefore, cable SoH methods were investigated. The literature study revealed Tan δ and partial discharge, which are in use at cable manufacturers and power distribution companies. These SoH methods can quantify the quality of cable insulation as well as connector and splice quality. Although, as was mentioned in previous sections, the SoH method will only capture the SoH of the current state wet, dry or other. Dry measurements can not ensure the quality in wet conditions. Although, PD and Tan δ can work as a benchmarking tool over time that can help with prioritizing cable replacements. Furthermore, the SoH methods mentioned above are also of interest to ADB-Safegate engineers who are commissioning new Safegate series circuits. The methods can help with evaluating if current series circuits can ensure the operation of Safegate fixtures and CCR:s.

Regarding future work within the area of series circuit fault location, the result of this study is that utilizing online substation terminal measurements is problematic and difficult. Although, large scale fault tests are recommended in order to verify the results of this study. Furthermore, one possibility of circumnavigating the problems associated with substation measurement methods is to abandon the substation and to utilize the logic and sampling possibilities of the light fixtures using ASP capabilities. Taking advantage of having a measurement node at each fixture and thus building a sensory network could solve the attenuation and dispersion problem related to series circuits. With sufficient resolution of current measurements in the light fixtures, high resistance ground faults can also be located by comparing current amplitudes at each fixture. If a difference in current between two adjacent fixtures is detected, there is reason to believe that a ground fault has occurred in the cable segment connecting the two fixtures.

This study has not resulted in a complete product, but has laid the foundation for future research and development within the area. The problem of series circuit fault location is still unsolved in the industry, and is more complex than initially anticipated. Automated fault location and SoH is a stepping stone to increased availability and minimized downtime of airside operations, which is an integral part of ADB-Safegate's vision of the future airport.

References

[1] Safegate Group (2016-04-04). *The future airport*. Available: http://www.safegate.com/home/the-future-airport [2016-04-28].

[2] Safegate Group (2016-04-04). *About Safegate Group*. Available: http://www.safegate.com/home/business-interaction [2016-04-28].

[3] EFLA Oy (2016-04-28). *AGL Transformers for Series Circuits*. Available: http://www.efla.net/products/agl-transformers-for-series-circuits/ [2016-04-28].

[4] Safegate Group (2016-04-04). *Airfield lighting manual - Inset Lights*. Available: http://www.safegate.com/tibet/template/media\%2CMediaObjectFile.vm?siteid=1040\&objectid=7313\&size=large [2016-04-28].

[5] Safegate Group (2016-04-04). *Airfield lighting manual - Elevated Lights*. Available: http://www.safegate.com/tibet/template/media\%2CMediaObjectFile.vm?siteid=1040\&objectid=7364\&size=large [2016-04-28].

[6] Safegate Group (2016-04-04). *Airfield lighting manual - Constant Current Regulator*. Available: http://www.safegate.com/home/safegate-solutions/airfield/afl-product-catalogue/safeccr-idm8000 [2016-05-16]

[7] Safegate Group (2016-04-04). *Airfield Smart Power Manual*. Available: http://www.safegate.com/data/safegate/files/file_element/245501f3296b7405605a9672ee9f772b/SG_ASP_Manual_v1.0_s_1.pdf [2016-05-16]

[8] Kabelwerk Eupen AG (2015-08-08). *Eupen Datasheet: FAA-L-824 - Type C - Brass tape screened 5kV* [Data Sheet]. Available: http://www.eupen.com/weimages/airfield/primary_cables/faa-l-824_typec_brass_tape_screened.pdf [2016-04-28].

[9] K. Steinbrich (2005). IEEE Explore - Digital library. *Influence of semiconducting layers on the attenuation behavior of single-core power cables*. Volume: 152.

[10] Qian. L. & Shan, Z. (2012), *Coaxial Cable Modeling and Verification*. Blekinge Institute of Technology. Bachelor of Science in Electrical Engineering.

[11] Schmitt, R. (2002). *Electromagnetics Explained: A handbook for wireless/RF, EMC, and high speed electronics*. Elsevier.

[12] McCammon, R. (2012). *SPICE Simulation of Transmission Lines by the Telegrapher's Method*. Part1-3. University of Texas Department of Electrical Engineering.

[13] Popović, Z. B., Popović, B.D. (2000), *Introductory Electromagnetics: Practice, Problems and Labs*. University of California: Prentice Hall.

[14] Glover ,J.D., Mulukutla, S.S., Overbye, T.J. (2012), *Power Systems Analysis and Design*. 5:th edition. Stamford: Cengage Learning.

[15] Coiner. P. (2011). *Calculating the propagation delay in coaxial cable*. http://www.gpssource.com/files/Cable-Delay-FAQ.pdf. [2016-04-29].

[16] Kabelwerk Eupen AG (2015-08-08). *Primary Airfield Lighting Cables - Shielded vs Unshielded*. Available: https://www.eupen.com/weimages/download_catalog/Primary-Airfield-Lighting-Cables-02-2013-def.pdf [2016-05-02].

[17] The Okonite Company (2016). *Shielding Discussion.* `http://www.okonite.com/engineering/shielding.html`. [2016-05-02].

[18] Alsharif, M., Wallace, P.A., Hepburn D.M., Zhou, C. (2012), *FEM Modelling of Electric Field and Potential Distributions of MV XLPE Cables Containing Void Defect.* Taraghin-Sebha, Libya: Department of Physics, Faculty of Arts, Sebha University.

[19] Meettechniek.info (2013-10-06). *Current Transformers.* Available: `http://meettechniek.info/instruments/current-transformer.html` [2016-05-02].

[20] efla.net *AGL-transformers for series circuits* Available: `http://www.efla.net/products/agl-transformers-for-series-circuits/` [2016-05-04]

[21] Texas Instruments Incorporated (2001). *Power Transformer Design.* Available: `http://www.ti.com/lit/ml/slup126/slup126.pdf` [2016-05-02].

[22] Ajaei, F.B. (2011). IEEE Explore - Digital library. *Compensation of the Current-Transformer Saturation Effects for Digital Relays.* Volume:26, Issue: 4. Tehran, Iran: ECE School, College of Engineering, University of Tehran.

[23] IEEE Explore - Digital library (2007). *IEEE Guide for Fault-locating Techniques on Shielded Power Cable Systems.* New York: The Institute of Electrical and Electronics Engineers.

[24] Saha, M.M., Izykowski, J., Rosolowski, E. (2010). *Fault location on power networks.* London: Springer.

[25] Flytkjær Jensen, C. (2014). *Online Location of Faults on AC Cables.* Switzerland: Springer.

[26] Ulrich, K.T., Eppinger, S.D. (2012). *Product Design and Development.* 5:th edition. New York: McGraw-hill.

[27] Krein, P.T. (1997). *Elements of Power Electronics.* US: Oxford University Press.

[28] Frank, R., Morton, C. (2005). IEEE Explore - Digital library *Comparative corrosion and current burst testing of copper and aluminum electrical power connectors.*

[29] IEEE Explore - Digital library (2005). *IEEE Guide for determining fault location on ac transmission and distribution lines.* New York: The Institute of Electrical and Electronics Engineers.

[30] Zhang, J., Liang, S. (2011). *Research on Fault Location on Power Cable with Wavelet Analysis.* Nanyang, China: Department of E.E. Henan Polytech. Inst.

[31] Engadget (2016-05-02). *super-mario-world-self-learning-ai.* Available: `http://www.engadget.com/2015/06/17/super-mario-world-self-learning-ai/` [2016-05-02].

[32] Densley, J. (2001). *Ageing Mechanisms and Diagnostics for power cables - an overview.* Ontario, Canada: Ontario Power Technologies.

[33] Patsch, R., Jung, J. (1999). *Water Trees in cables: generation and detection.* Germany: Inst. of Mater. & Diagnostics in Electr. Eng., Siegen Univ.

[34] Bao, M., Tang, S., He, J., Yin, X., Wang, Q., Wu, G., Yang, Y. (2012). *The initiation phenomena of electrical treeing in XLPE cable insulation.* China: Chongqing Electric Power Research Institute.

[35] Jia-bin, L., Quan, Z., Shijun, C., Tao, Y., Ruijin, L., Di, Y. (2008). *Analysis on Secondary Growth Characteristics of Electrical Trees in XLPE Cable.* China: State Key Laboratory of Power Transmission Equipment & System Security and New Technology, Chongqing University.

[36] Mroczkowski, R.S. (1998). *Concerning reliability modeling of connectors*. USA: AMP Inc., Harrisburg.

[37] Oussalah, N., Zebboudj, Y., Boggs, S.A. (2007). *Partial Discharge Pulse Propagation in Shielded Power Cable and Implications for Detection Sensitivity*. Volume:23, Issue: 6.

[38] Thayoob, Y.H.M., Visvanathan, Y.S., Ahmed, S.K.,Ghani, A.B.A. (2015). *Analysis and characterization of water tree condition in XLPE cables from dielectric spectroscopy measurement in frequency domain*. Selangor, Malaysia: College of Engineering, University Tenaga Nasional Jalan IKRAM-UNITEN.

[39] Gong, Y., Mynam, M., Guzmán, A., Benmouyal, G., Shulim, B. (2012). *Automated fault location system for nonhomogeneous transmission networks*. Schwitzerland: Schweitzer Engineering Laboratories, Inc.

[40] Pozar, D.M. (2011). *Microwave Engineering*. 4th edition. John Wiley & sons inc.

[41] Misiti, M., Misiti, Y., Oppenheim, G., Poggi, J.M. (1996). *Wavelet Toolbox, For use with MATLAB. User Guide.*. The MathWorks, inc.

[42] Linear Technology (2016-06-10). *LTspice*. Available: `http://www.linear.com/designtools/software/#LTspice` [2016-06-12].

Appendix A LTspice

A.1 LossyTL Constructor

```
.param len=1 ; in meters
.param Lcon=10n ; convergence inductance
+ C=124e-12 ; the value of capacitance at dc (/m)
+ Gdc=0.5n ; the value of conductance at dc (1000ft)
+ Rdc=2m ; the value of resistance at dc of (/m)
+ Ldc=0.24e-6 ; the value of inductance at dc (/m)
+ Linf=0.22e-6 ; inductance at infinite frequency of (/m)
+ Ldel=(Ldc-Linf) ; inductance parameter
+ Zinf=(Linf/C)**0.5 ; characteristic impedance at infinite frequency
+ Yinf=1/Zinf ; characteristic conductance at infinite frequency
+ F2=5e6 ; the highest frequency in Hz
+ W2=6.28318*F2 ; the highest frequency in rad/sec
+ G1=23u ; the value of conductance at F1 (1000ft)
+ G2=36u ; the value of conductance at F2 (1000ft)
+ Rac=0.0666 ; the value of resistance at F2 (/m)
+ F1=3e6 ; the second highest frequency in Hz
+ A=1.6 ; inductance parameter
+ k=Log(G2/G1)/Log(F2/F1)/2 ; conductance parameter
+ WL=6.28318*161000 ; inductance parameter
+ WR=W2*(Rdc**2)/(((Rac**4)-(Rdc**4))**0.5) ; resistance parameter

.subckt single_mode_xline L1 R1
G1 N1 0 N1 0 Laplace={{{{{Gdc+G2*(-(s/w2)^2)^k)+s*C)/
+ ((Rdc*(1-(s/wR)^2)^0.25)+s*(Linf+Ldel/(1+A*((-(s/wL)^2)^0.5)-
+ (s/wL)^2)^0.25)))^0.5))-Yinf}}
G2 0 N1 N2 0 1
G3 0 L1 N2 0 1
V1 L1 N1 0 Rser=0
H1 N4 0 V1 1
G4 N6 0 N6 0 Laplace={{{{{Gdc+G2*(-(s/w2)^2)^k)+s*C)/
+ ((Rdc*(1-(s/wR)^2)^0.25)+s*(Linf+Ldel/(1+A*((-(s/wL)^2)^0.5)-
+ (s/wL)^2)^0.25)))^0.5))-Yinf}}
G5 0 N6 N5 0 1
G6 0 R1 N5 0 1
V2 R1 N6 0 Rser=0
H2 N3 0 V2 1
R1 N6 0 {Zinf}
R2 N1 0 {Zinf}
G7 0 N2 N3 0 Laplace= Exp(-len*( (((Rdc*(1-(s/wR)^2)^.25)+
+ s*(Linf+Ldel/(1+A*((-(s/wL)^2)^.5)-(s/wL)^2)^.25))*
+ (Gdc+G2*(-(s/w2)^2)^k+s*C))^.5))/(s*Lcon+1)
L1 N5 0 {Lcon} Rser=1
G8 0 N5 N4 0 Laplace= Exp(-len*( (((Rdc*(1-(s/wR)^2)^.25)+
+ s*(Linf+Ldel/(1+A*((-(s/wL)^2)^.5)-(s/wL)^2)^.25))*
+ (Gdc+G2*(-(s/w2)^2)^k+s*C))^.5))/(s*Lcon+1)
L2 N2 0 {Lcon} Rser=1
.ends single_mode_xline
```

A.2 Complete airport circuit Schematic

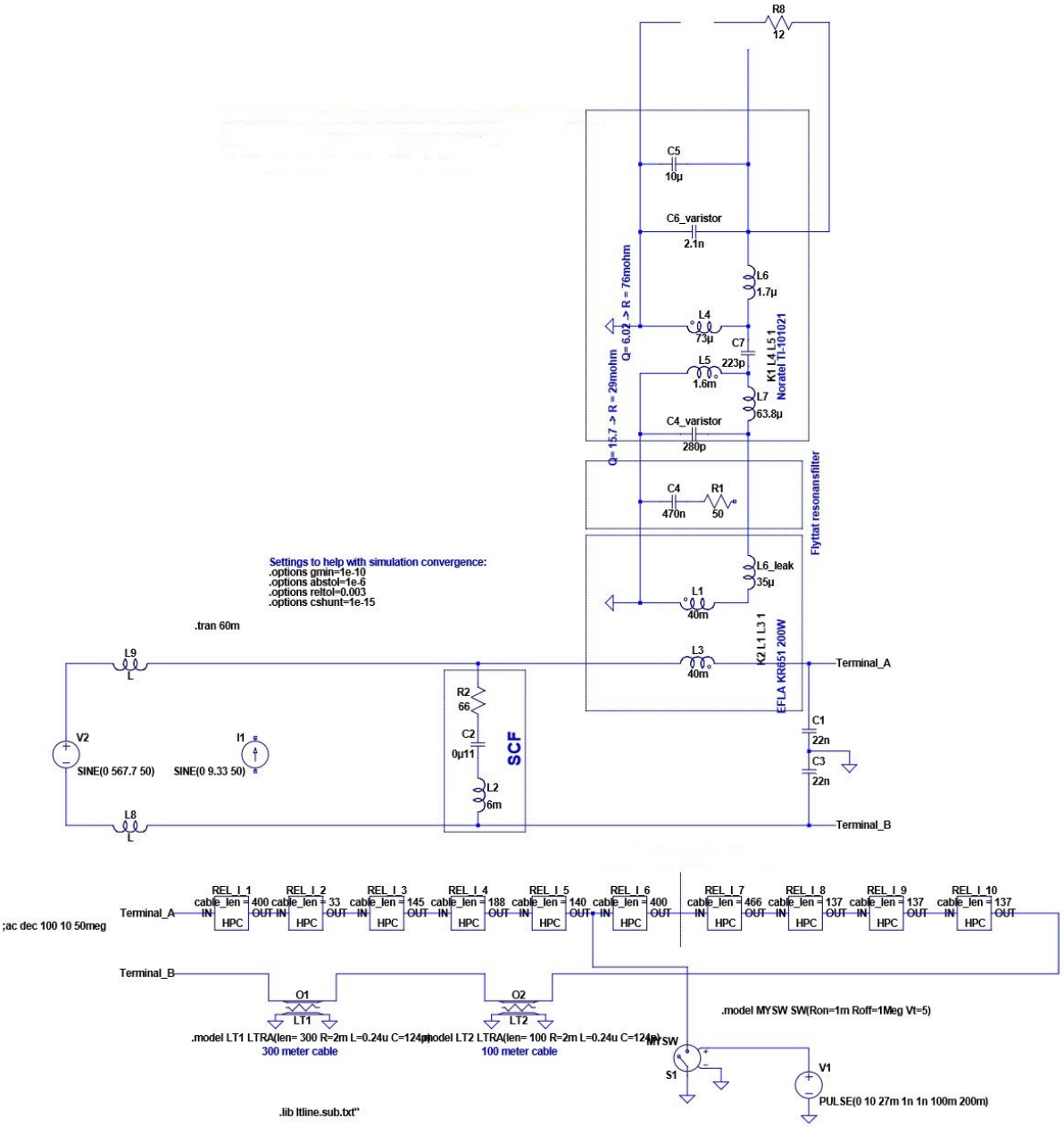

Appendix B Test Data & Calculations

B.1 Inter-turn Capacitance Calculation

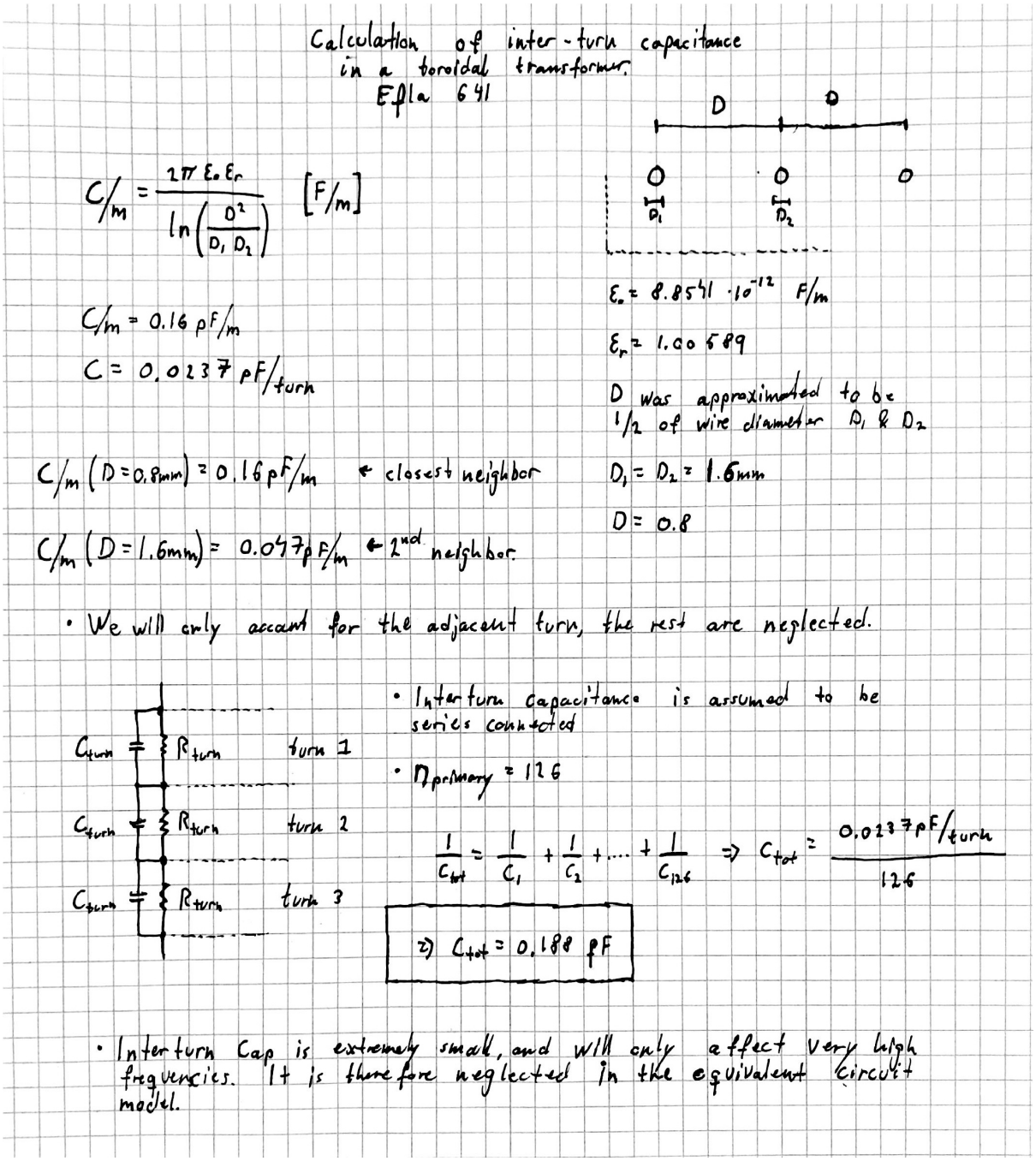

Figure 79: Our inter-turn capacitance calculation of a EFLA 641 transformer.

B.2 Transformer Data

Failopen tester

Isoladins trafo mätningar

Peter

1 Mätningar av olika isolationstrafos
2 Testobjekt och testfall
3 Tester
3.1 Test 1, olika trafotyper och CCR-strömmar
3.2 Test 2, lastberoende
3.3 Försök med LC-länkar som belastning

1. Mätningar av olika isolationstrafos:

Trafo	*Kapacitans mellan lindningar*	*Induktans primär*	*Induktans sekundär*	*Induktans kortsluten primär*	
300W Efla KR561	99 pF	44,7 mH	44,1 mH Q=2,31	3,85 mH	Q=17,1
200W Efla KR651	233 pF	14,67 mH	14,48 mH Q=1,35	0,056 mH	Q=0,88
100W Efla KR641	209 pF	14,9 mH	14,7 mH Q=1,62	0,036 mH	Q=0,76 $\begin{cases} L_{mag}=14mH \\ L_{leak}=40\mu H \end{cases}$
100W Efla KR541	85 pF	30,8 mH	30,3 mH Q=1,16	1,82 mH	Q=18,2
30/45W KR531	51 pF	3,76 mH	3,61 mH Q=1,6	0,55 mH	Q=8,7
300W Amerace	78 pF	64,8 mH	62,7 mH Q=3,5	2,18 mH	Q=14,8
30/45W Amerace	49 pF	11,3 mH	10,8 mH Q=0,95	0,28 mH	Q=4,6

Trafo resonansfrekvenser:

Trafo	f_{res_sc}	f_{res_open}
KR561	143 kHz	55 kHz
KR641	2,27 MHz	omätbar (låg parallell-kapacitans)
KR541	244 kHz	125+370 kHz överlagrade, svaga
KR531	588 kHz	333 kHz+1,1 MHz överlagrade, svaga
Amerace 300W	322,6 kHz	66,7 kHz, svag
Amerace 30/45W	1,17 MHz	526 kHz, svag

Detta är mätt från "lampsidan". Det blir då lätt att kortsluta på "slingsidan" vid behov.
Frekvenserna ändras endast marginellt om man mäter på det omvända hållet.

Appendix C Simulations Raw Data

C.1 Inception Angle

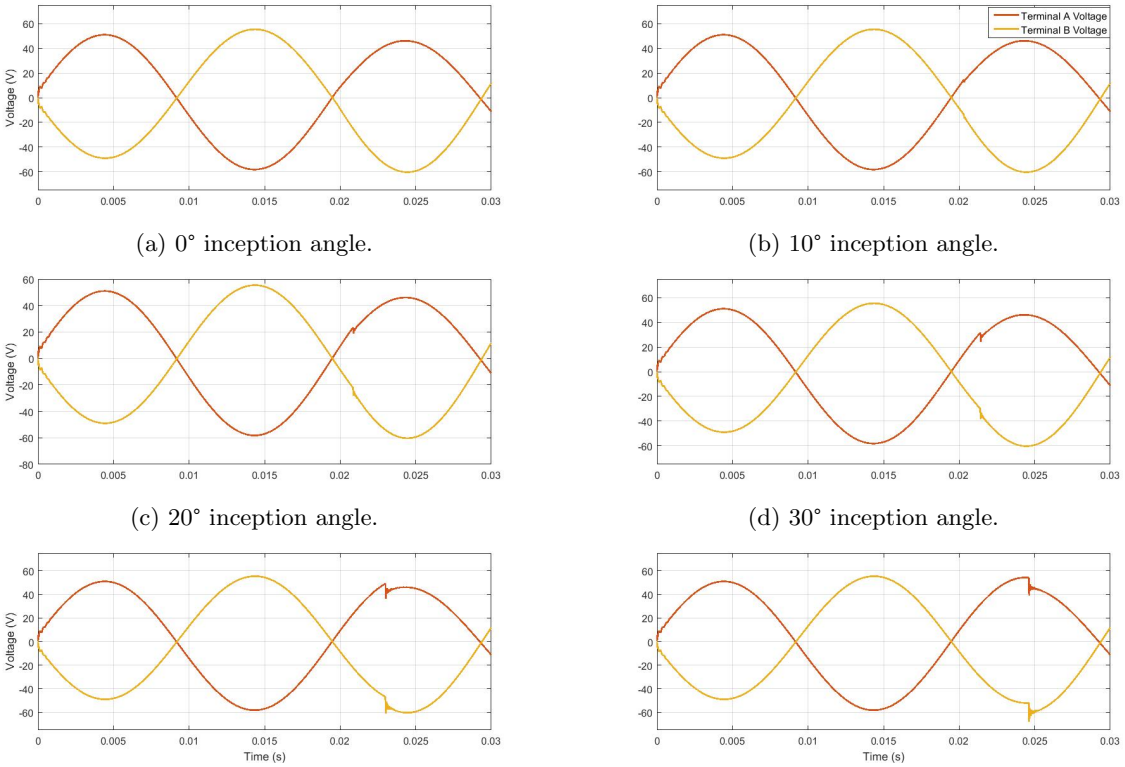

(a) 0° inception angle.

(b) 10° inception angle.

(c) 20° inception angle.

(d) 30° inception angle.

(e) 60° inception angle.

(f) 90° inception angle.

Figure 80: Effect of fault inception, obtained terminal data from the airport transient simulations. $R_f = 1m\Omega$ and $d_{fault} = 906m$ from terminal A.

C.2 Fault Resistance

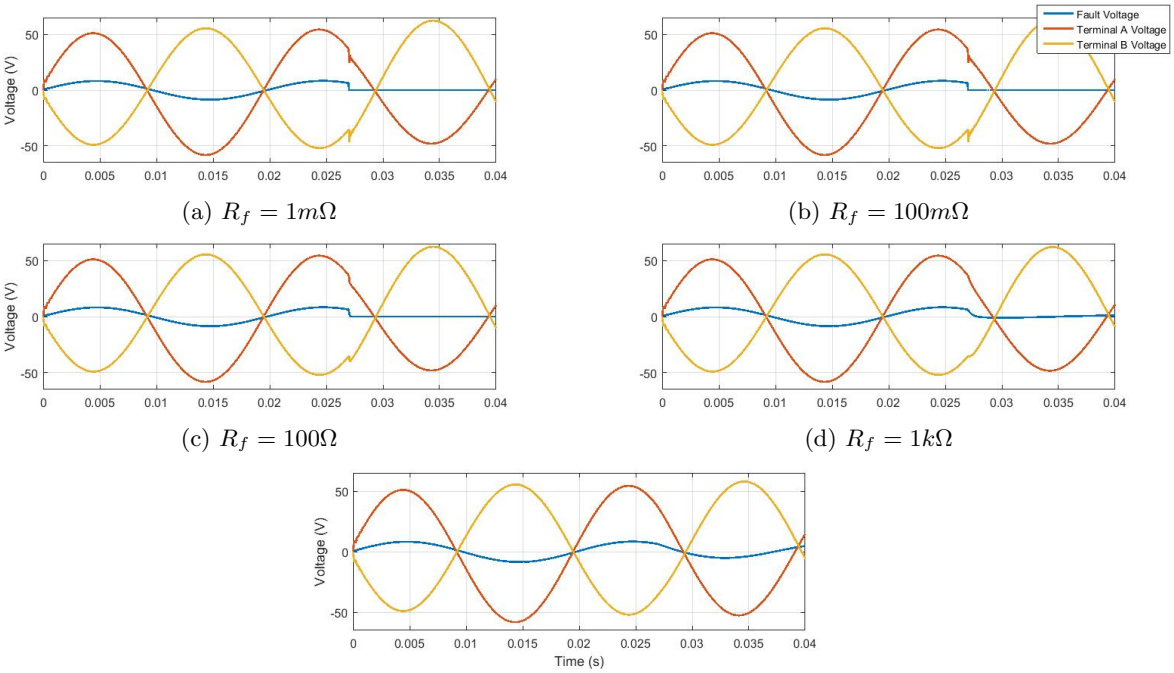

(a) $R_f = 1m\Omega$

(b) $R_f = 100m\Omega$

(c) $R_f = 100\Omega$

(d) $R_f = 1k\Omega$

(e) $R_f = 10k\Omega$

Figure 81: Effect of R_f, obtained terminal data from airport transient simulations. $t_{fault} = 27ms$ and $d_{fault} = 906m$ from terminal A.

C.3 Fault Location

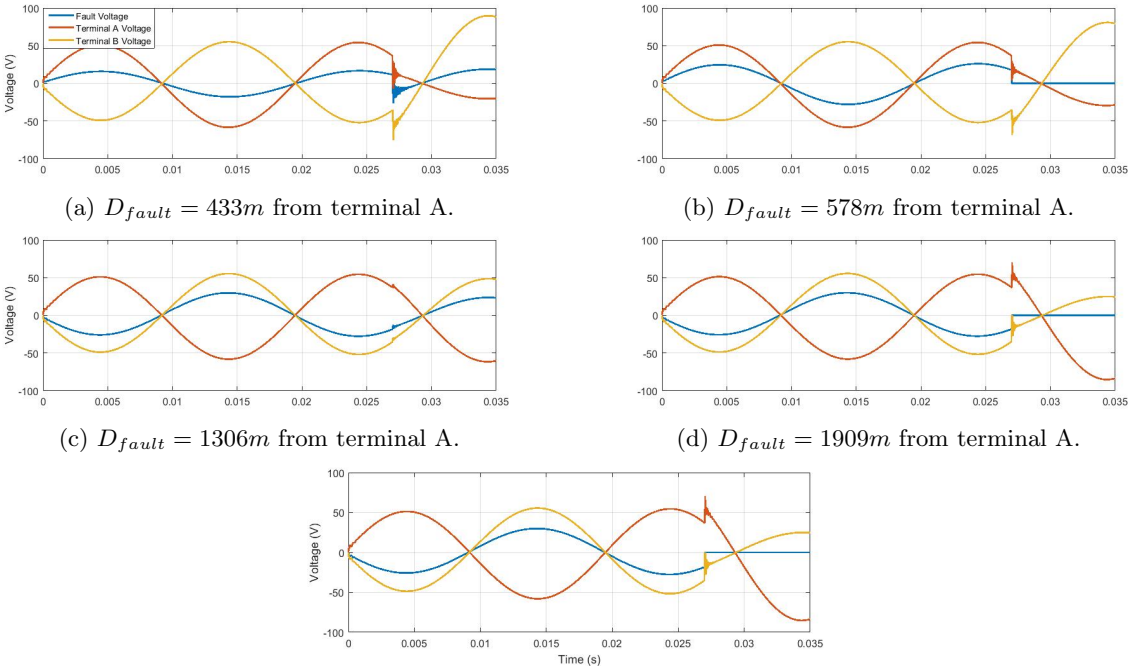

(a) $D_{fault} = 433m$ from terminal A.

(b) $D_{fault} = 578m$ from terminal A.

(c) $D_{fault} = 1306m$ from terminal A.

(d) $D_{fault} = 1909m$ from terminal A.

(e) $D_{fault} = 2046m$ from terminal A.

Figure 82: Effect of fault location, obtained terminal data from airport transient simulations. $R_f = 1m\Omega$ and $d_{fault} = 906m$ from terminal A.